DEANSHIP OF GRADUATE STUDIES
AL-QUDS UNIVERSITY

Spectroscopic Investigations of Propofol and L-arginine Interactions with Beta-amyloid (1-40)

Shurook Yousef Mohammed Aiaidah

M.Sc. Thesis

Jerusalem-Palestine

1435 / 2014

Spectroscopic Investigations of Propofol and L-arginine Interactions with Beta-amyloid (1-40)

Prepared by:

Shurook Yousef Mohammed Aiaidah

B.Sc. physics (Al-Quds University) (Jerusalem)

Supervisor: Prof. Saqer Darwish

A thesis submitted in partial fulfillment of requirements for the degree of master of physics department –Al-Quds University

1435/2014

Al-Quds University

Deanship of Graduate Studies

Physics Department

Thesis approval

Spectroscopic Investigations of Propofol and L-arginine Interaction with Beta-amyloid (1-40)

Prepared by: Shurook Yousef Mohammad Aiaidah

Registration No.: 21012420

Supervisor: Prof. Saqer Darwish

Master thesis submitted and accepted, Date: 1/2/2014

The names and signatures of the examining committee members as follows:

1- Head of Committee: …….. Signature ……
2- Internal Examiner: ……. Signature ……
3- External Examiner: ……. Signature ……

Jerusalem- Palestine

1435 / 2014

Dedication

I dedicate this thesis to all members of my lovely family who supported me throughout my life and encouraged me to achieve my goals:

To my father and my mother for their unconditional love, guidance, and support, to my brothers and sisters, to my children Qutada and Istabraq who gave me more reasons to succeed, and great thanks to my husband Ajwad for his support and encouragement in all stages of my life. I love you all…….

Shurook Yousef Mohammad Aiaidah

Declaration:

I certify that this thesis submitted for the degree of master is the result of my own research, except where otherwise acknowledged, and that this thesis (or any part of the same) has not been submitted for a higher degree to any other university or institution.

Name: Shurook yousef Mohammad Aiaidah

Signed:

Date: / /

Acknoledgements

At first and last my great commendation and thanks to Allah, who gave me the ability to accomplish this work, and put in my way such a nice supporting people

I would like to thank all peoples who deserve my gratitude and made this work possible and enjoyable experience for me

My great thanks to my supervisor Prof. Saqer Darwish for the support he gave me during the research and for providing me the ability to work. He has been an excellent teacher and a brilliant guidance for his wisdom, patience, encouragement, positive criticism, and assistance in bringing this work to completion. You are a teacher who I will not forget all my life, I sincerely thank you…

My great thanks also to all teachers in the physics department especially my wonderful teacher Prof. Imad Al-Barghouthi.

Great thanks to Lina Al-Qawasmi for her help in taking the AFM images for my samples.

Abstract

The interaction of propofol and L-arginine with β-amyloid (1-40) (Aβ) have been investigated by using UV-absorption spectroscopy, fluorescence spectroscopy, Fourier transform infrared (FTIR) spectroscopy, and atomic force microscopy (AFM). The binding constants have been determined by both UV-absorption spectroscopy and fluorescence spectroscopy. The values of the binding constants calculated at 293K are ($2.13x10^2M^{-1}$, $2.81x10^2M^{-1}$) for propofol, and ($0.35x10^2M^{-1}$, $0.37x10^2$ M^{-1}) for L-arginine. The Stern-Volmer quenching constant values were found to be $1.21x10^3L.mol^{-1}$ for propofol and $1.49x10^3L.mol^{-1}$ for L-arginine.

The fluorescence data reveals a decrease in Aβ-drug emission intensity with the increase of propofol and L-arginine concentration. This decrease in intensity indicates that both propofol and arginine have strong ability to quench the intrinsic fluorescence of Aβ through static quenching mechanism.

All peak positions in the amide I and amide II regions have been assigned, and any effect due to concentration changes have been investigated. The FTIR spectra measurements indicate a change in the intensity of the absorption bands due to the change in ligand concentration. An increase in the intensity of anti-parallel β-sheet bands with increasing propofol concentration has been observed. This increase is associated with the formation of oligomers or fibrils in the Aβ. On the other hand a decrease in the intensity of anti-parallel β-sheet band with increasing L-arginine concentration has been observed. It has been found that L-arginine decreased the rate of oligomerization and amyloid fibrils formation.

It has been found that changing temperature have no effect on the intensity of the absorption bands of parallel and anti parallel β-sheet in Aβ free. For Aβ-propofol complex the intensity of anti-parallel β-sheet band has increased gradually with increasing temperature, this increase in the intensity of anti-parallel β-sheet band is accompanied with a decrease in parallel β-sheet band intensity. For Aβ-L-arginine complex the intensity of anti parallel β-sheet band has decreased accompanied with an increase in parallel β-sheet band intensity until the temperature is 33^0C, then the intensity of anti-parallel β-sheet band starts to increase and that of parallel β-sheet starts to decrease gradually.

AFM images were also taken for Aβ-free, Aβ-propofol complex, and Aβ-L-arginine complex to compare the effect of these ligands on Aβ and verify our results. AFM images showed an increase in the size of oligomers after propofol addition to Aβ.

List of tables:

List of Figures

List of symbols:

symbol	description
λ	Wavelength
c	Speed of light
ν	Frequency
E	Energy
E_{total}	Total energy of a molecule
E_{rot}	Rotational energy
E_{vib}	Vibrational energy
E_{el}	Electronic energy
I	Intensity of the transmitted light
I_0	Intensity of the incident light
ε	Beer's law molar absorptivity coefficient (or extinction coefficient)
l	Length of the light path
A	Absorbance
V_i	Vibrational energy states
h	Plank's constant
ν_i	Vibrational frequency
x_i	Anharmonicity constant
$\tilde{\nu}$	Wavenumber
k	Binding constant
μ	Reduced mass of the system
$f(t)$	Radiant power as a function of time (t)
$G(\omega)$	Radiant power as a function of angular frequency (ω)
K	Stern-Volmer quenching constant
k_q	Biomolecular quenching constant
l	Quencher concentration
F_0	Fluorescence intensity without a quencher
F	Fluorescence intensity with a quencher

List of abbreviations:

symbol	Abbreviation representation
EMW	Electromagnetic Waves.
IR	Infrared
FTIR	Fourier Transform Infra-red.
HOMO	Highest Occupied Molecular Orbital
UV	Ultraviolet
LUMO	Lowest Unoccupied Molecular Orbital
Aβ	Beta-Amyloid
APP	Amyloid Precursor Protein.
FSD	Fourier Self Deconvolution
Tyr	Thyrosin
Phe	Phenylalanine
Trp	Tryptophan
nm	Nanometer
AFM	Atomic Force Microscopy
AD	Alzheimer Disease
NMR	Nuclear Magnetic Resonance
KDa	Kilodalton
LED's	Light Emitting Diodes
DTGS	Deuterium Triglycine sulfate
MCT	Mercury Cadimium Telluride
CNS	Central Nervous System
AMU	Atomic Mass Unit
PBS	Phosphate Buffer Saline

Chapter one:

Introduction

Introduction

This research is concerned with using spectroscopic techniques such as Fourier Transform Infrared Spectroscopy (FTIR), UV-Vis spectroscopy, Fluorescence spectroscopy, in addition to Atomic Force Microscopy (AFM) to investigate the effect of propofol, and L-arginine on Beta-Amyloid (Aβ) (1-40). Aβ is a peptide that is secreted from neurons under normal conditions after cleavage of amyloid precursor protein (APP). Aβ is considered as one of the byproducts of APP processing (Jimenez 2005). Several studies have been performed using several spectroscopic techniques and discovered that Aβ protein is one of the major components of amyloid plaques, which are deposits that are found in the brains of the patients with Alzheimer disease (AD) (Takahashi et al 2002, Lin 2003, El-Agnaf et al 2000).

AD is characterized by loss of memory and language skills. Studies on Aβ have been done and it has shown that due to the toxicity of Aβ, fibrillar Aβ can directly kill the neurons or initiate a series of events leading to a neuronal cell death (Walsh et al 1999, Fodale et al 2006).
Many researches have been done throughout the world to develop compounds that interfere with amyloid aggregation. It has been found that amyloid oligomers and fibrils were characterized by β-sheet secondary structural arrangement (Murphy 2002, kirkitadze et al 2001, Lindgren& Hammarstrom 2010). This research examines the effect of L-arginine and propofol in forming oligomers in Aβ.

Propofol is a fast effective anesthetic drug that is widely used in surgery throughout world (Aschenbrenner & Venable 2009, Silverstein et al 2008). L-arginine is a complex amino acid found in proteins and enzymes, kidneys produce about 60% of L-arginine in human body, and it may be synthesized in the liver. The best diet sources of L-arginine are meat, peanuts, soybeans and eggs (Stayton et al 2008, Stargrove 2008).

The first spectroscopic technique that is used in the process is FTIR which is used in order to investigate the conformational changes on the secondary structure of Aβ upon the addition of different concentrations of propofol and L-arginine on it. Investigation of structural changes includes changes in peak positions and changes in the relative intensities of the secondary structural elements are performed. Also the effect of temperature on Aβ-free, Aβ-propofol complex, and Aβ-L-arginine complex are examined.

UV-absorption spectroscopy is the second spectroscopic technique that is used to investigate the strength of interaction between Aβ with propofol and L-arginine. The binding constant between the ligands and Aβ will be determined.

Fluorescence spectroscopy was used to confirm the calculation of binding constants as an indication of the strength of interaction. The Stern-Volmer quenching constants for propofol and L-arginine interaction with Aβ will also be calculated.

AFM images of Aβ free, Aβ-propofol complex, and Aβ-L-arginine complex will be taken. These images are used to investigate changes of the sizes of upon addition of propofol or L-arginine to Aβ.

The first chapter is an introduction. It shows the purpose and the importance of this work. It also gives information about each chapter in this thesis.

In the second chapter of this thesis the physical background and theoretical considerations of the spectroscopic will be discussed, then a brief introduction to spectroscopic technique used in this research will be given. A brief introduction to proteins, their structural levels, and protein misfolding are given, also AD will be introduced, then information about materials used (Propofol, L-arginine, and Aβ) are given.

In chapter three the experimental part of the study is discussed in details. Sample preparation from the moment of taking the solid protein sample to the moment of inserting the sample inside FTIR equipment is explained. A brief discussion of the instruments is given, and then the experimental procedure followed in taking the needed data is mentioned.

In chapter four results are analyzed and discussed. The UV-absorption spectroscopy results are plotted and used to calculate the binding constant between Aβ and both propofol and L-arginine. The absorption spectra of Aβ with different concentrations of propofol and L-arginine are shown.

A plot of the fluorescence emission spectra of Aβ in the absence and presence of propofol and L-arginine are shown. The binding constant, Stern-Volmer quenching constants and the quenching rate constant of the bio-molecule will be calculated.

FTIR has been used to investigate the conformational changes in Aβ after binding to propofol or L-arginine. Changes in amide I and e II peaks positions for Aβ with different concentrations of propofol and L-arginine are investigated, also changes in the intensity of the component bands of the secondary structure as a result of changing concentrations of propofol and L-arginine have been shown. The effect of changing temperature on the peak positions and on the intensity of β-sheet bands for Aβ free, Aβ-propofol complex, and Aβ-L-arginine complex have been examined.

AFM images for Aβ in the absence and presence of propofol and L-arginine are shown. Comparison between the three images will assist in distinguishing the effect of each ligand on Aβ.

The last chapter contains the conclusion and it also recommends future work that can be done in this field.

Chapter two:

Background and Theoretical Consideration

This chapter discusses spectroscopy in general and explains the physical principles of the spectroscopic techniques that have been used in the work. A brief introduction to proteins and Alzheimer disease, Aβ, propofol, and L-arginine is given.

2.1 ELECTROMAGNETIC RADIATION

Electromagnetic waves (EMW) are transverse oscillating waves composed of electric and magnetic fields perpendicular to each other and perpendicular to the direction of propagation. EMW propagate as a sine or cosine waves at the speed of light in vacuum (Stuart 2004).

The electromagnetic spectrum consists of radio waves, microwaves, infrared radiation, visible light, ultraviolet radiation, X-rays and gamma rays as show in (Figure 2.1).

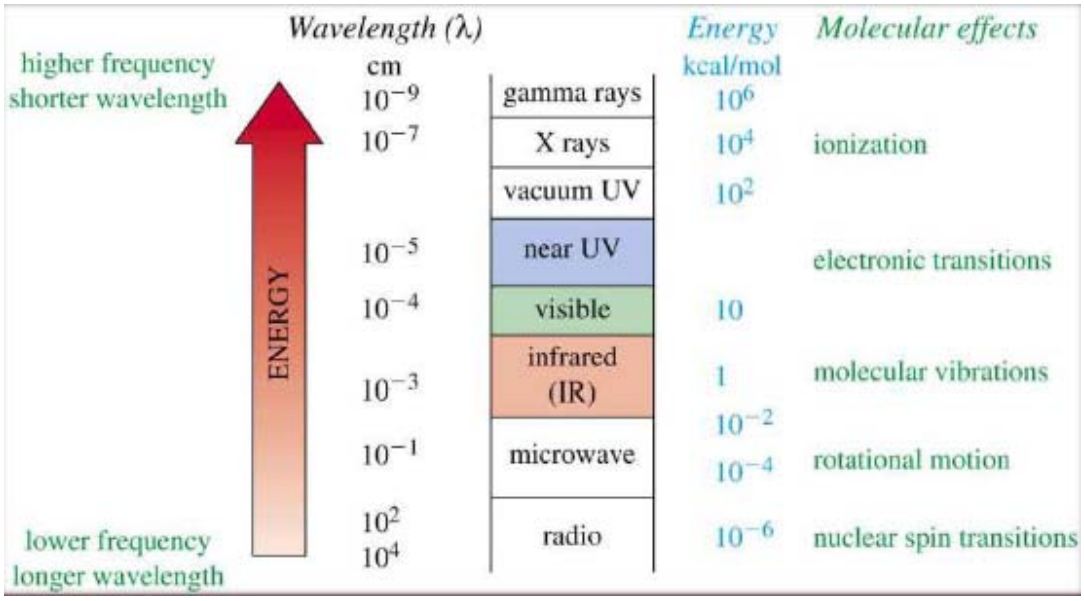

Figure 2.1: The electromagnetic spectrum (Sharma 2007, Ball 2001).

Wavelength (λ) is inversely proportional to frequency(ν) and it is governed by the relation:

$$\lambda = \frac{c}{\nu} \qquad (1)$$

Where c is speed of light and ν is the frequency.

Electromagnetic radiation is composed of multiple electromagnetic waves or photons, which carry energy, momentum and angular momentum.

The energy of each photon is given by Planck–Einstein equation:

$E = h\nu = h\frac{c}{\lambda}$ ---------- (2)

Where E is the energy, h is Planck's constant, ν is frequency, and λ is wavelength (Pavis et al 2008, Yadav 2005, Williams 1976, Ball 2001).

The atomic spectra arise from the transition of electron between atomic energy levels, while molecular spectra arise from three types of energy transitions due to molecular rotation, molecular vibrational, and electronic transition. According to Born Oppenheimer approximation, the total energy of the molecule is given by :

$E_{total} = E_{rot} + E_{vib} + E_{el} + \cdots$ ---------- (3)

Where: E_{rot}: is rotational energy due to the molecule rotation about the axis passing the center of gravity for the molecule.

E_{vib}: is vibrational energy due to the periodic displacement of atoms around their equilibrium positions

E_{el} : is related to the energy of the molecule's electrons (Sharma 2007).

When radiation falls on a sample it may be absorbed, this occur when the energy of radiation matches the difference in energy levels of the sample, otherwise it may be either transmitted or scattered by the sample. A simplified representation of the quantized electronic and vibrational states is represented in (Fig 2.2). It is clear that transitions between electronic energy states require more energy than transitions between vibrational energy states (Hollas 2004, Turro 1991, Ball 2001).

IR radiation does not have enough energy to induce electronic transitions as seen with UV and visible light. Absorption of IR is appropriate to excite vibrational and rotational states of a molecule as shown in (Fig 2.1)

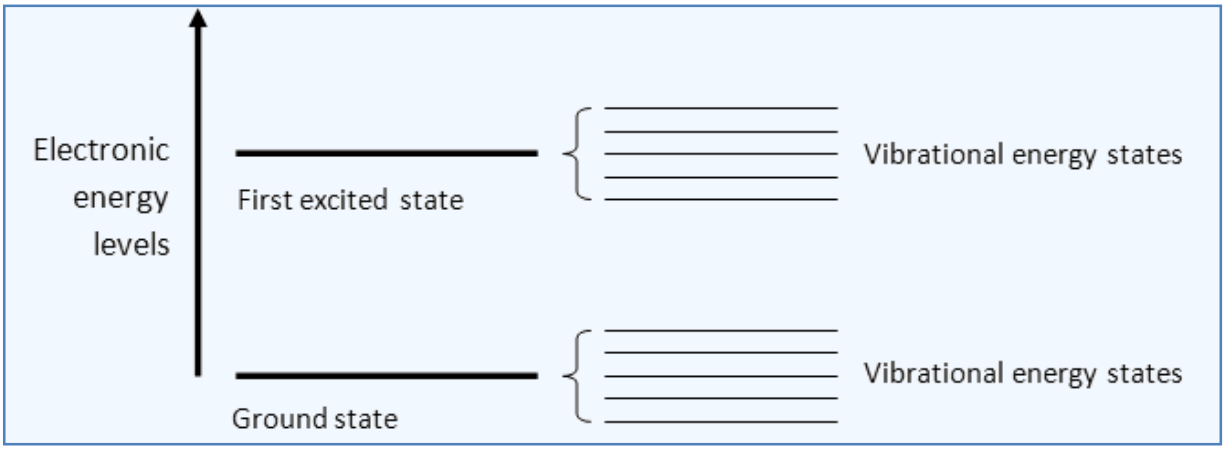

Figure 2.2: A schematic representation of the quantized electronic and vibrational energy levels of a molecule.

Intensity of the light absorbed to produce a given transition is given by Beer-Lambert law:

$\frac{I}{I_0} = 10^{-\varepsilon cl}$---------- (4)

In which I and I_0 are the intensity of light transmitted through the absorber and incident upon it respectively. ε: is the molar absorption coefficient or (molar extinction coefficient), c: is the concentration of absorbing molecule in the sample, and l: is the length of the light path in the sample. The above equation can be represented in logarithmic form:

$A = \log_{10} \frac{I_o}{I} = \varepsilon(v)cl$ ---------- (5)

Where A is called Absorbance (Hollas 2004, Schulman 1977). A setup for an absorption instrument is shown in (Fig 2.3).

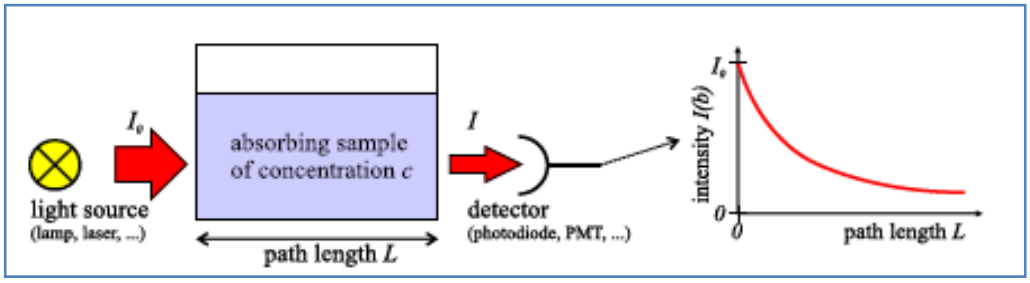

Figure 2.3: A setup of an absorption measurement

2.2 MOLECULAR VIBRATIONS

When the temperature is above absolute zero all atoms in the molecule undergoes vibrational motion with respect to each other, if the incident radiation has energy that matches the difference in energy between vibrational levels of atoms in the molecules, the molecule will absorb energy and become excited.

There are two types of molecular vibrations, stretching (change in bonds length) and bending (change in bonds angel). The bond can stretch in phase (symmetrical stretching) or out of phase (asymmetric stretching) (Stuart 2004, Griffith & Haseth 2007, Williams 1976).

A polyatomic molecule with N atoms has a total of (3N) degrees of freedom; three of which are translational, and three rotational for nonlinear molecules, while two rotational degrees of freedom for linear molecules. The remaining degrees of freedom are for vibrational motion. They are 3N-6 for nonlinear molecules and 3N-5 for linear molecules, as shown in (Table 2.1) (Stuart 2004).

Table 2.1: Molecule degrees of freedom. (Stuart, 2004)

Type of degrees of freedom	Linear	Non-linear
Translational	3	3
Rotational	2	3
Vibrational	$3N-5$	$3N-6$
Total	$3N$	$3N$

Not all of these fundamental vibrations are IR active, only those produce a net change in dipole moment will give an IR-absorption spectrum.

Each mode of vibration involves harmonic displacement of the atom from their equilibrium position, for any mode (i), the atom vibrates with frequency (ν_i) , the potential energy V(r) for harmonic oscillator is shown by the dashed line in (Fig. 2.4) as a function of the distance between the atoms (r). For any mode in which the atoms vibrate with simple harmonic motion, the vibrational energy states can be described by:

$$V_i = h\nu_i\left(n_i + \frac{1}{2}\right)\text{---------- (6)}$$

Where h: Plank's constant, ν_i: fundamental frequency for a particular mode, n_i: vibrational quantum number for the ith mode (n= 0, 1,2,…). Note here that the frequency ν_i is measured in Hertz (Griffith & Haseth 2007).

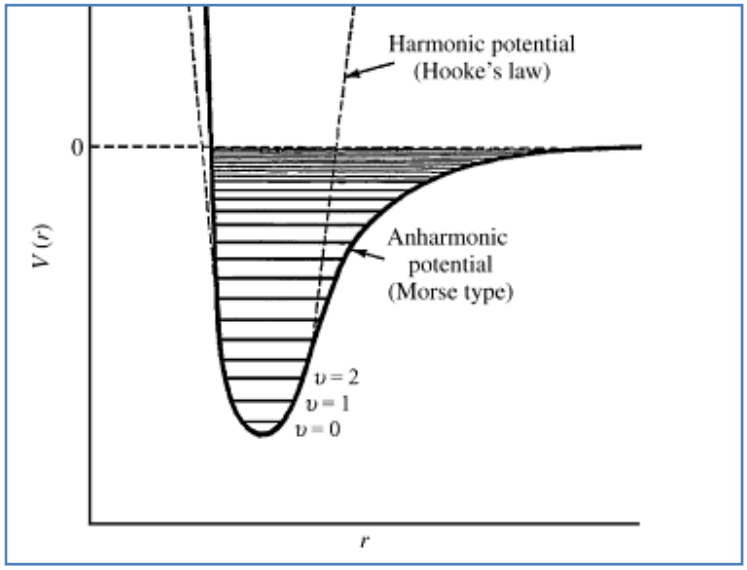

Figure 2.4: Potential energy for a diatomic molecule as a function of atomic displacement during vibration for a harmonic oscillator (dashed line) and anharmonic oscillator (solid line).

The actual vibration of the potential energy as a function of displacement is given by (Fig 2.4 solid line). It is clear that (equation 6) is valid only at low values of vibrational quantum number and is not valid when n_i is large. In practice the potential energy must be described by

the model of anharmonic oscillator (Morse-type potential function). To a first approximation it is given by the following equation:

$$V_i = h\nu_i\left(n_i + \frac{1}{2}\right) + h\nu_i x_i (n_i + \frac{1}{2})^2 \quad \text{----------(7)}$$

Where x_i: is the anharmonicity constant that is dimensionless and has typical values between 0.001-0.02 depending on the mode of vibration (sathyanariana 1983).

For many vibrational modes a large number of atoms in the molecule are almost stationary and only few of them have large displacements. The frequency of such mode is characteristic of the functional group of these molecules and it is almost unaffected by other atoms in the molecule, which enabled scientist to assign each absorption band in the infrared region to a typical functional group (Griffith & Haseth 2007). The assigned wave number for each function group is shown in (Table 2.2).

Table 2.2: Typical bond stretching and angel-bending group vibrations (Hollas 2004).

Bond-stretching		Bond-stretching		Angle-bending	
Group	ω/cm^{-1}	Group	ω/cm^{-1}	Group	ω/cm^{-1}
≡C–H	3300	–C≡N	2100	≡C–H	700
=CH	3020	>C–F	1100	=CH$_2$	1100
except: O=CH	2800	>C–Cl	650	–CH$_3$	1000
>C–H	2960	>C–Br	560	>CH$_2$	1450
–C≡C–	2050	>Cl–I	500	C≡C–C	300
>C=C<	1650	–O–H	3600[a]		
>C–C<	900	>N–H	3350		
>Si–Si<	430	>P=O	1295		
>C=O	1700	>S=O	1310		

2.3 SPECTROSCOPY

Spectroscopy is experimental techniques deal with absorption, emission, or scattering of electromagnetic radiation by atoms or molecules, it deals with interaction between EM radiation and matter (Michael Hollas, 2004).

An incident photon that can induce transition between rotational levels of a molecule is found in the microwave region, while the transition between vibrational levels is induced by a photon in the infrared region, electronic transitions in atoms or molecules give radiation in the visible and UV (Ultraviolet) region (Sharma 2007).

2.3.1. Infrared spectroscopy:

Infrared spectroscopy is a technique based on the absorption of infrared radiation by molecules, when molecules absorb infrared radiation they will be excited to a higher vibrational energy states. This absorption of infrared radiation process is quantized as a molecule absorbs only selected frequencies of infrared radiation (Pavis et al 2008).
Sometimes radiation have a frequency that matches the natural vibrational frequencies of the bonds in the molecule but the bonds are not capable of absorbing it, the reason is that for bonds to be capable of absorbing infrared radiation it must possess a dipole moment that changes as a function of time at the same frequency as the incoming radiation, an example of infrared inactive molecule is homo-nuclear diatomic molecule because it's dipole moment remain zero (Stuart 2004, Raaman 2006).

Infrared radiation is an electromagnetic radiation lies between visible light and microwave region. It is divided into three sub regions, near, far, and mid infrared region.

Near infrared region is assumed to lie between (0.78 - 3μm) or (12820 – 4000 cm^{-1}), mid infrared region lies between (3-30 μm) or (4000-400 cm^{-1}), and far infrared region between (30-300 μm) or (400 - 33cm^{-1}) (Griffith & Haseth 2007).

The presence of hydrogen bonding is of great importance in infrared spectroscopy, it is defined as the attraction that occurs between a highly electronegative atom carrying a non-bonded electron pair (such as fluorine, oxygen or nitrogen) and a hydrogen atom, itself bonded to a small highly electronegative atom as shown in (Fig 2.5).

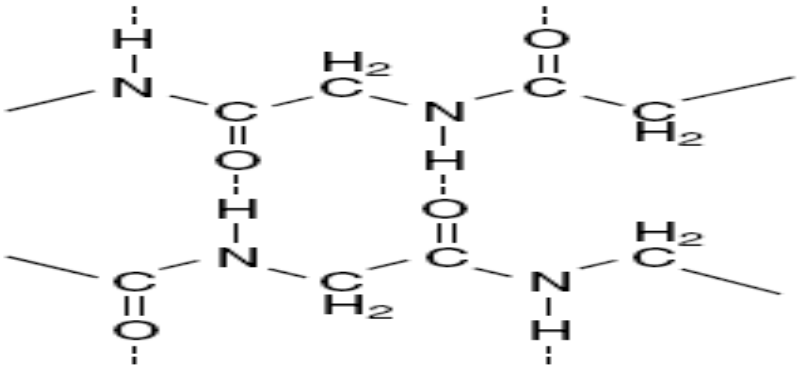

Figure 2.5: Intramolecular hydrogen bonding in a protein (dashed line).

The hydrogen bonding influences the bond stiffness and so alters the frequency of vibration. For example, for a hydrogen bond in an alcohol, the O–H stretching vibration in a hydrogen-bonded dimer is observed in the 3500–2500 cm^{-1} range, rather than in the usual 3700–3600 cm^{-1} range (Stuart 2004, Griffith & Haseth 2007).

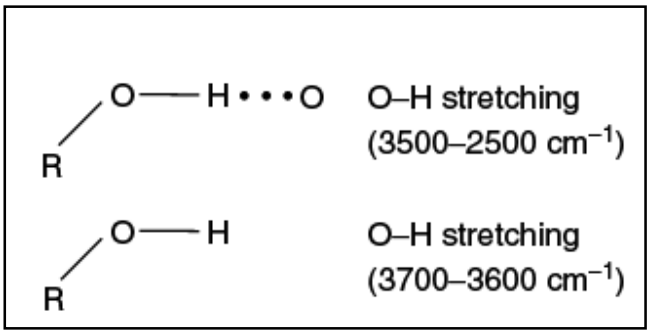

Figure 2.6: Effect of hydrogen bonding on an O–H stretching vibration (Stuart 2004).

2.3.2. Fourier transforms infrared spectroscopy (FTIR):

When a sample is exposed to infrared radiation some of this radiation will be absorbed and some will pass through the sample (transmitted). The resulting spectrum shows the molecular

absorption or transmission and creates a molecular fingerprint of the sample as shown in (Fig 2.7). No two molecular structures produce the same spectrum, and this make FTIR useful in studying several types of molecules.

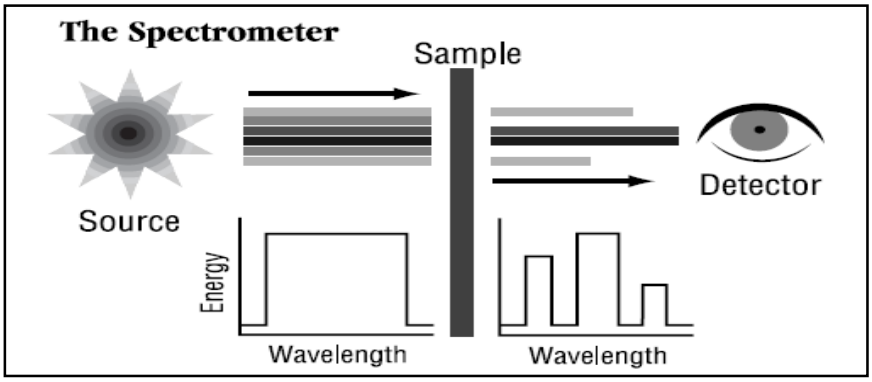

Figure 2.7: Incident and transmitted IR-radiation upon passing through a sample.

Organic molecules can absorb IR radiation between 4000 cm^{-1} and 400 cm^{-1} which corresponds to absorption of energy between 1.24meV-1.7eV. This amount of energy initiates transitions between vibrational states of bonds contained within the molecule (Buxbaum 2011).

Transitions between vibrational energy levels follow the same equation as for a classical harmonic oscillator:

$$\tilde{\nu} = \frac{1}{2\pi c}\sqrt{\frac{k}{\mu}} \quad \text{---------- (8)}$$

Where $\tilde{\nu}$: is wave number in cm^{-1}

k: is the force constant.

μ: is the reduced mass of the system, which is given by:

$$\mu = \frac{m_1 m_2}{m_1 + m_2} \quad \text{---------- (9)}$$

From the above equations it can be noticed that as the value of force constant (k) increases the vibrational frequency and so the energy will increase, and energy will decrease when the masses increase.

The design of optical pathway produce a pattern called interferogram.

FTIR uses an interferometer to process the energy that passes through the sample. In the interferometer the infrared source energy passes through a beam splitter; a mirror placed at angel 45^0 to the incoming radiation; that divides the beam into two perpendicular beams. As shown in the schematic diagram in (Fig.2.8). The deflected beam goes to a fixed mirror and is then returned to the beam splitter. The un-deflected light beam goes to a movable mirror and return back to the beam splitter, the path length of the second beam varies as a result of mirror motion. The two beams then recombine when they meet at the beam splitter forming a destructive or constructive interference as a result of path length difference between the two beams, and so the merged beams will cover a wide range of wavelengths.

For a single IR frequency, when the two arms of the interferometer are of equal length, the two split beams travel through the exact same path length and are totally in phase with each other, thus they interfere constructively and lead to a maximum in the detector response. This position of the moving mirror is called the point of zero path difference (ZPD). When the moving mirror travels in either direction by the distance (λ/4), the optical path (beamsplitter–mirror–beamsplitter) is changed by 2 (λ/4), or (λ/2). The two beams are 180° out of phase with each other, and thus interfere destructively. As the moving mirror travels another (λ/4), the optical path difference is now 2 (λ/2), or (λ). The two beams are again in phase with each other and result in another constructive interference.

When the mirror is moved at a constant velocity, the intensity of radiation reaching the detector varies in a sinusoidal manner to produce the interferogram output, the interferogram is a record of the interference signal, and it is a time domain spectrum (a plot of intensity of radiation versus time). Then a mathematical operation “Fourier Transform” will convert the interferogram to the final IR spectrum which is a frequency domain that is a plot of intensity versus frequency (Aruldhas 2007, Griffith & haseth 2007, Raaman 2006).

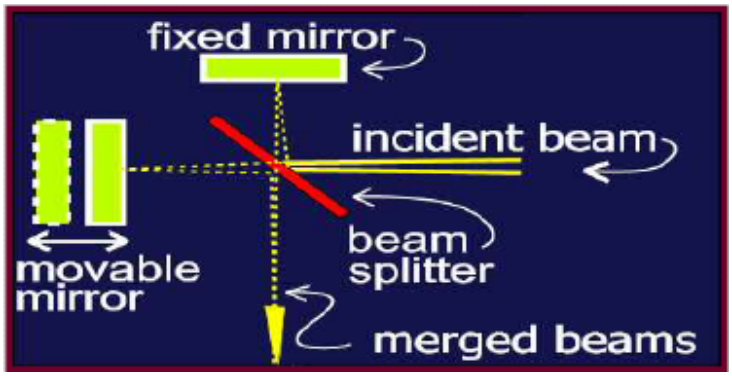

Figure 2.8: Michelson interferometer.

The Fourier transform pairs are mathematical relations used in transformation from time domain spectrum (the changes in the radiant power $f(t)$ is recorded as a function of t) into frequency domain spectrum (which records the radiant power $G(\omega)$ as a function of ω) and vice versa, these two equations are:

$$G(\omega) = \frac{1}{\sqrt{2\pi}} \int_{-\infty}^{\infty} f(t) e^{i\omega t} dt \quad \text{---------- (10)}$$

$$f(t) = \frac{1}{\sqrt{2\pi}} \int_{-\infty}^{\infty} G(\omega) e^{-i\omega t} d\omega \quad \text{---------- (11)}$$

Where ω is the natural angular frequency (Barbara Stuart 2004, G. Aruldhas 2007).

The transformed interferogram is then oriented toward the sample, the sample absorbs all the frequencies that match its natural vibrations. The remaining spectrum then reaches the detector (Pavis et al 2008, Smith 2011). The layout and components of FTIR are shown in (Fig 2.11).

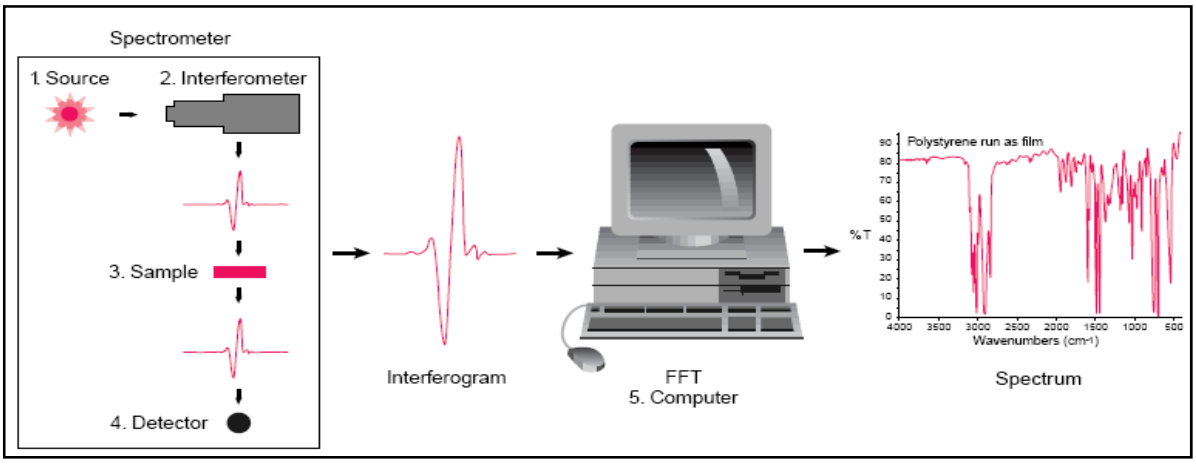

Figure 2.9: the layout and the main components of FTIR.

Amide bands:

There are nine infrared absorption bands for a polypeptide or a protein which are: amide A, B, and I-VII. The amide I and II bands are the two most prominent vibrational bands of the protein backbone. The most sensitive spectral region for the protein secondary structure is the amide I band (1700-1600 cm^{-1}), which is due almost entirely to the C=O stretching vibrations. The amide II is mainly from the in-plane NH bending vibration and from CN stretching vibrations. Other amide vibrational bands are very complex depending on the details of the force field, the nature of side chains, and hydrogen bonding. So it is rarely used in the studying of protein structure. All characteristic amide bands are shown in (Table 2.3) (Kong & Yu 2007, Smith 2011, Raaman 2006).

Table 2.3: Characteristic amide bands of peptide linkage (Kong &Yu 2007, Smith 2011).

Designation	Approximate frequency (cm^{-1})	Description
Amide A	3300	NH stretching
Amide B	3100	NH stretching
Amide I	1600–1690	C=O stretching
Amide II	1480–1575	CN stretching, NH bending
Amide III	1229–1301	CN stretching, NH bending
Amide IV	625–767	OCN bending
Amide V	640–800	Out-of-plane NH bending
Amide VI	537–606	Out-of-plane C=O bending
Amide VII	200	Skeletal torsion

In amide I region (1700-1600 cm^{-1}), molecular geometry and hydrogen bonding pattern will give rise to different C=O stretching vibration. The amide I band contour consists of overlapping component bands (α-helix, parallel β-pleated sheet, anti parallel β-pleated sheet, random coils, and β-turns).characteristic software is used to assign each component band (Kong &Yu 2007).

Deuterium oxide (D_2O) is employed in infrared studies more than water (H_2O) since water absorbs strongly in the spectral region that overlap with amide I band and therefore it can

affect the spectra, on the other hand D_2O has relatively low absorbance in the region between 1400-1800 cm^{-1}(Bai & Nussinov 2007).

Some proteins frequencies and the assigned secondary structural element in amide I band when employing H_2O or D_2O are shown in (Table 2.4)

Table 2.4: Deconvoluted amide I band frequencies and assignments to secondary structure for protein in D_2O and H_2O media (Kong &Yu 2007).

H_2O[↑]		D_2O[↕]	
Mean frequencies	Assignment	Mean frequencies	Assignment
1624±1.0	β-sheet	1624±4.0	β-sheet
1627±2.0	β-sheet		
1633±2.0	β-sheet	1631±3.0	β-sheet
1638±2.0	β-sheet	1637±3.0	β-sheet
1642±1.0	β-sheet	1641±2.0	3_{10} Helix
1648±2.0	Random	1645±4.0	Random
1656±2.0	α Helix	1653±4.0	α-Helix
1663±3.0	3_{10} Helix	1663±4.0	β-Turn
1667±1.0	β-Turn	1671±3.0	β-Turn
1675±1.0	β-Turn	1675±5.0	β-sheet
1680±2.0	β-Turn	1683±2.0	β-Turn
1685±2.0	β-Turn	1689±2.0	β-Turn
1691±2.0	β-sheet	1694±2.0	β-Turn
1696±2.0	β-sheet		

2.3.3. Ultraviolet-Visible Spectroscopy (UV-vis):

UV-Vis spectrum results from interaction between electromagnetic radiation in the UV-Vis region and molecules, the absorption of radiation in this region depends on the electronic structure of the absorbing species, when the incident photon energy matches the difference in the energy of these electronic levels (Sharma 2007).

To obtain UV-Vis Spectrum the sample is irradiated with electromagnetic radiation varied over a range of wavelengths in the UV or visible regions. A monochromatic radiation is employed at a time; the intensity of radiation absorbed at each wavelength is plotted against wavelength to obtain the spectrum.

The characteristics of UV-Vis spectrum depend on the structure and concentration of the absorbing species in solution (Kalsi 2004).

The wavelength of the radiation that will be absorbed by organic molecule is determined by the difference in energy between ground state and the various excited electronic states of the molecule. Atoms in organic molecules are bonded through σ and π bonds, and the possible transitions between them is shown in (Fig. 2.10), as a rule the transition occur from HOMO (Highest Occupied Molecular Orbital) to LUMO (Lowest Unoccupied Molecular Orbital). Of all the six transitions shown in (Fig 2.10), only the two of lowest energy ($n \rightarrow \pi^* \; and \; \pi \rightarrow \pi^*$) can be achieved with radiation available in the range 200-650 nm which corresponds to UV-vis region (Yadav 2005, Kalsi, 2004, Raaman 2006).

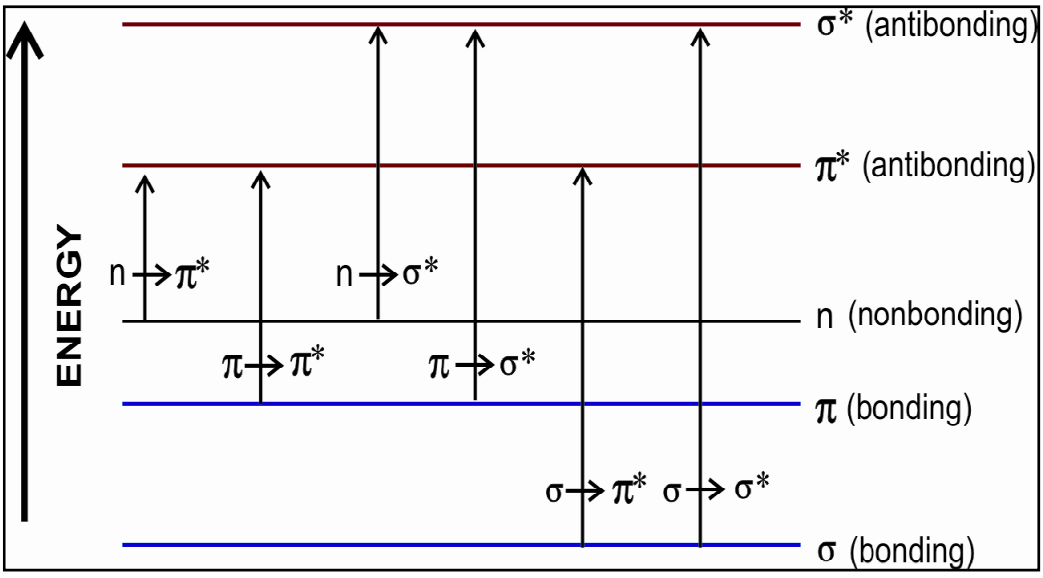

Figure 2.10: Generalized molecular orbital energy level diagram and possible transitions for organic compounds (Yadav 2005, Raaman 2006).

The $\pi \rightarrow \pi^*$ transitions are generally intense while $n \rightarrow \pi^*$ transitions are weak, so only molecules that have π bonds and atoms with non bonding electrons absorb light in the range 200-700nm and it is called chromophores. A list of some chromopheric bonds and their absorption characteristics are given in (Table 2.5), and absorption ranges for various electronic transitions are shown in (Fig 2.11) (Kalsi, 2004).

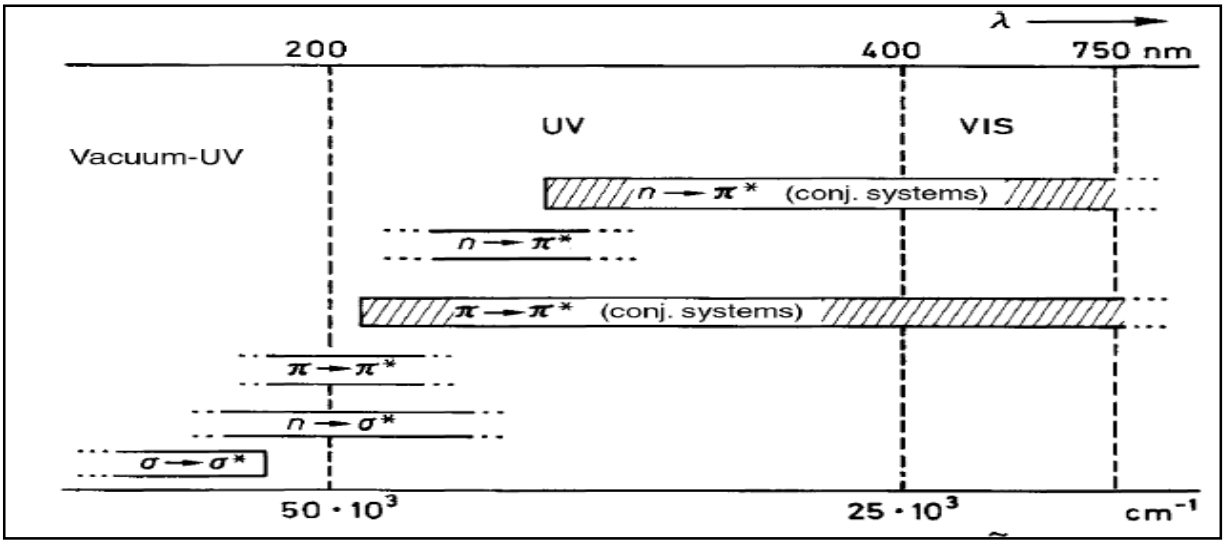

Figure 2.11: Absorption ranges for various electronic transitions.

Table 2.5: Absorption characteristics of some common chromophoric groups (Kalsi, 2004).

Chromophore	Example	λ_{max}	Type of Transition
>C = C<	C_6H_{13} CH = CH_2	177	$\pi \rightarrow \pi^*$
–C ≡ C–	C_5H_{11} C ≡ C – CH_3	178	$\pi \rightarrow \pi^*$
>C = O	CH_3CO CH_3	186 280	$n \rightarrow \sigma^*$ $n \rightarrow \pi^*$
	CH_3CHO	180 293	$n \rightarrow \sigma^*$ $n \rightarrow \pi^*$
–COOH	CH_3COOH	204	$n \rightarrow \pi^*$
$–CONH_2$	CH_3CONH_2	214	$n \rightarrow \pi^*$
–N = N–	$CH_3N = NCH_3$	339	$n \rightarrow \pi^*$
$–NO_2$	CH_3NO_2	280	$n \rightarrow \pi^*$
–N = O	C_4H_9 NO	300 665	- $n \rightarrow \pi^*$

2.3.4. Fluorescence:

Luminescence is the emission of light from atoms when it is electronically exited. It is divided into two categories fluorescence and phosphorescence.

Fluorescence:

At room temperature most of the electrons occupy the lowest vibrational level of the ground electronic state (S_0) , and when they absorb light they produce exited states, the transitions to the first and the second excited states (S_1, S_2 respectively) are shown in (Fig. 2.12) (Schulman, 1977).

When a molecule absorbs energy, it reaches a higher vibrational level of the excited state, if it maintains its spin, it is a singlet state (S) while if its spin i changed it is a triplet state (T), the excited molecule then rapidly loses its excess of vibrational energy and falls to the lowest vibrational level of the excited state. Returning from singlet state to the ground state is fast while returning from triplet state requires spin reversal and so is slower and less likely to occur. As shown in (Fig. 2.12) there are sub states associated with each singlet or triplet states they are caused by vibration and rotation of the molecule. If the energy of the sub-states of the ground state and those of the excited state overlap, direct return of the electron to the ground state is possible by internal conversion, the energy difference is converted to molecular vibration, that is, heat.

If the energy of the sub-states of the ground state and those of the excited state do not overlap, then direct returning to the ground state is impossible, instead the electron first falls to S_1 via internal conversion, and from there it returns to S_0 by emission of light as shown in (Fig. 2.12), the energy difference between S_2 and S_1 is lost as molecular vibration (heat), and thus the light emitted will have less energy and so longer wave length than that absorbed this phenomena is called fluorescence (Lakowicz 2002, Sharma 2007, Buxbaum 2011).

Fluorescence usually occurs from fluorescent substances such as aromatic molecules called fluorophores. Fluorophores are divided into two main classes: intrinsic fluorophores which occur naturally such as amino acids (aromatic amino acids Tryptophan, tyrosine, and phenylalanine), and extrinsic fluorophores which are added to the sample to provide

fluorescence when it does not exist or to change the spectral properties of the sample (Lakowicz 2006).

Phosphorescence:

Upon production of excited states by promotion of an electron into a higher orbital the direction of spin of the electrons is preserved, since most of molecules have an even number of electrons they will be arranged in pairs. However, it is possible for the spin of the promoted electron to be reversed so that it is no longer paired and the molecule has two independent electrons of the same spin in different orbitals. Quantum theory predicts that such a molecule can exist in three forms that differs slightly, but normally indistinguishable in their energy, and the molecule is said to exist in a triplet state. The indirect process of conversion from the excited state which is produced by absorption energy from singlet state to a triplet state is known as intersystem crossing (Fig. 2.12) and can occur in many substances when the lowest vibrational level of the excited singlet state, S_1, has the same energy level as an upper vibrational level of the triplet state (Sheehan 2009).

Direct transition from the ground state, usually singlet state, for a molecule with an even number of electrons, to an excited triplet state is theoretically forbidden, which means that the reverse transition from triplet to ground state will be difficult. Thus, while the transition from an excited singlet state, for example, S_1, to the ground state with the emission of fluorescence can take place easily and within 10^{-9} –10^{-6} seconds, the transition from an excited triplet state to the ground state with the emission of phosphorescence requires at least 10^{-4} seconds and may take as long as 10^{2} seconds, so phosphorescence can be defined as the transitions from the triplet state to the ground state (Sharma 2007, Lakowicz 2006).

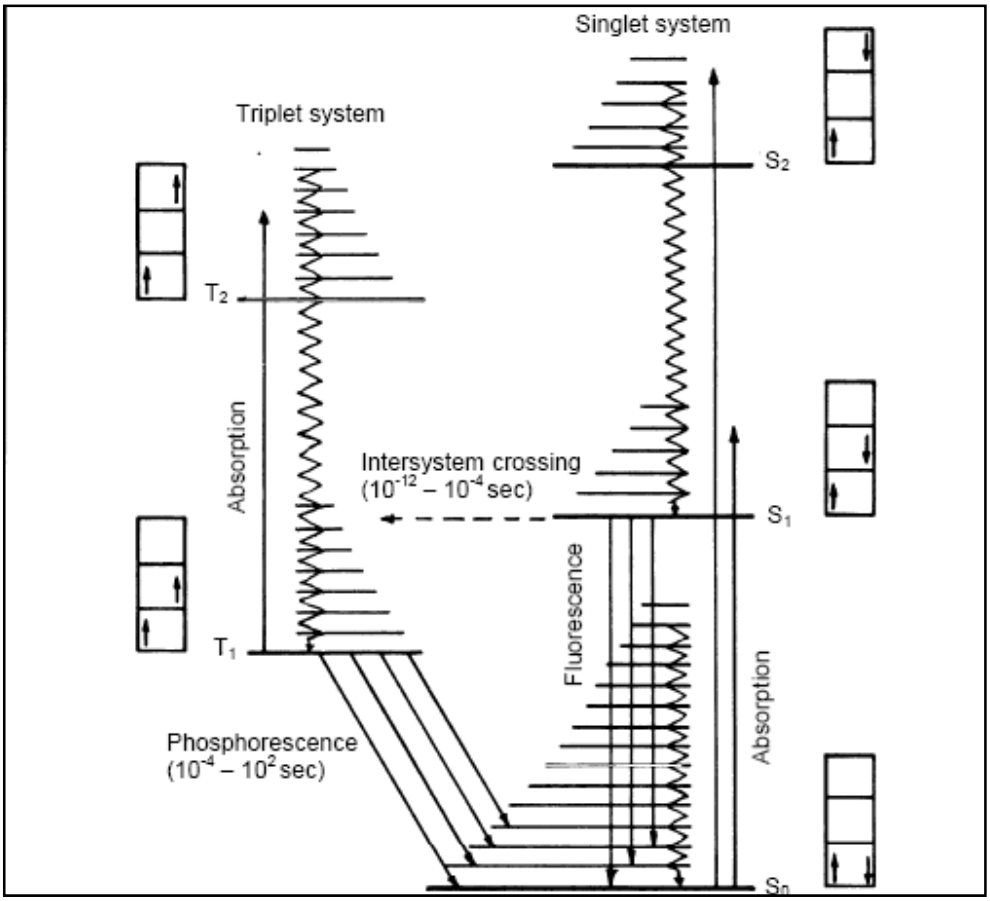

Figure 2.12: one form of Jablonski diagram shows how fluorescence and phosphorescence occur (Lakowicz 2006).

2.3.5. Quenching:

Decrease of fluorescence intensity by interaction of the excited state of the fluorophores with its surroundings is known as quenching and is relatively rare. Quenching can occur in several mechanisms, collisional quenching occurs when exited state fluorophores are deactivated upon contact with some other molecule in solution, which is called quencher (Sheehan 2009). For collisional quenching the decrease in intensity is given by Stern-Volmer equation:

$$\frac{F_0}{F} = 1 + K[l] = 1 + k_q \tau_0 [l]$$

Where K is Stern-Volmer quenching constant, k_q is biomolecular quenching constant, τ_0 is the unquenched lifetime, and l is the quencher concentration. The quenching constant K indicates the sensitivity of the fluorophores to the quencher. There are a wide variety of molecules that acts as a collisional quencher such as oxygen, halogen, amines, and electron-deficient molecules like acrylamide. Quenching mechanism differ according to fluorophores quencher pair, for instance quenching of indole by acrylamide occur as a result of electron transfer from indole to acrylamide, while quenching by halogens and heavy atoms occurs as a result of spin orbit coupling and intersystem crossing to the triplet state (Lakowicz, 2006, Sheehan 2009).

Static quenching is another type of quenching. It occur in the ground state and does not rely on diffusion or molecular collisions. It occurs as a result of complex formation in the ground state between fluorophores and quencher (Turro, 1991).

2.3.6. Atomic force microscopy (AFM):

AFM is a high resolution type of scanning probe microscopy; its resolution is in the order of fractions of nanometer. It can examine rigid surfaces either in air or in liquid (Braga & Ricci 2004).

AFM consists of a cantilever with a sharp tip used to scan the specimen surface; the tip is made of silicon or silicon nitride. It has a radius of curvature in the order of (10-20) nanometers. Forces between the sample and tip cause deflection in cantilever. This deflection can be measured using a laser spot reflected from the top surface of the cantilever, as any deflection in the cantilever will change the position of the laser spot on the photodetector that consists of two side by side photodiodes (Samori 2008, Bowen & Hilal 2009).

The amount of force between the probe and the sample is dependent on the spring constant of the cantilever and the distance between the probe and the sample surface. This force can be described by Hook's law:

$$F = -kx$$

Where k: is the spring constant and x: is the cantilever deflection (Wilson & Bullen).

2.4 PROTEINS

In this work we investigate proteins. Proteins are polymers composed of 20 different amino acids joined by peptide bonds. The structure of an amino acid contains an amino group, a carboxyl group, and R-group which is usually carbon based and gives the amino acid its specific properties. The basic structure of amino acid is shown in (Fig 2.13).

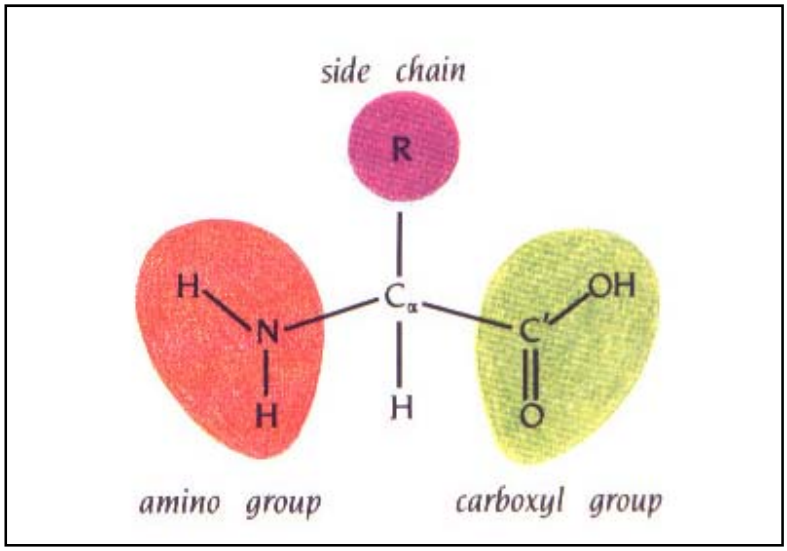

Figure 2.13: Basic amino acid structure.

Peptide bond is that bond between amino group of one amino acid and carboxyl group of the other. As a result of this reaction dipeptide is formed and a water molecule is eliminated. Peptide bond is responsible for the main chain or backbone of poly peptide chain. As an example the peptide bond between Glycine and Alanine is shown in (Fig. 2.14) (Whitford 2005).

Proteins are found in every living organism, they are responsible for a wide variety of functions, and proteins accomplish their tasks in the body by three-dimensional tertiary and quaternary interactions between various substrates

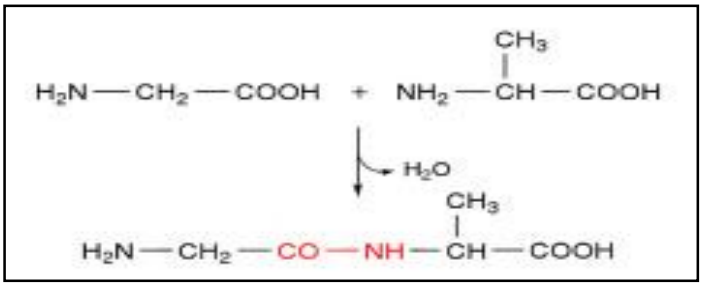

Figure 2.14: the peptide bond between Glycine and Alanine to form Glycylalanine. The peptide bond is shown on red and arrow assign to it.

2.4.1. Structural levels of protein:

There are four levels of protein structure, the primary structure which is determined by the linear sequence of amino acids in poly peptide, secondary structure can take the form of either α-helix or β-strands which is formed as a result of hydrogen interaction between N-H and C=O group in the invariant parts of amino acids in the poly peptide backbone. Elements of either α-helix, or β-sheets, or both, or loops, and unstructured elements are folded into a tertiary. A number of Tertiary structured polypeptides associate to constitute the Quaternary structure of protein. These structural levels are shown in Fig. 2.15 (Petsko & Ringe 2004).

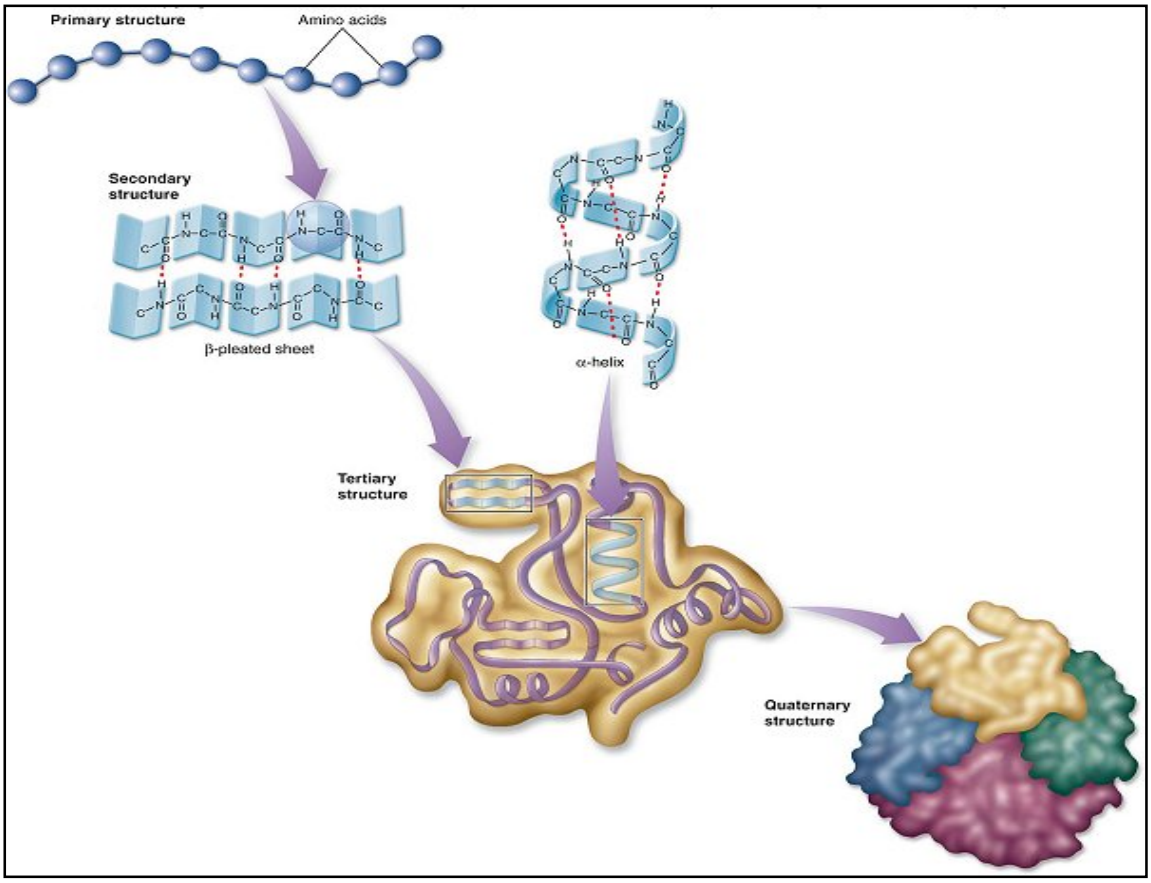

Figure 2.15: structural levels of protein.

2.4.2. Protein structural forms:

The secondary structure of a protein includes four particularly structural forms. α-helix which is formed when the amino acid backbone curls around. Alpha helix is stabilized by hydrogen bonds between the carbonyl oxygen of one amino acid and the backbone nitrogen of a second amino acid located four positions away. β-sheets consist of beta strands connected by at least two or three backbone hydrogen bonds, forming a generally twisted, pleated sheet. β-sheets have two categories, parallel, in which all carboxyl terminal end are at the same side, or anti-parallel. The other elements of secondary structure include β-turns, random coils, and unordered structure. β-turns are sharp turns that connect the adjacent strands in an anti-parallel β-sheet. Unordered structures are loops that form near the surface of protein and join other elements of secondary structure. Alpha helix and beta-sheets are shown in (Fig. 2.16) below (Fasman 1990, Petsko & Ringe 2004, Buxbaum 2007).

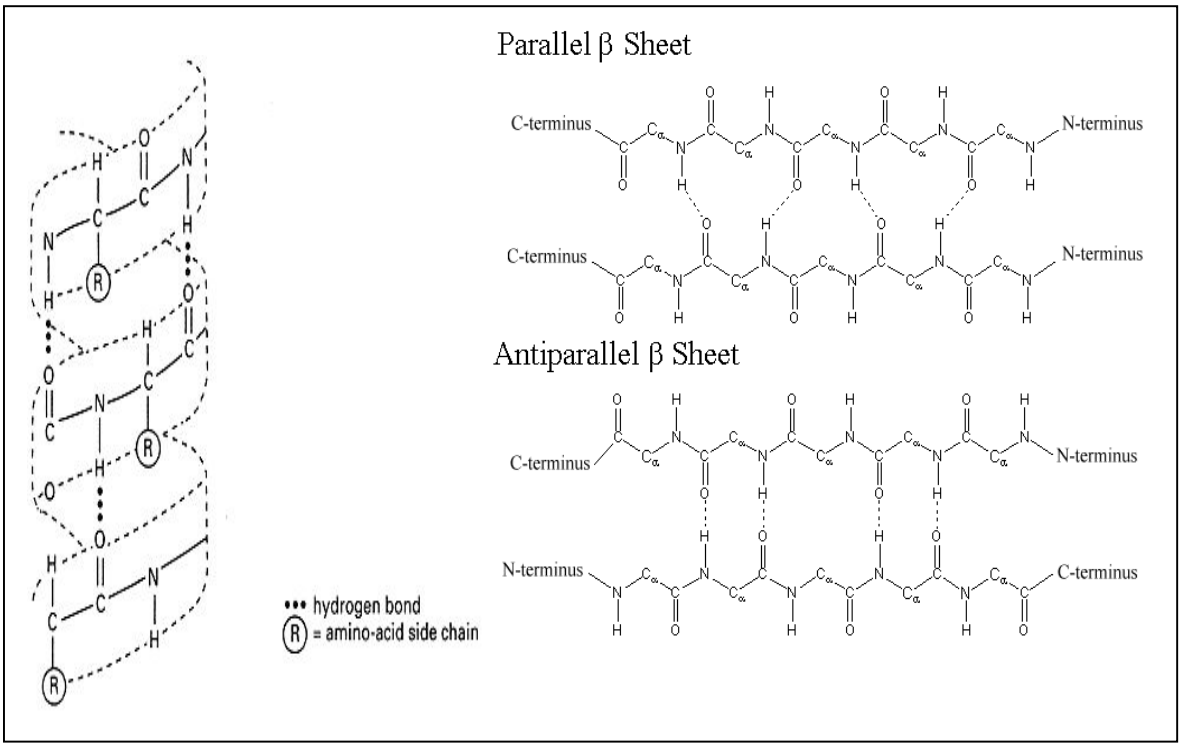

Figure 2.16: Representation of alpha helix, parallel beta sheets, and anti parallel beta sheets.

2.4.3. Protein misfolding:

Protein misfolding (or protein conformational) diseases occur when protein fail to adopt or remain in its functional form, the larger group of misfolding diseases are related to a specific peptide called Amyloid, in a process called Amyloidosis (Chiti 2006).

Amyloidosis is any pathological state associated with the formation of extracellular amyloid deposits of insoluble fibrils or plaques, which form when the normally soluble amyloid misfold and self associate in abnormal matter (Lindgren & Hammarstrom 2010). There are over 20 diseases related to Amyloidosis such as AD, Parkinson's, diabetes type II, Huntington disease, and the prion diseases. Each one of these diseases is associated with a deposition of a poly peptide that aggregates and accumulates in the tissue in an irreversible manner to form amyloid fibrils or plaques in a specific body organ (Robin et al 2010). Until now there is no effective treatment for any of the cardiovascular, systemic, or neurodegenerative amyloidosis, including AD (Wang, 2008).

2.5 Alzheimer disease (AD)

Alzheimer disease (AD), was first described by Alois Alzheimer in 1906, as a progressive neurodegenerative disorder disease characterized by multiple pathological changes in the brain, leading to memory loss (Juszczyk 2009). AD is the most known cause of dementia worldwide (Kirkitadze et al 2001). In the united states alone it affects about 4.5 million people, and the number is expected to exceed 13 million by the year 2050 (Stein et al. 2004, Collins & Dawes 2007). It affects more than 27 million people worldwide (Lee 2010). 5% of people over the age of 65 and 20% of people over the age of 80 are affected with Alzheimer disease (Collins & Dawes 2007). AD is characterized by β-amyloid aggregation and plaque formation (Walsh et al 1999, lee & Chapman 2010).

Recent reports have suggested that AD might be accelerated by aesthesia and surgeries at old and earlier ages (Carnini 2007, Bohnen 1994). A study by California Alzheimer Disease Diagnostic and Treatment Centre Program examined the different risk factors related to AD; they discovered that general anesthesia is a risk factor for AD (V. Fodale et al. 2010, Eckenhoff et al. 2004).

Hence, it is important to understand the effect of anesthetic drugs on the proteins related to AD. Different analytical techniques such as, light scattering, filtration assay, electron microscopy and nuclear magnetic resonance (NMR) spectroscopy has been used to characterize the effect of anesthetic drugs on proteins related to AD through enhancement of peptide oligomerization (Pravat et al. 2006, Eckenhoff et al. 2004).

AD is characterized by the accumulation of β-Amyloid 40/42 peptides in senile plaques and also the presence of neurofibrillary tangles inside the neurons (Cerf et al. 2009, Atassi 2006). Multiple studies have shown that in the cases of AD the levels of β-Amyloid peptide in cerebrospinal fluid are often low (Ramirez et al. 2010).

It has been found that high concentrations of Fe^{+3}, Cu^{+2}, and Zn^{+2} are found in the neurophils of AD patients and on within the core and periphery senile plaques. It has been suggested that

as a result of binding between metal ions and Aβ the kinetic energy barrier for Aβ precipitation is lowered (Lee 2010, Duce et al. 2010).

A promising alternative to the pharmacotherapy for AD is the inhibition of oligomerization using small molecules or peptides that can induce Aβ to fold into α-helix or random rather than β-sheet and so block β-Amyloid aggregation (Kumar 2011).

2.6 Propofol

Propofol (2,6-Diisopropylphenol) is a non barbiturate, sedative, hypotonic agent. Propofol is the prototype of parental anesthetics; Anesthetics are drugs that causes anesthesia (Miller & Pardo 2011). Propofol appears as a milky white solution, because it is formulated in a solution with soybean oil, glycerol and egg phospholipids (Aschenbrenner & Venable 2009, Silverstein et al. 2008). The Pka for propofol is 11 and pH is 7-8.5, its molecular weight is 178.27g/mol, and it is slightly soluble in water. It has also shown anti-oxidant activity because of the presence of phenolic hydroxyl group in its structure. The negative ionotropic effect of propofol is due to reduced myocardial intracellular calcium availability caused by Ca^{+2} influx inhabitation (Collins & Dawes 2007).

Propofol is important for maintenance of anesthesia. It is highly lipophilic drug that is rapidly distributed into vessel-rich organs. It is administrated intravenously and is distributed fast to all tissues in the body, loss of consciousness usually occurring within 40 seconds (cote, 2009). Its cumulative effect in the body is low, since it is extensively metabolized by hepatic enzymes. It has some benefits over other induction agents such that it is associated with more rapid awakening and recovery, with a less residual CNS (Central Nervous System) (Miloroet al. 2004).

Propofol is metabolized by the lever by hepatic conjugation to be later excreted by the kidneys; about 50% of the metabolic byproducts are in the form of glucuronide conjugate. The elimination half life of propofol is 0.5-1.5 hours (Curey & Garavaglia 2008). The chemical structure for propofol is shown in (Fig 2.17)

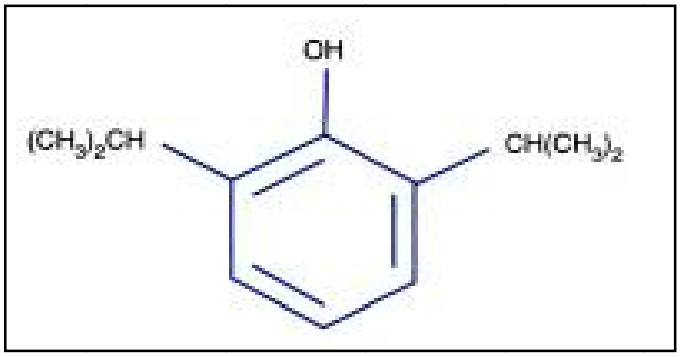

Figure 2.17: Chemical structure of Propofol (Miloro et al. 2004).

2.7 L-Arginin

L-arginine is a complex amino acid that is found in the active site of proteins and enzymes. The first discovery of L-arginine was in 1886 when it was first isolated from lupine seedlings, L-arginine is obtained from the diet although mammals can synthesize it. The main site of the net L-arginine synthesis is the kidney, accounting for about 60% of L-arginine stores. The other site of L-arginine synthesis is the liver (M. Stayton2008). L-Arginine is glycogenic and has a lot of functions, it plays a role in the synthesis innumerable proteins, and it is an intermediate in the urea cycle (Ignarro 2000, Rice & Correl 2008).

The best dietary sources of L-Arginine are meat, peanuts, soybeans, hazelnut, shrimp, eggs, and milk products, other foods containing significant amount of L-Arginine are almond, cashews, Brazil nuts, chocolate, brown rice, and corn (Stargrove 2008). The chemical structure of L-arginine is shown in (Fig 2.18).

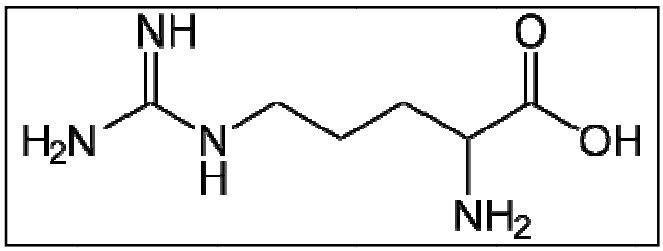

Figure 2-18: Chemical structure of Arginine (Ignarro 2000).

2.8 Beta-Amyloid (Aβ)

Aβ is a peptide of (35-43) amino acids that is generated by sequential intracellular cleavage of Amyloid Precursor Protein (APP) by β and γ secretases. APP is an oriented membrane protein of unclear function with its amino terminus within the lumen/extracellular space and its carboxyl terminus within the cytosol. APP is subjected to two principle processing pathways the amyloidogenic pathway and a non amyloidogenic one, β-Amyloid is produced during amyloidogenic pathway by consecutive action of β and γ secretases (Takahashi 2002, Lee 2010). In anti amyloidogenic pathway APP is cleaved approximately in the middle of β-Amyloid region by α-secretase, and so enhancement of α-secretase lowers the formation of amyloid plaques (Haass et al. 2012, planque 2007). "Cell biological studies have demonstrated that β-Amyloid is generated in the Endoplasmic reticulum (ER), Golgi, and endosomsl/lysosomal system" (Takahashi 2002, Haass et al. 2012).

The sequence of amino acids in Aβ(1-40) is [H-Asp-Ala-Glu-Phe-Arg-His-Asp-Ser-Gly-Tyr-Glu-Val-His-His-Gln-Lys-Leu-Val-Phe-Phe-Ala-Glu-Asp-Val-Gly-Ser-Asn-Lys-Gly-Ala-Ile-Ile-Gly-Leu-Met-Val-Gly-Gly-Val-Val-OH] (Tjernberg et al. 1998).

Studies on Aβ have been done and they have shown that due to the toxicity of Aβ, fibrillar Aβ can directly kill the neurons or initiate a series of events leading to neuronal cell death (Walsh et al. 1999).

Depending on environment, the cleavage sites, and on many other factors, these hydrophobic, unstable peptides self associate and a change in the secondary structure from α-helix and random coils to β-sheet are induced (Eckenhoff et al. 2004, Chiti 2009, Pravat et al. 2006).

β-Amyloid fibrilization passes multiple of steps as shown in (Fig. 2.19). It involves formation of dimmers then small larger soluble oligomers, which are soluble spherical aggregates of 2-20nm. Oligomers formation is followed by protofibrills formation leading to insoluble fibrils and consequently forming β-Amyloid plaques or deposits (Kumar 2011, Walsh et al.1999,

Vetri 2010, Jimenez 2005). Amyloid fibrils tend to be long (> 1μm), thin (10-20 nm) straight and unbranching (Krebs et al. 2005).

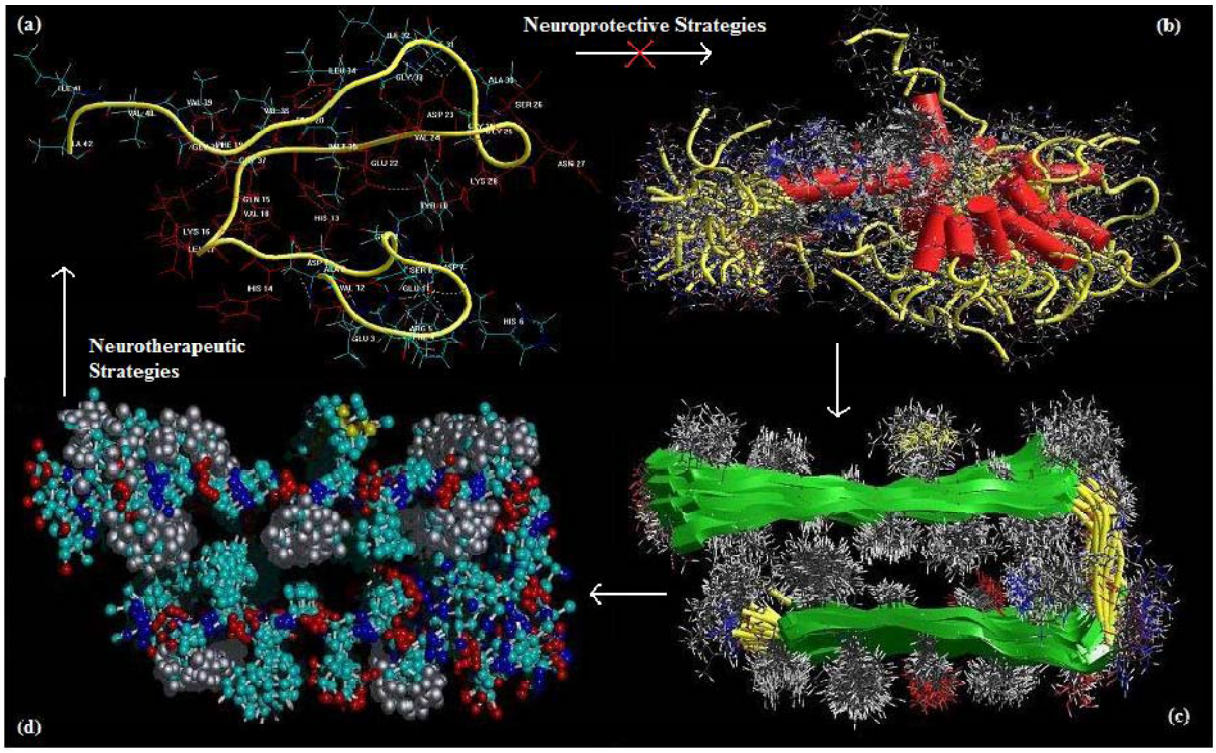

Figure 2.19: self assembly of β-Amyloid protein (a) amyloid-β protein oligomer, (b) proto-fibril, (c) fibril, and (d) plaque deposit (Kumar et al. 2011).

It has been proven through studying the β-amyloid conformation during protofibrill and fibril assembly that during the conversion of unstructured, unassembled β-Amyloid into β-sheet rich fibril as a transition mode an increase in α-helix content occurs (Kirkitadze et al. 2001, Juszczyk 2009, Cerf et al. 2009, Wang 2008). Because of amyloid fibrils noncrystallinity and insolubility it was difficult to obtain high resolution fibril structure, so neither the assembly mechanism nor the atomic structure of the amyloid fibrils are known, but some few general principles that governs protein aggregation have been suggested (Thirumalai et al. 2003).

It has been revealed that FTIR can be used to study the aggregation properties of Aβ peptides, and the effect of environmental variables on aggregation. Investigations have shown that Aβ peptides are weakly soluble in physiological conditions, and the conformation of these peptides in a solution is highly dependent on the solvent itself, Ph, temperature, pressure, and the presence of co-solvent (Szabo et al.1999, Lee 2010, Chiti & Dobson 2009, planque 2007).

It is now widely accepted that soluble oligomers of Aβ are more neurotoxic and play a role in amyloid pathogenesis than Aβ fibrils (Cerf et al. 2009, Vetri, 2010, Wang 2008).

It has been discovered that Aβ (1-42) and Aβ (1-40) are the two major components of Amyloid plaques (Cerf et al. 2009, Atassi 2006, planque 2007, Lin 2003). NMR studies have shown that monomers of Aβ(1-40) and Aβ(1-42) have no α-helical or β-sheet structure, and they exist as random extended chains (Atassi 2006).

Chapter three:

Experimental part

In this chapter experimental procedure has been discussed in details including sample preparation for FTIR, UV-vis spectroscopy, fluorescence spectroscopy, and AFM. The instrumentation of Fluorospectrometer (NanoDrop 3300), UV-vis spectrometer (NanoDrop 1000), Bruker IFS 66/S, and Micro cantilever, OLYMPUS spectrometer has been discussed briefly. The experimental procedure followed in this research has been explained.

3.1 SAMPLES PREPARATION

In this study Aβ (1-40) have been used in powder form. It has a molecular weight of about (4329.82 AMU), with the chemical formula ($C_{194}H_{295}N_{53}O_{58}S$), and propofol (2, 6-Diisopropylphenol) in solution form with a chemical formula ($C_{12}H_{18}O$) and a molecular weight (178.3 g/mol). As for L-arginine in powder form with chemical formula ($C_6H_{14}N_4O_2$) and a molecular weight (174.2 g/mol), and phosphate buffer saline were used to prepare all the samples. All above chemicals were purchased from Sigma Aldrich Company and used without further purification. Optical grade silicon windows (NICODOM Ltd) were used as spectroscopic cell windows. These windows were purchased from Sigma Aldrich Company.

FTIR measurements were carried out using several samples in the form of thin films of Aβ, Aβ-propofol, and Aβ-L-arginine solutions. UV-vis and fluorescence measurements were done using the liquid samples of the mentioned solutions.

3.1.1. Stock solutions:

Beta-Amyloid stock solution:

0.5 mg of Aβ (1-40) was dissolved in 250 µl of triple distilled water to yield a concentration of 0.462 mM.

Propofol stock solutions:

The density of propofol is 962 gL^{-1}, the molarity of propofol solution was found to be 5.396M. This solution was used to prepare different solutions with these concentrations of propofol (3.82, 2.88, 1.92, 1.44, 0.96, and 0.72 mM) using phosphate buffer saline (PBS) (pH 7.4) and depending on the molarity dilution equation ($M_iV_i = M_fV_f$).

PBS pH 7.4 was directly prepared by dissolving one foil pouch in one liter double distilled water.

L-Arginine stock solutions:

1.338 mg of L-arginine was dissolved in 2 ml of PBS to prepare 3.84mM arginine stock solution. Different concentrations of L-arginine (3.84, 2.88, 1.92, 1.44, 0.96, 0.72, and 0.48 mM) were prepared in PBS solution using molarity dilution equation.

3.1.2. Aβ-ligand solutions:

The final concentration of Aβ-propofol solution were prepared by mixing equal volumes of Aβ and propofol stock solutions. Aβ concentration in all samples will be 0.231mM, and the propofol concentrations in the final protein-drug solution are (1.92, 1.44, 0.96, 0.72, 0.48, 0.36, and.0.24mM).

The final concentrations of Aβ-arginine samples were prepared by mixing equal volumes of Aβ and L-arginine stock solutions. Aβ concentration in all samples will be 0.231mM, and the arginine concentrations in the final protein-drug solution are (1.92, 1.44, 0.96, 0.72, 0.48, 0.36, and.0.24mM).

3.1.3. Thin films preparation:

After cleaning silicon windows very well, 40 μL of each sample were applied on a certain area on the silicon window plate and left to dry at room temperature inside the incubator for 24 hours. The dehydrated films are prepared with the desired concentration of propofol and L-arginine while keeping the concentration of Aβ constant in all of them.

For background measurement, a clean silicon window has been kept in the same incubator together with the rest of samples, in order to have all samples in the same environment.

3.2 Instruments

The following instruments are used in taking the required measurements:

3.2.1. Fluorospectrometer:

Fluorescence measurements had been done using Flourospectrometer (NanoDrop ND-3300) at 25^0C.

The excitation source comes from one of three solid-state light emitting diodes (LED's), which are oriented 90° to the detector. A 2048-element CCD array detector, covering 400 – 750 nm, is connected by an optical fiber to the optical measurement surface. The spectrometer is configured with a cut filter to eliminate light transmission below 395 nm.

A 1-2 µl sample is pipette onto the end of the lower measurement pedestal (the receiving fiber). A non-reflective "bushing" attached to the arm is then brought into contact with the liquid sample causing the liquid to bridge the gap between it and the receiving fiber. The gap, or path length, is controlled to 1mm. Following excitation with one of the three LEDs, emitted light from the sample passing through the receiving fiber is captured by the spectrometer. The NanoDrop 3300 is controlled by software run from a PC. The image below lists some of common fluorophores that can be measured using the NanoDrop 3300 along with the most appropriate excitation LED.

The excitation source option includes the UV-LED with maximum excitation at 365nm, the blue-LED with maximum excitation at 470nm, and the white-LED in the range 500-650nm.

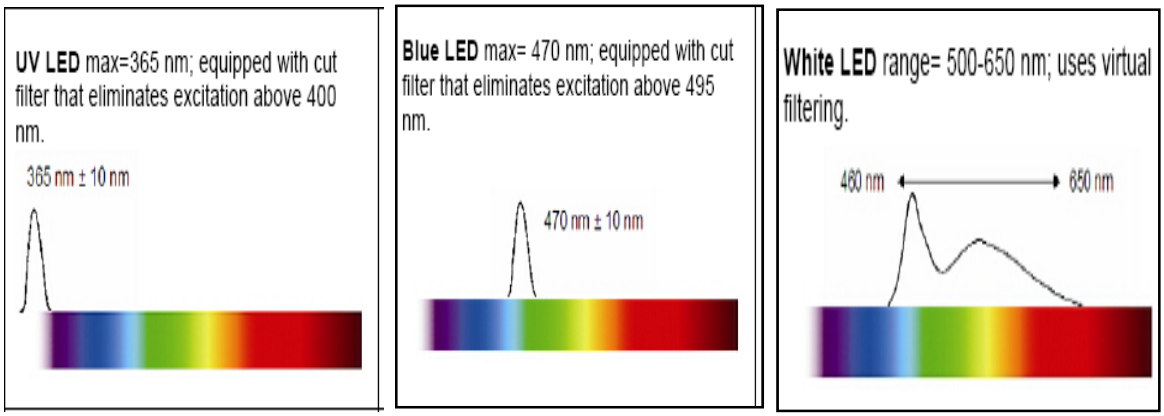

Figure 3.1:Excitation LEDs.

3.2.2. UV-VIS spectrophotometer:

The Thermo Scientific NanoDrop 1000 Spectrophotometer measures 1 µl samples with high accuracy and reproducibility. The full spectrum (220nm-750nm) spectrophotometer utilizes sample retention technology that employs surface tension alone to hold the sample in place. This eliminates the need for cumbersome cuvettes and other sample containment devices and allows for clean up in seconds. In addition, the NanoDrop 1000 Spectrophotometer has the capability to measure highly concentrated samples without dilution (50X higher concentration than the samples measured by a standard cuvette spectrophotometer).

The sample is pipette at the end of a fiber optic cable, and then a second fiber optic cable is brought in contact with the sample causing the liquid to bridge the gap between the fiber optic ends which is controlled between 1-0.2mm. A pulsed xenon flash lamp provides the light source that pass through the sample. The excitation is made at 210nm and emission occurs at 280nm.

The sample size is not critical but the liquid column must be formed so that the gap between the upper and lower pedestals is bridged with the sample.

3.2.3. Fourier Transform Infrared Spectroscopy (FTIR):

The FTIR measurements were obtained on Bruker IFS 66/S spectrophotometer, equipped with liquid nitrogen –cooled MCT detector and a KBr beam splitter the spectrometer was continuously purged with dry air during measurement. The absorption spectrums in the mid infrared region (4000-400 cm^{-1}) were taken and measured.
Because of the need to a relative scale for the absorption intensity, a background spectrum must also be measured. This is normally a measurement with no sample in the beam.

The two most popular detectors for a FTIR spectrometer are deuterated triglycine sulfate (DTGS) which is a pyroelectric detector that delivers rapid responses because it measures the changes in temperature rather than the value of temperature, and "our detector" mercury cadmium telluride (MCT) which is a photon (or quantum) detector that depends on the quantum nature of radiation and also exhibits very fast responses. It must be maintained at liquid nitrogen temperature (77 °K) to be effective. Generally MCT detectors are faster more sensitive than DTGS detectors.

3.2.4. Atomic force microscopy (AFM):

Images for the surface of the samples have been taken using (Olympus, tips). The motion of the probe across the surface is controlled using feedback loop or piezoelectronic scanners. A semiconductor diode laser is bounced off the back of the cantilever onto a position suitable for photodiode detector. This detector measures the bending of the cantilever while the tip is scanning over the sample. The measured deflections are then used to generate a map for the surface topography (Wilson & Bullen).

Other equipments were used in sample preparation and making measurements such as Digital balance, vortex, incubator, plate stirr, micropipettes, volumetric flask, beakers, and test tubes.

3.3 Experimental Procedures

3.3.1. Fluorospectrometer procedure:

The prepared liquid samples of Aβ free, Aβ-propofol and Aβ-L-arginine solutions were used to make the fluorescence Measurements in the following steps:

With the sampling arm open, pipette the sample onto the lower measurement pedestal.

Close the sampling arm and initiate a measurement using the operating software on the PC. The sample column is automatically drawn between the upper bushing and the lower measurement pedestal and the measurement is made.

When the measurement is complete, open the sampling arm and blot the sample from both the upper bushing and the lower pedestal using low lint laboratory wipe to prevent sample carryover and avoid residue buildup

3.3.2. UV-VIS spectrometer (ND-1000):

The same samples used in UV-vis measurements were used following these steps:
With the sampling arm open, pipette the sample onto the lower measurement pedestal.

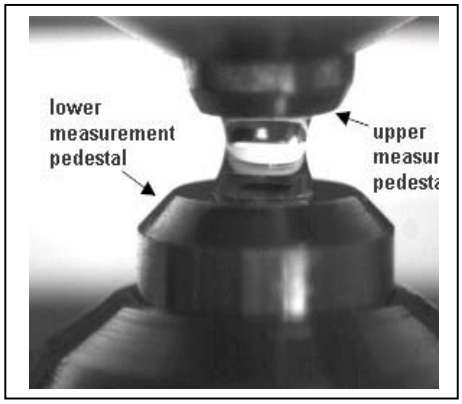

Close the sampling arm and initiate a spectral measurement using the operating software on the PC. The sample column is automatically drawn between the upper and lower measurement pedestals and the spectral measurement made.

When the measurement is complete, open the sampling arm and wipe the sample from both the upper and lower pedestals using a soft laboratory wipe. Simple wiping prevents sample carryover in successive measurements.

When the NanoDrop ND-1000 and NanoDrop ND-3300 spectrophotometers are blanked, a spectrum is taken for the reference material, and stored in computer memory as an array of light intensities by wavelength. When a measurement of a sample is taken the intensity of light that has been transmitted through the sample is recorded, and then the sample intensity with the blank intensity was used to calculate the sample absorbance according to the following equation:

$$\textbf{Absorbance} = A = -\log\left(\frac{\textbf{Intensity}_{\textbf{sample}}}{\textbf{Intensity}_{\textbf{blank}}}\right)$$

Both the intensity of the blank and of the sample is needed to give the absorbance at a given wavelength.

3.3.3. Fourier Transform infrared (FTIR) spectroscopy:

The nitrogen gas cylinder is switched on by turning the switch on the top of the cylinder anti-clockwise. When the gas reaches the mirror then a green led will start flashing at the base of

the spectrometer. Liquid nitrogen must be employed inside the instrument and the prepared samples then can be delivered starting with the background sample.

Each measurement is taken at a resolution of 4 cm^{-1} and an average 60 scans to increase signal to noise ratio, the aperture used in this study was 8mm, since it has been founded that this aperture gives best signal to noise ratio. Many manipulation techniques have been performed on all the spectra by OPUS software (Optic User Software) such as baseline correction, normalization, and peak areas calculations. The peak positions were determined using second derivative of the spectra.

For temperature dependence study Aβ-drug complexes on silicon windows were placed into an infrared cell window. The temperature of the cell was controlled by an external water path and was increased gradually from 20^0C to 80^0C at 3^0C per 5 minutes scan rate.

Peak positions were determined using second derivative at 9 smoothing points by OPUS software, calculation of areas under the different curves were performed using Fourier self deconvolution (FSD) techniques by OPUS software.

The advantages of the FTIR instrument is the high speed and sensitivity, as it acquire the interferogram in less than a second. Modern FTIR spectrometers have a powerful computerized data system, as it can perform many data processing tasks (Jilie Kong, 2007), a brief explanation of these tasks is given below:

1. Baseline correction:
   The offset correction is performed by selecting a single point of multiple points on a spectrum and adding to them or subtract a y-value to correct the baseline offset. This processing step is used to bring the minimum point to zero, or to align the baseline of two or more spectra causing them to overlap.

2. Derivatives:
   Derivatives are used to remove offset and slope due to background differences. In our study we have used second derivative to determine the positions of peaks for Aβ-free, Aβ-Propofol complexes, and Aβ-L-arginine complexes.

3. Fourier self deconvolution:

   It is the band narrowing technique that is most widely used in infrared spectroscopy of biological material. The aim of FSD is to enhance the apparent resolution of a spectrum, or to decrease the line width. So the broad and overlapping lines of spectrum can be separated into sharp single lines.

   The deconvolution correspond to a multiplication of the interferogram I(x) using the exp^{ax} deconvolution function for Lorentzian and exp^{ax^2} for Gaussian shapes, which will intensifies the interferogram edges.

   The deconvolution factor is the maximum value of these functions at the end of the interferogram, deconvolution factors of 100, 1000, and 5000 correspond to a maximum amplification of 3.4, 12.8, and 40 in the case of Lorentzian shape, and 1.06, 3.2, and 16 in the case of Gaussian shapes. If you work with Lorentzian shapes it is recommended to increase the deconvolution factor in the order of 50, 100, 1000, 5000, and to stop if the resultant spectrum shows artificial oscillations (Bruker, 2004). Successful application of FSD will enhance peak separation on overlapping absorption bands. The application of FSD on amide I, and amide II regions is a key step in the determination of proteins secondary structure, conformational changes, structural dynamics and stability studies of proteins. (Jilie Kong 2007)

4. Curve fitting:

   The curve fitting command allows calculating single components in a system of overlapping bands, a model that consists of an estimated number of bands. A baseline should be generated before the fitting calculation is started. The model can be set up interactively on the display and is optimized during the calculation (Brucker, 2004).

3.3.4. Atomic force microscopy:

AFM is used to give high resolution picture for Aβ-free, Aβ-propofol , and Aβ-L-arginine solutions. 10 µl of the liquid Aβ-drug solution after washing with water to remove un-adsorbed material was placed on a certain area of a freshly cleaved mica substrate and left to

dry at room temperature. Aβ free, Aβ-propofol, and Aβ-L-arginine solutions were characterized by AFM equipped with 4x4μm^2 piezoelectric scanner. Analysis was carried out using tapping mode at room temperature using AFM cantilevers with a spring constant 2N/m (Micro cantilever, OLYMPUS). All scanned images were analyzed using WSxM 5.0 Develop 3.2 software.

Chapter Four

Results and discussion

The experimental results are presented as follows: the first section deals with UV-absorption spectroscopy. The second section discusses fluorescence spectroscopy results. The third section discusses Fourier transform infrared spectroscopy results. In the last section AFM images for Aβ free and Aβ-propofol complexes and Aβ-L-arginine complexes will be shown.

4.1 UV-absorption spectroscopy

UV-absorption spectroscopy was used to determine the binding constants between Aβ and a drug (propofol or arginine). The strength of interaction between Aβ and drugs is dependent on the binding constant which can be calculated using graphical analysis of the absorbance spectrum.

The absorption spectra for Aβ-propofol and Aβ- L-arginine complexes with different concentrations of propofol and L-arginine were recorded and shown in (Fig 4.1, and 4.2 respectively). The excitation has been done at 210 nm, while the absorption is recorded at 280 nm. The UV absorbance intensity of Aβ has increased with increasing propofol concentration, while it has decreased with increasing L-arginine concentration. The change in the absorbance intensity of Aβ with increasing drug concentration is an indication that an interaction has occurred between Aβ and propofol and L-arginine.

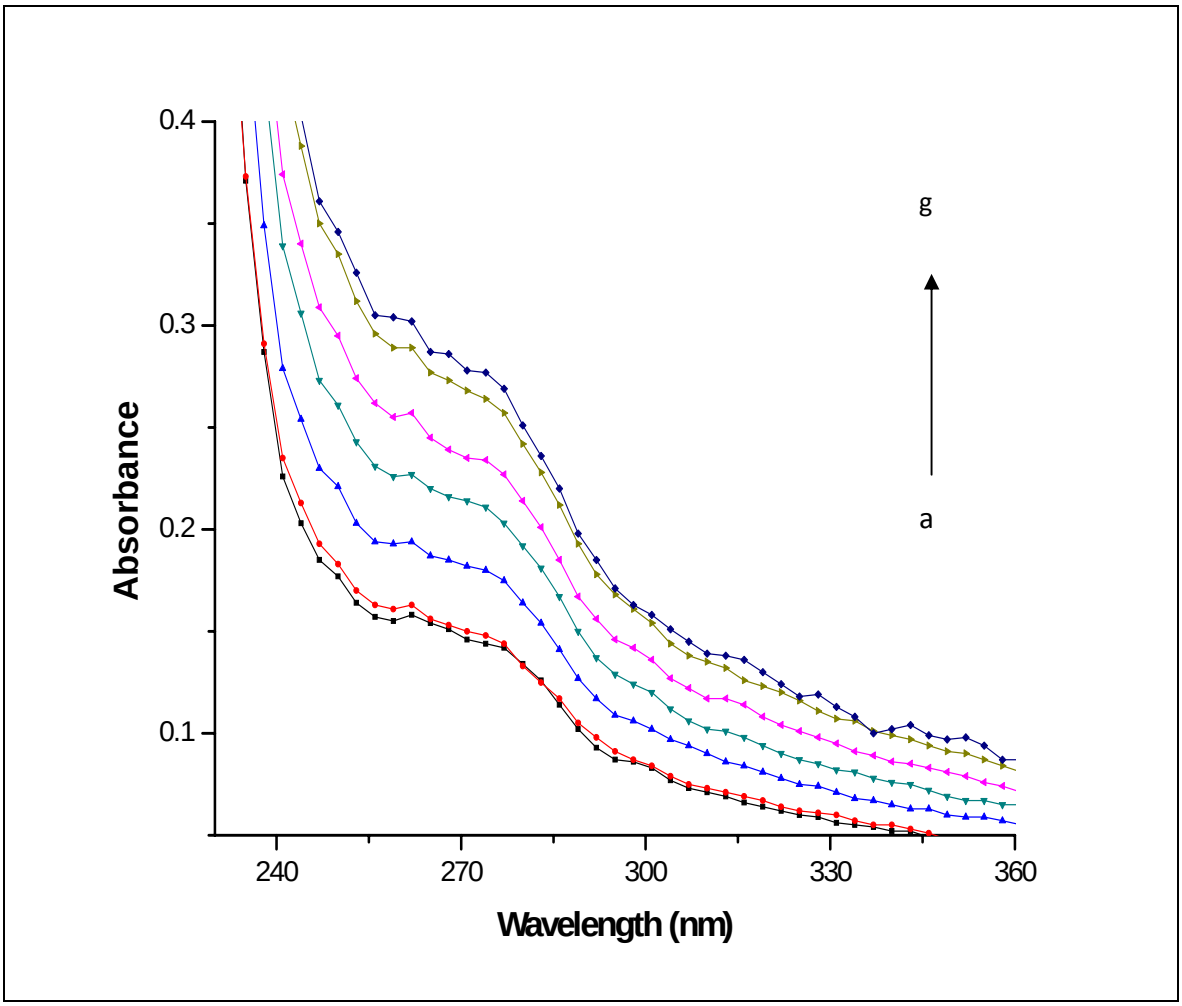

Figure 4.1: UV absorbance spectra of Aβ-propofol complexes at different propofol concentrations (a: 0.0mM, b: 0.36mM, c: 0.48mM, d: 0.72mM, e: 0.96mM, f:1.44mM, and g: 1.92mM)

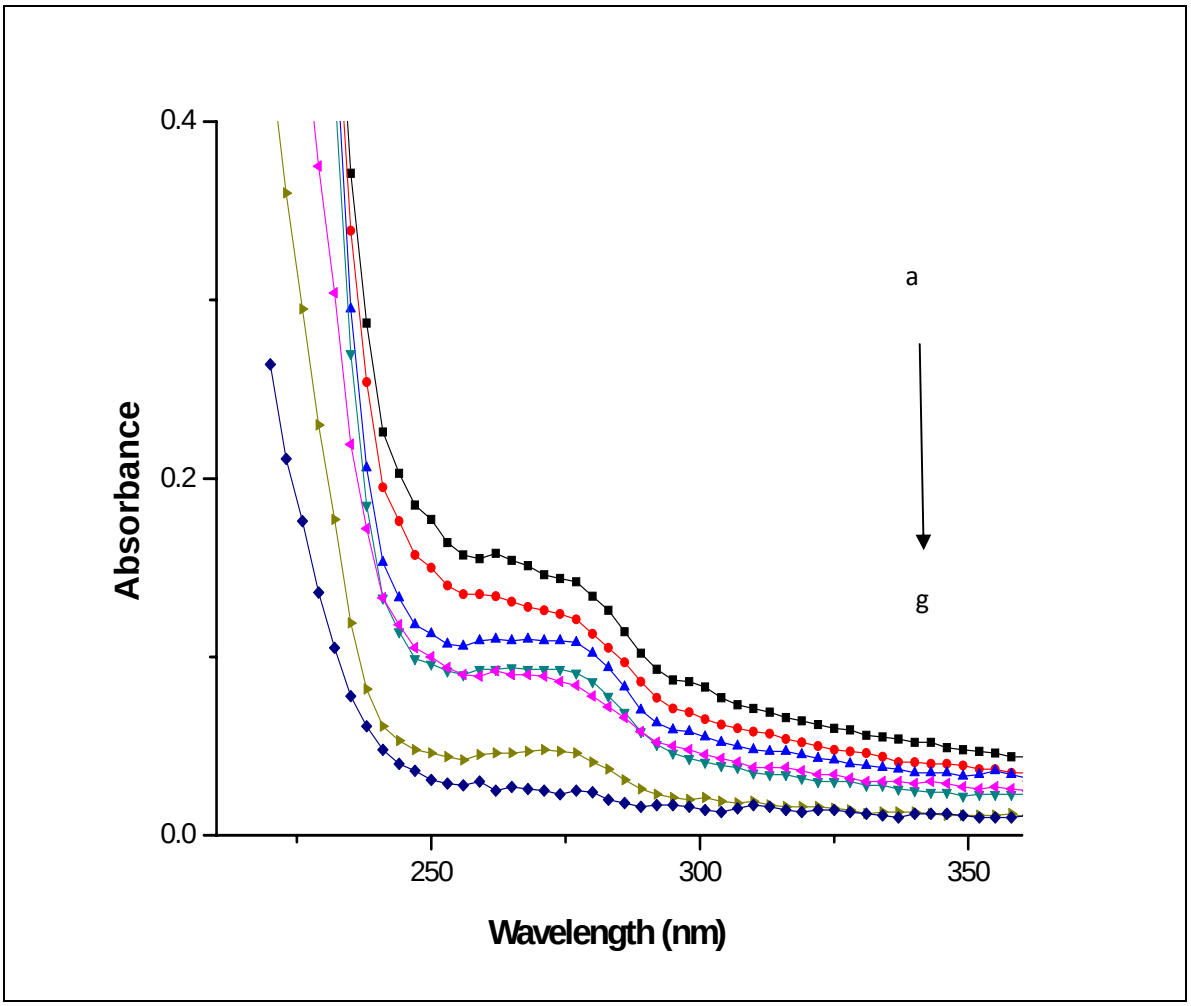

Figure 4.2: UV absorbance spectra of Aβ-L-arginine complexes at different L-arginine concentrations (a: 0.0mM, b: 0.36mM, c: 0.48mM, d: 0.72mM, e: 0.96mM, f: 1.44mM, and g: 1.92mM)

4.1.1. Determination of binding constants (K) by UV absorption spectroscopy:

To determine the binding constant (k) by UV-Vis. spectroscopy a plot of $\frac{1}{A-A_0}$ vs $\frac{1}{L}$ is made. This plot indicates a linear relation and the binding constant (k) is found by taking the ratio of the intercept to the slope, which can be seen clearly from the following equation (Darwish et al. 2012).

$$\frac{1}{(A-A_0)} = \frac{1}{(A_{\infty}-A_0)} + \frac{1}{K(A_{\infty}-A_0)}\frac{1}{L}$$

Where A_0 corresponds to the absorption of protein at 280nm in the absence of a ligand, while A_{∞} is the final absorption of protein after it binds to the ligand, and A is the recorded absorption at the different concentrations of the ligand (L), the ligand in our case is either propofol or L-arginine.

A plot of $\frac{1}{A-A_0}$ vs. $\frac{1}{L}$ for different concentrations of propofol in Aβ-propofol complexes is shown in (Fig. 4.3), and for different concentrations of L-arginine in Aβ-L-arginine complexes is shown in (Fig. 4.4).

The binding constant for Aβ-propofol is calculated to be 2.13×10^2 M^{-1}, and for Aβ-L-arginine complexes is calculated to be $0.35 \times 10^2 M^{-1}$. The binding constant for Aβ-L-arginine is lower than that of Aβ-propofol. Drugs with low binding constants are shown to be more effective in binding with protein (Bhattacharya et al 2000).

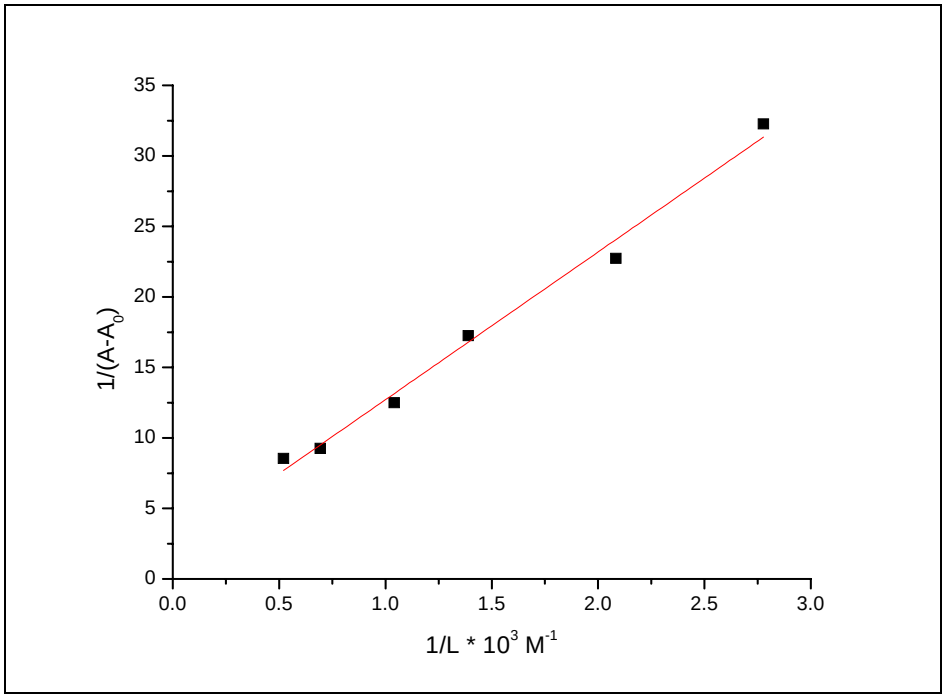

Figure 4.3: the plot of $\frac{1}{A-A_0}$ vs $\frac{1}{L}$ for Aβ with different concentrations of propofol.

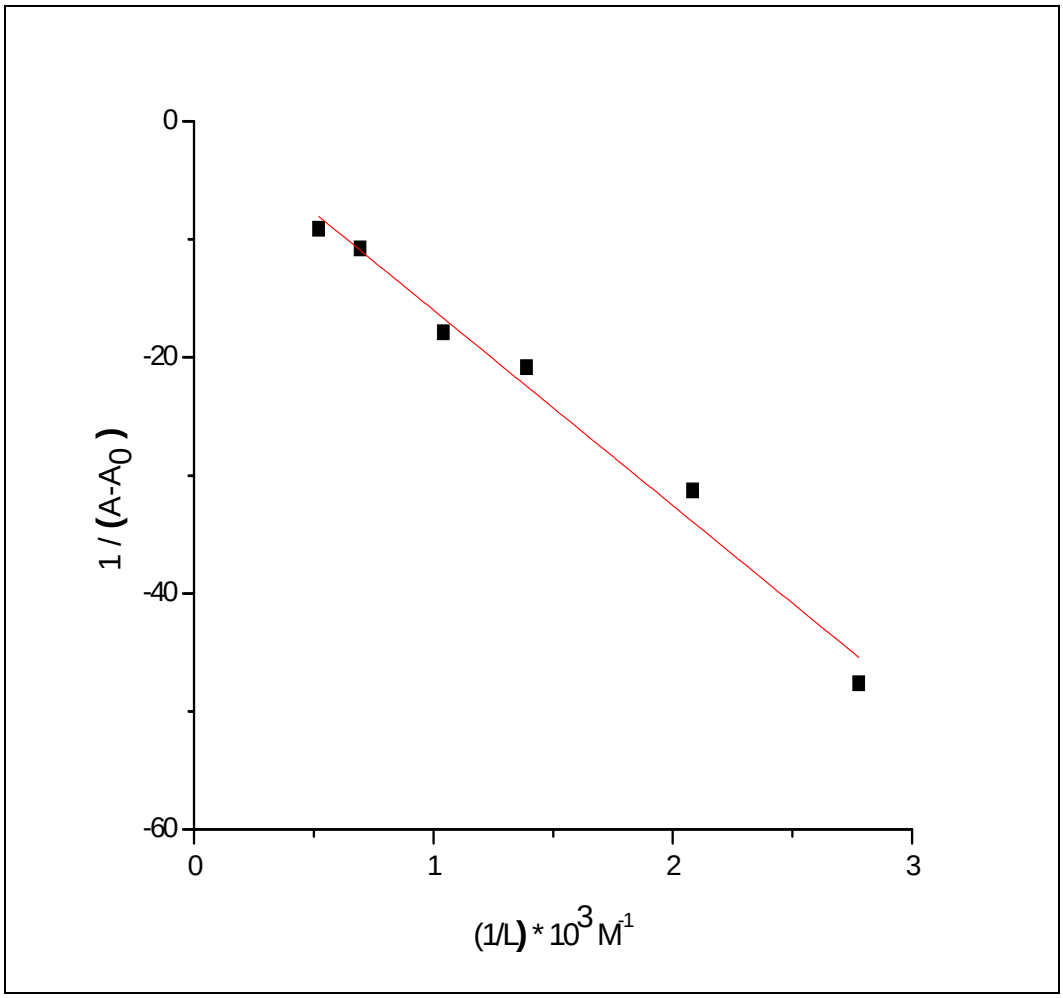

Figure 4.4: the plot of $\frac{1}{A-A_0}$ vs $\frac{1}{L}$ for Aβ with different concentrations of L-arginine.

4.2 Fluorescence spectroscopy

Fluorescence spectroscopy is another technique that is used widely to study binding between protein and ligand. In Aβ(1-40) intrinsic fluorescence is mainly due to tyrosine (tyr) residue, since no tryptophan (Try) is found in the structure of Aβ(1-40) and phenylalanine (Phe) has very low quantum yield (Sarroukh et al. 2011, Amaro et al. 2013).

Various molecular interactions can decrease the fluorescence intensity of a compound such as molecular rearrangements, exited state reactions, energy transfer, ground state complex formation, and collisional quenching (Turro 1991, Sheehan 2009). The excitation is done on 350 nm and emission occurs at 431 nm.

The fluorescence emission spectra of Aβ with various concentrations of propofol (0.24, 0.36, 0.48, 0.96, 1.44, and 1.92 mM) are shown in (Fig 4.5).The emission fluorescence spectra of Aβ with various L-arginine concentrations (0.24, 0.36, 0.48, 0.96, 1.44, and 1.92 mM) are shown in (Fig 4.6).

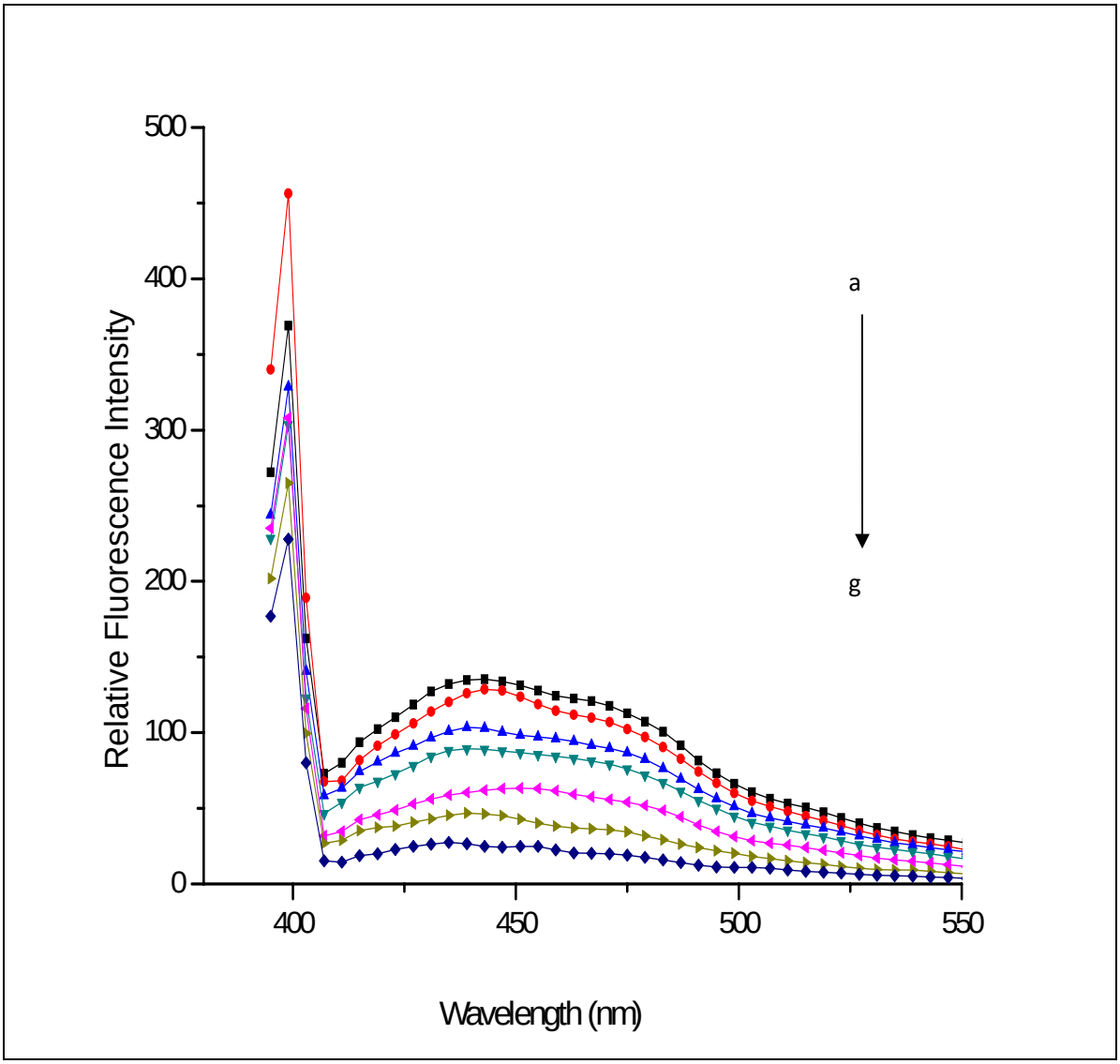

Figure 4.5: The fluorescence emission spectra of Aβ with various concentrations of propofol (a= 0.0, b=0.24, c= 0.36, d= 0.48, e= 0.96, f= 1.44, and g=1.92 mM)

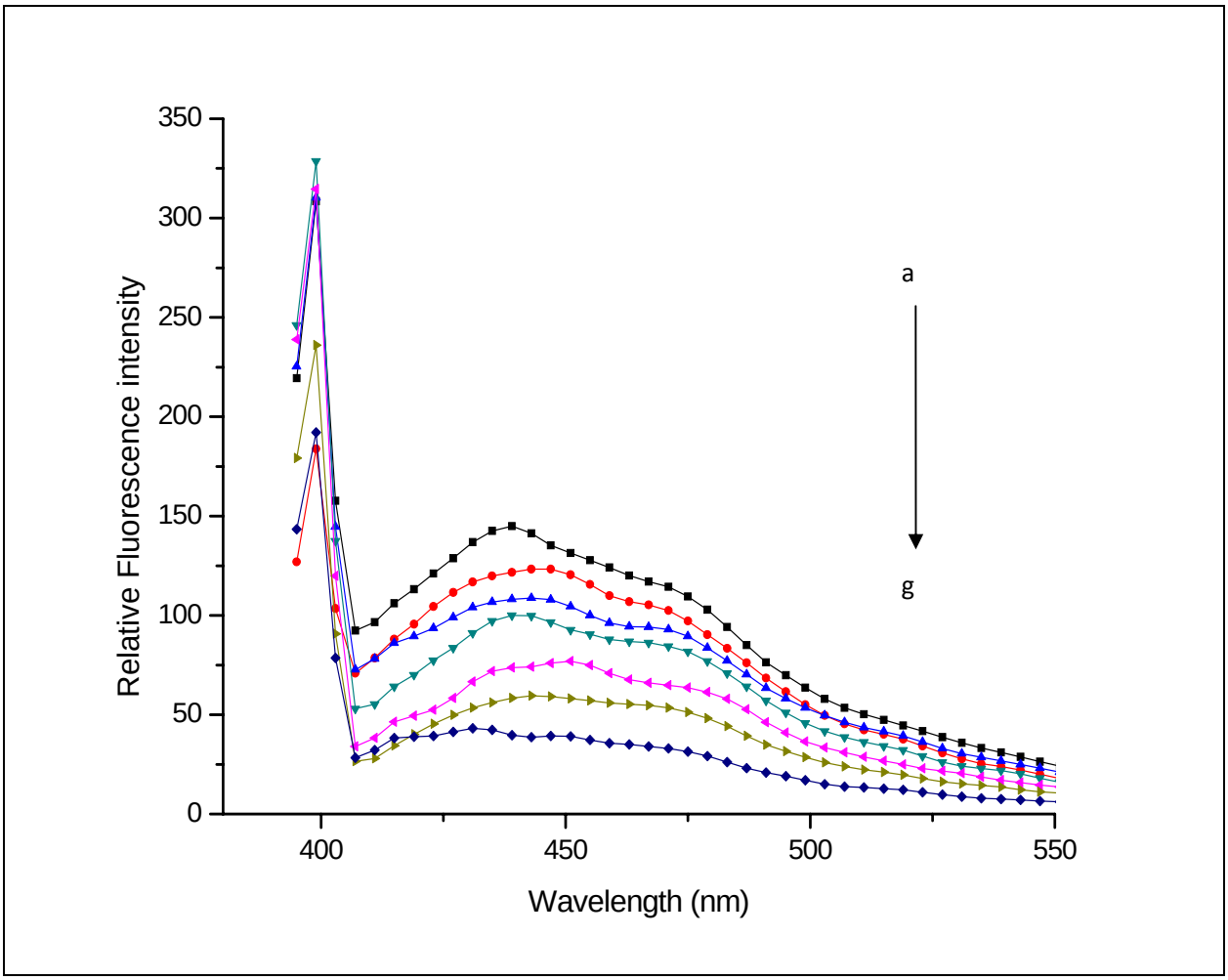

Figure 4.6: The fluorescence emission spectra of Aβ with various concentrations of L-arginine (a=0.0, b=0.24, c=0.36, d=0.72, e=0.96, f=1.44, and g=1.92 mM)

4.2.1. Determination of Stern-Volmer quenching constants (Ksv) and the quenching rate constant (Kq):

Fluorescence quenching can be induced by different mechanisms that were usually classified into static quenching and dynamic quenching. Dynamic quenching arises from collisional encounters between the fluorophores and quenchers while static quenching results from the formation of a ground state complex between the fluorophores and the quenchers (Turro 1991).

For dynamic quenching, the decrease in fluorescence intensity is described by Stern-Volmer equation (Lakowicz 2006, Sheehan 2009).

$$\frac{F_0}{F} = 1 + K_{sv}[L] = 1 + k_q\tau_0[L]$$

Where F and F_0 are the fluorescence intensities with and without quencher, k_q is the quenching rate constant, K_{sv} is the Stern-Volmer quenching constant, (L) is the concentration of propofol or L-arginine, and τ_0 is the average lifetime of the biomolecule without quencher. The Stern-Volmer quenching constants K_{sv} were obtained by finding the slope of the linear curve obtained when plotting $\frac{F_0}{F}$ vs (L). The quenching rate constant k_q can be calculated using the fluorescence lifetime of Aβ to be 1.1ns (Amaro et al.2013).

The plots of $\frac{F_0}{F}$ vs [L] for Aβ-propofol and Aβ-arginine complexes are shown in (Fig 4.7, and 4.8 respectively). From these plots the Stern-Volmer quenching constants for Aβ-propofol and Aβ-L-arginine complexes were found to be 1.21×10^3 M and 1.49×10^3 M respectively. The quenching rate constants for Aβ-propofol and Aβ-arginine were then calculated to be 1.1×10^{12} L Mol^{-1} s^{-1} and 1.35×10^{12} L Mol^{-1} s^{-1} respectively. The obtained values of the quenching rate constants for both propofol and L-arginine are larger than the maximum dynamic quenching constants for various quenchers with biopolymers (2×10^{10} L Mol^{-1} s^{-1}) which confirms that static quenching is dominant in these complexes (Wang et al. 2008, Darwish et al. 2012).

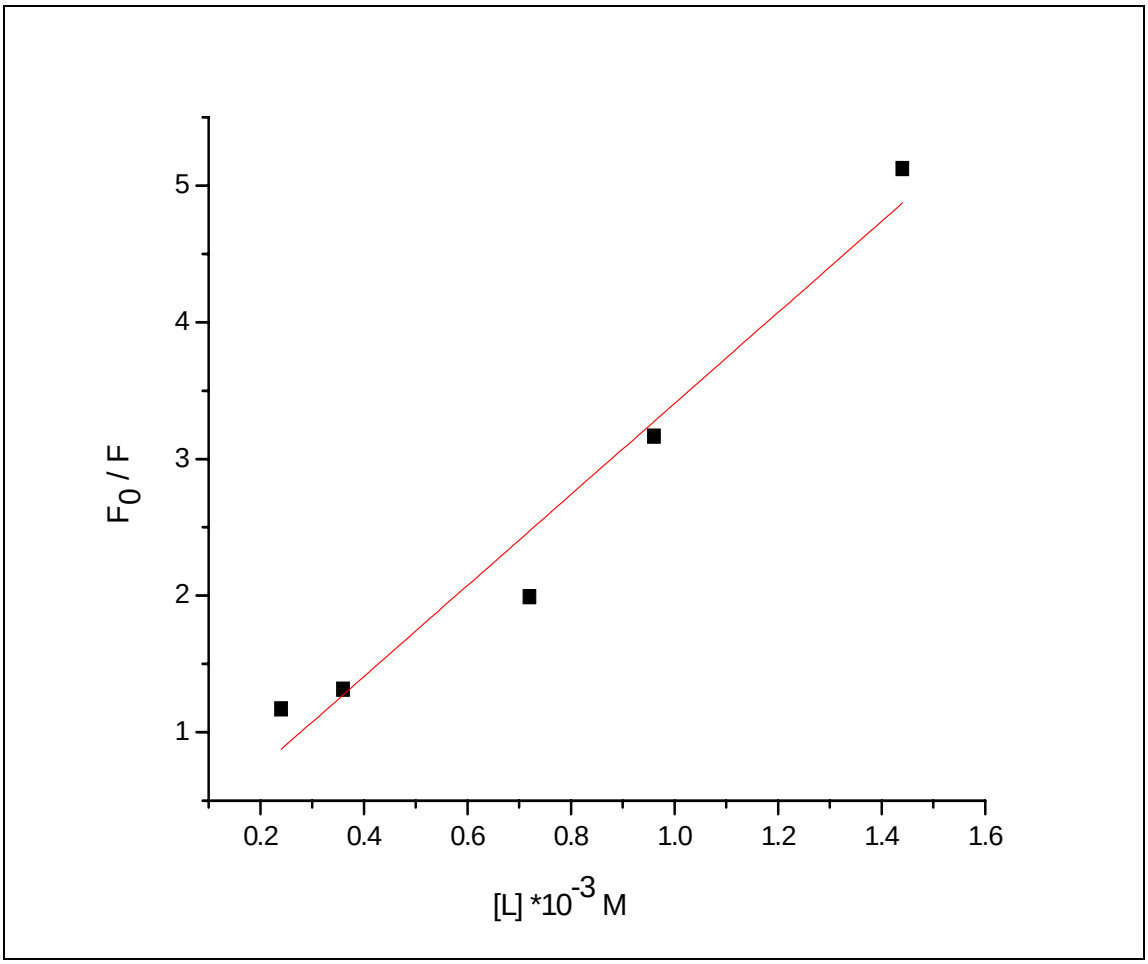

Figure 4.7: The plot of $\frac{F_0}{F}$ vs [L] for Aβ-propofol

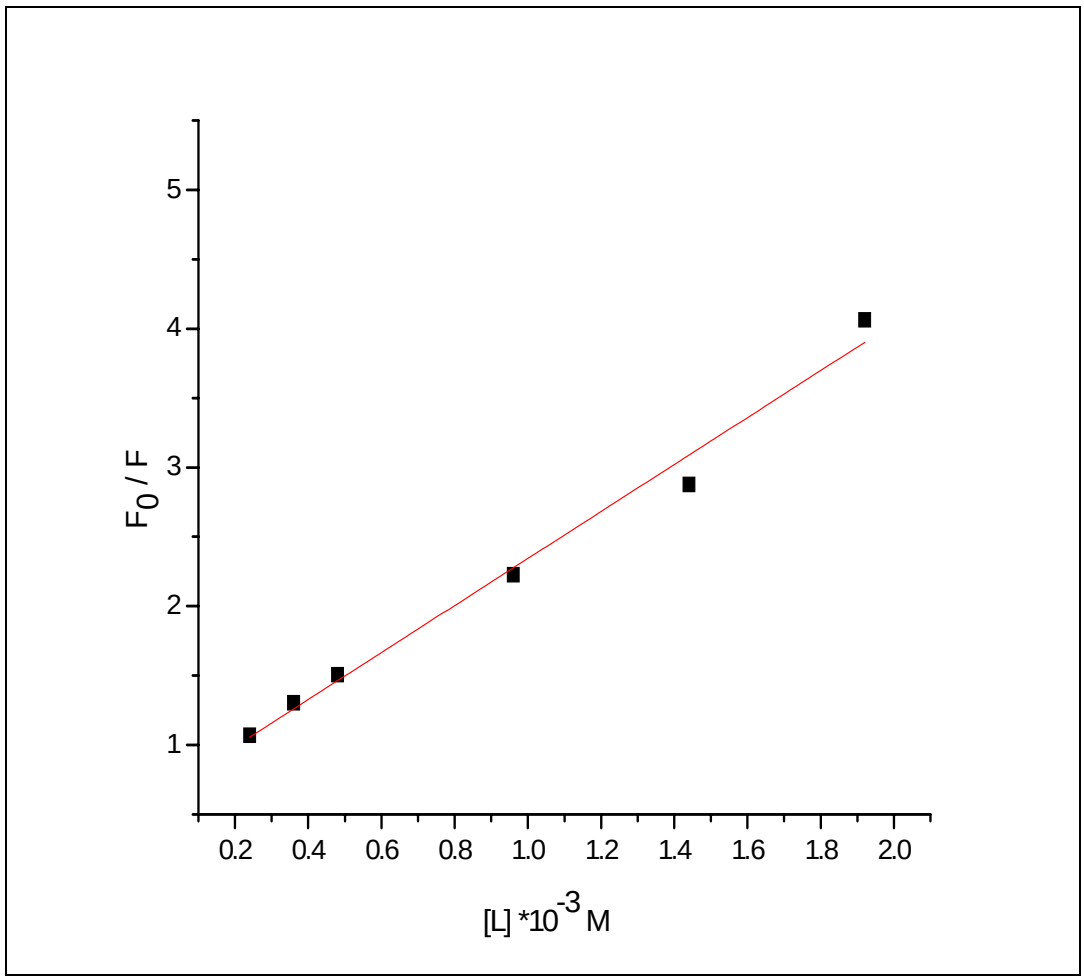

Figure 4.8: The plot of $\frac{F_0}{F}$ vs [L] for Aβ-L-arginine

4.2.2. Determination of the binding constants (K) by fluorescence spectroscopy:

For static quenching, the following equation is used to determine the binding constant between Aβ and the drug.

$$\frac{1}{F_0 - F} = \frac{1}{F_0 K(L)} + \frac{1}{F_0}$$

Where K is the binding constant of drug with Aβ. To determine the binding constants of Aβ-propofol and Aβ-arginine systems, a plot of $\frac{1}{F_0 - F}$ vs $\frac{1}{l}$ for different propofol and L-arginine concentrations is made. The plots are linear and have a slope of $\frac{1}{F_0 K}$ and intercept $\frac{1}{F_0}$ according to the above equation. By taking the quotient of the intercept and the slope, the binding constants K(L) can be calculated.

The plot of $\frac{1}{F_0 - F}$ vs 1/L for Aβ-propofol and Aβ-L-arginine complexes are shown in (Fig 4.9, and Fig 4.10 respectively). The binding constants for propofol and L-arginine with Aβ have been calculated from the slope and the intercept in (Fig. 4.9, and 4.10 respectively) and are found to be 2.81×10^2 M^{-1} for Aβ-propofol and 0.37×10^2 M^{-1} for Aβ-L-arginine.

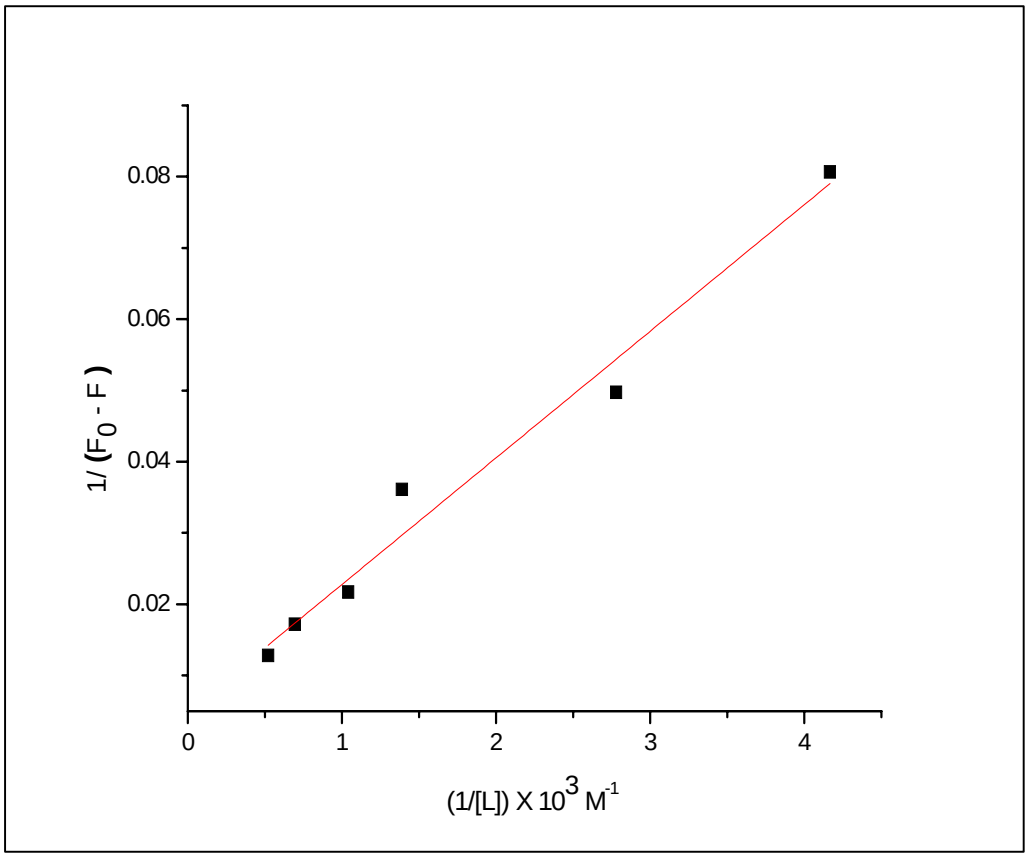

Figure 4.9: The plot of $\frac{1}{F_0-F}$ vs 1/L for Aβ-propofol complexes.

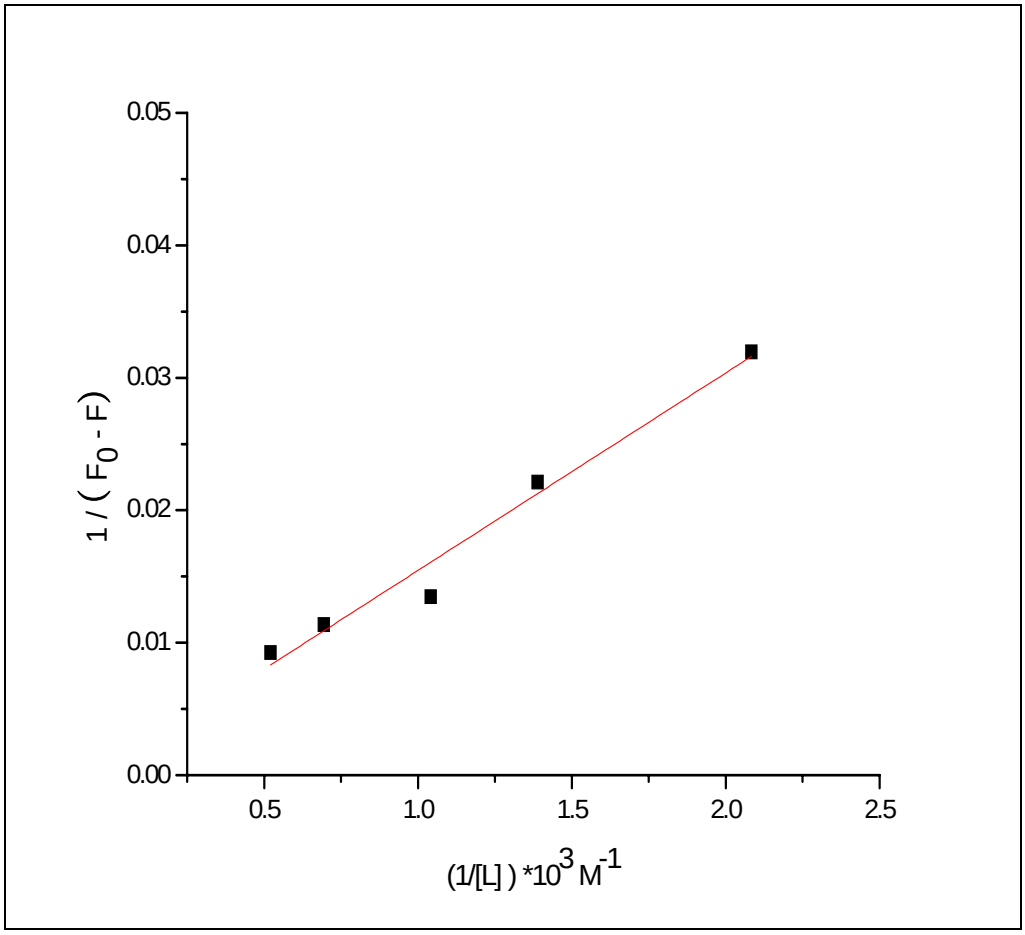

Figure 4.10: The plot of $\frac{1}{F_0-F}$ vs 1/L for Aβ-L-arginine complexes.

4.3 Fourier transform infrared (FTIR) spectroscopy

FTIR spectroscopy has special characteristics made it suitable to analyze the protein-ligand interaction in all kinds of physiological conditions (Stuart 2004). These characteristics are the high sensitivity, fast analysis, and low demanding sample preparation (Susi & Bayler1983). The infrared spectra exhibit a number of amide bands and changes in these bands have been noticed and used to follow aggregation and to explore the effects of environmental properties and temperature on the structure of protein. Any changes in the molecular structure of the protein can be noticed from the changes in the amide regions, mainly amide I and amide II. Changes in the intensities of the absorption bands of β-sheets have been studied in great details. This research focused on β-sheets as it has been shown that amyloid fibrils are rich in β-sheet especially the more stable anti-parallel β-sheet (Kirkitadze et al. 2001, Juszczyk 2009, Cerf et al. 2009, Wang 2008, Zandomeneghi et al.2004).

Amide I and amide II bands are the two most prominent vibrational bands of the protein backbone. The most sensitive spectral region for the protein secondary structure is the amide I band, therefore most investigations concentrated on amide I band (Kong & Yu 2007, Smith 2011, Raaman 2006).

In this study FTIR has been used to investigate the conformational changes in Aβ after binding to propofol and L-arginine. First we have studied changes in the peak positions of amide I and amide II regions for Aβ with different concentrations of propofol and L-arginine and at different temperatures. In addition the changes in the intensity of the component bands in the secondary structure of Aβ with changing propofol and L-arginine concentrations have been investigated. The effect of changing temperature on the intensity of β-sheet bands for Aβ free, Aβ-propofol complex, and Aβ-arginine complex have been examined.

4.3.1. Peak positions:

The second derivative technique and Fourier self deconvolution (FSD) can be used to obtain the peaks positions of the FTIR spectrum. The second derivative of the FTIR spectrum for Aβ-

free in amide I and amide II bands are shown in (Fig 4.11.A, and Fig 4.12.A) The FTIR spectra of Aβ-propofol thin films with concentrations (0.0, 0.48, 0.72, 0.96, and 1.92mM), and the spectra of Aβ-L-arginine thin films with concentrations (0.0, 0.24, 0.36, 0.48, and 0.72mM) are shown in (Fig 4.11.B, and 4.12.B respectively).

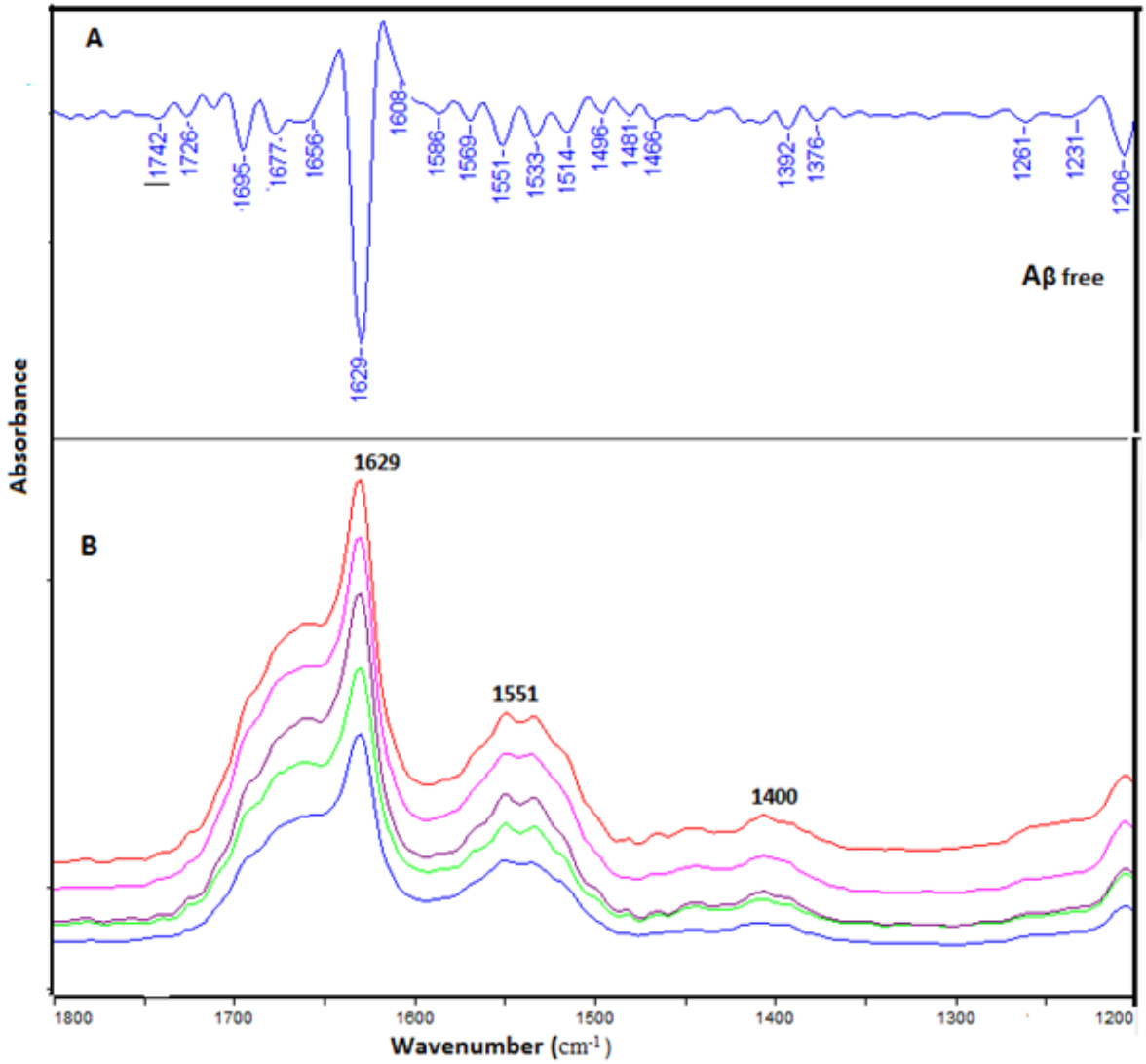

Figure 4.11: the spectra of A: Aβ free (second derivative) and B: Aβ-propofol complexes with concentrations (a=0.0mM, b= 0.48mM, c=0.72mM, d=1.44mM, and e=1.92 mM).

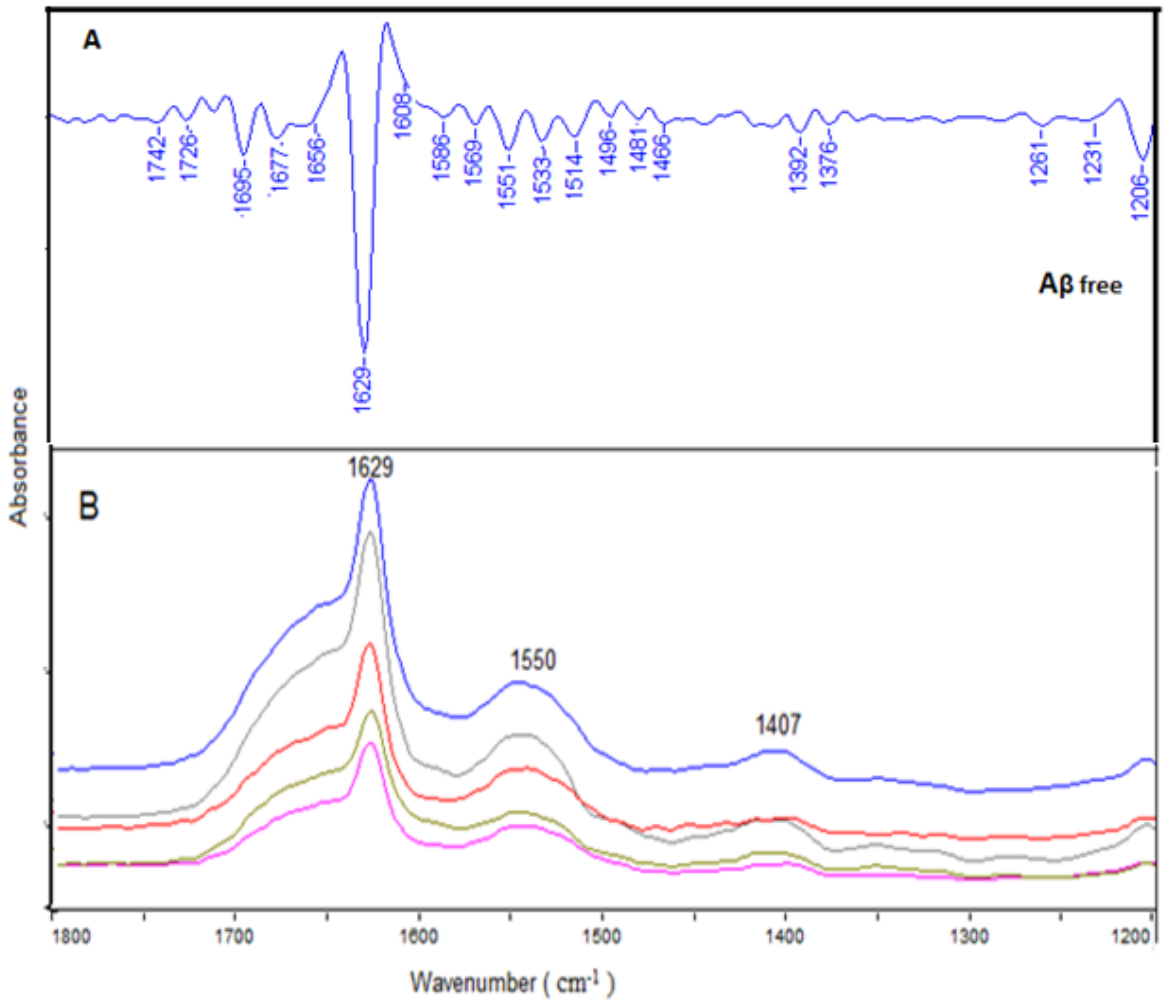

Figure 4.12: the spectra of A: Aβ free (second derivative) and B: Aβ-L-arginine complexes with concentrations (a=0.0mM, b= 0.24mM, c=0.36mM, d=0.48mM, and e=0.72 mM).

The peak positions of Aβ with different propofol and L-arginine concentrations in amide I and amide II are shown in (Table 4.1, Table 4.2 respectively). For Aβ-propofol spectrum we notice peak shifts in amide I band: 1622 to 1624 cm^{-1}, 1636 to 1638 cm^{-1}, 1661 to 1662 cm^{-1}, 1693 to 1694 cm^{-1}, while the peak at 1677cm^{-1} has not been changed. In amide II region the shifts are: 1489 to 1499 cm^{-1}, 1509 to 1515 cm^{-1}, 1528 to 1531 cm^{-1}, 1551 to 1550 cm^{-1}, 1666 to 1568 cm^{-1}, and 1591 to 1592 cm^{-1}.

For Aβ with different L-arginine concentrations in amide I band we notice peak shifts as follows: 1622 to 1621cm^{-1}, 1636 to 1638cm^{-1}, 1661 to 1662, 1677 to 1678cm^{-1}, while the peak at 1693 cm^{-1} has not been shifted and the peak at 1608cm^{-1} has disappeared as its intensity was small and addition of L-arginine has reduced its intensity to zero. In amide II region the shifts are: 1489 to 1487 cm^{-1}, 1509 to 1507 cm^{-1}, 1528 to 1525cm^{-1}, 1551 to 1548 cm^{-1}, 1666 to 1568 cm^{-1}, and 1591 to 1593 cm^{-1}.

The peak shifts for Aβ-propofol system to a higher wave number can be attributed to a newly imposed hydrogen bonding on the C=O upon the addition of propofol (Sarver & Krueger 1991, Lee 1986). In amide II region the peak shifts are more clear as we notice the shift from 1489 to 1499 cm^{-1}, and from 1509 to 1515 cm^{-1}, the shifts indicates that the binding constant for the NH and CN bonds (which are responsible for the amide II spectra) (Kong & Yu 2007) has changed upon interaction with propofol. The shifts in these peaks are toward higher wave numbers which indicates that the strength of the bond has increased. On the other hand for Aβ-L-arginine systems the shifts are toward smaller wavelength which indicates that the strength of the bond have been decreased upon L-arginine addition.

The vibrational energy is proportional to the frequency of oscillation. Shifts to higher wave numbers means that the frequency of oscillation has increased and so a photon of higher energy is needed to break the bond and it can be said that shifts toward higher wave numbers indicates an increase in the strength in the bond and vice versa.

Table 4.1: Band assignment in the absorbance spectra of Aβ with different propofol concentrations in amide I, and amide II.

Bands	Aβ free	Aβ+Propofol 0.48mM	Aβ+Propofol 0.72mM	Aβ+Propofol 0.96mM	Aβ+Propofol. 1.44mM	Aβ+Propofol 1.92mM
Amide I	1608	1607	1607	1608	1608	1608
	1622	1623	1623	1623	1624	1623
	1636	1638	1638	1638	1637	1638
	1661	1662	1662	1662	1662	1662
	1677	1677	1677	1677	1677	1676
	1693	1694	1694	1694	1694	1694
Amide II	1489	1497	1496	1498	1498	1499
	1509	1511	1515	1514	1515	1515
	1528	1532	1531	1532	1532	1531
	1551	1550	1550	1550	1550	1550
	1566	1567	1569	1567	1567	1568
	1591	1593	1592	1592	1592	1592

Table 4.2: Band assignment in the absorbance spectra of Aβ with different L-arginine concentrations in amide I, and amide II.

Bands	Aβ free	Aβ+L-aginine 0.24mM	Aβ+L-arginine 0.36mM	Aβ+L-arginine 0.48mM	Aβ+L-arginine 0.72mM	Aβ+L-arginine 1.92mM
Amide I	1608					
	1622	1620	1621	1620	1620	1621
	1636	1639	1639	1638	1638	1638
	1661	1661	1661	1662	1662	1662
	1677	1676	1676	1678	1677	1678
	1693	1693	1692	1693	1692	1693
Amide II	1489	1493	1487	1484	1487	1487
	1509	1510	1506	1508	1509	1507
	1528	1530	1521	1529	1526	1525
	1551	1549	1546	1547	1546	1548
	1566	1568	1567	1568	1567	1568
	1591	1593	1593	1593	1593	

The difference spectra [(protein + propofol or L-arginine) – (protein)] were obtained to show the intensity variation, and the results are shown in (Fig 4.13, and Fig 4.14). For Aβ-propofol interaction; (Fig 4.13 A) shows FTIR spectra in amide I and amide II regions. The difference spectra for Aβ with different propofol concentrations in amide I and amide II regions are shown in (Fig 4.13 B).

In amide I region there is one strong positive feature at 1630 cm^{-1} in addition to a one weak positive feature at 1670 cm^{-1}. For amide II region there is one strong positive feature at 1550 cm^{-1}. These features were obtained at propofol concentrations (0.48, 0.72, and 1.44 mM).

For Aβ-L-arginine interaction: (Fig 4.14 A) shows FTIR spectra in amide I and amide II regions. (Fig 4.14 B) shows the difference spectra of Aβ with different L-arginine concentrations in amide I and amide II regions. In amide I region there is one strong negative feature at 1629 cm^{-1}, and another weak negative feature at 1668 cm^{-1}, while in amide II region there is one strong negative feature at 1538 cm^{-1} and another weak negative feature at 1493 cm^{-1}.

It is clearly shown that the strong positive features in amide I and amide II become stronger as propofol concentration was increased, on the other hand the strong negative features in amide I and amide II become stronger with increasing L-arginine concentration except for the weak negative feature at 1493 cm^{-1} with a little shift in its position.

The observed positive features are attributed to the increase in the intensity of the amide I band at 1630, and 1670 cm^{-1}, and amide II band at 1550 cm^{-1} as a result of propofol interaction with Aβ. This increase in the intensity is due to the increase in the number of β-sheet bonds. (Darwish et al. 2012) The negative featured noticed in the difference spectra of [Aβ-(L-arginine) – Aβ] are due to the decrease in the intensity with increasing L-arginine concentration. This decrease in the intensity is due to the decrease in the number of β-sheet bonds.

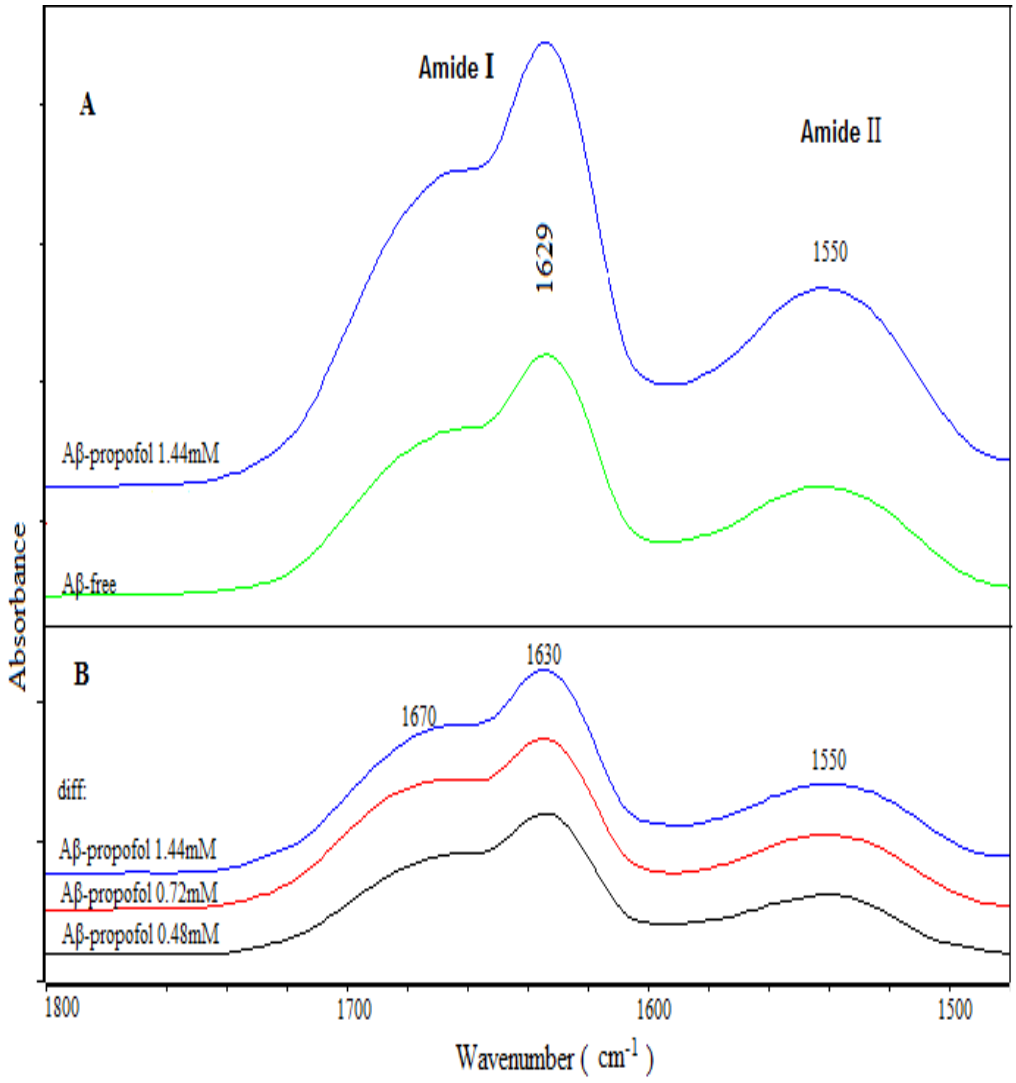

Figure 4.13: A: The FTIR spectra for Aβ free and Aβ-propofol complex 1.44mM, and B: difference spectra of Aβ and its complexes with different propofol concentrations in the region (1800-1480 cm^{-1}).

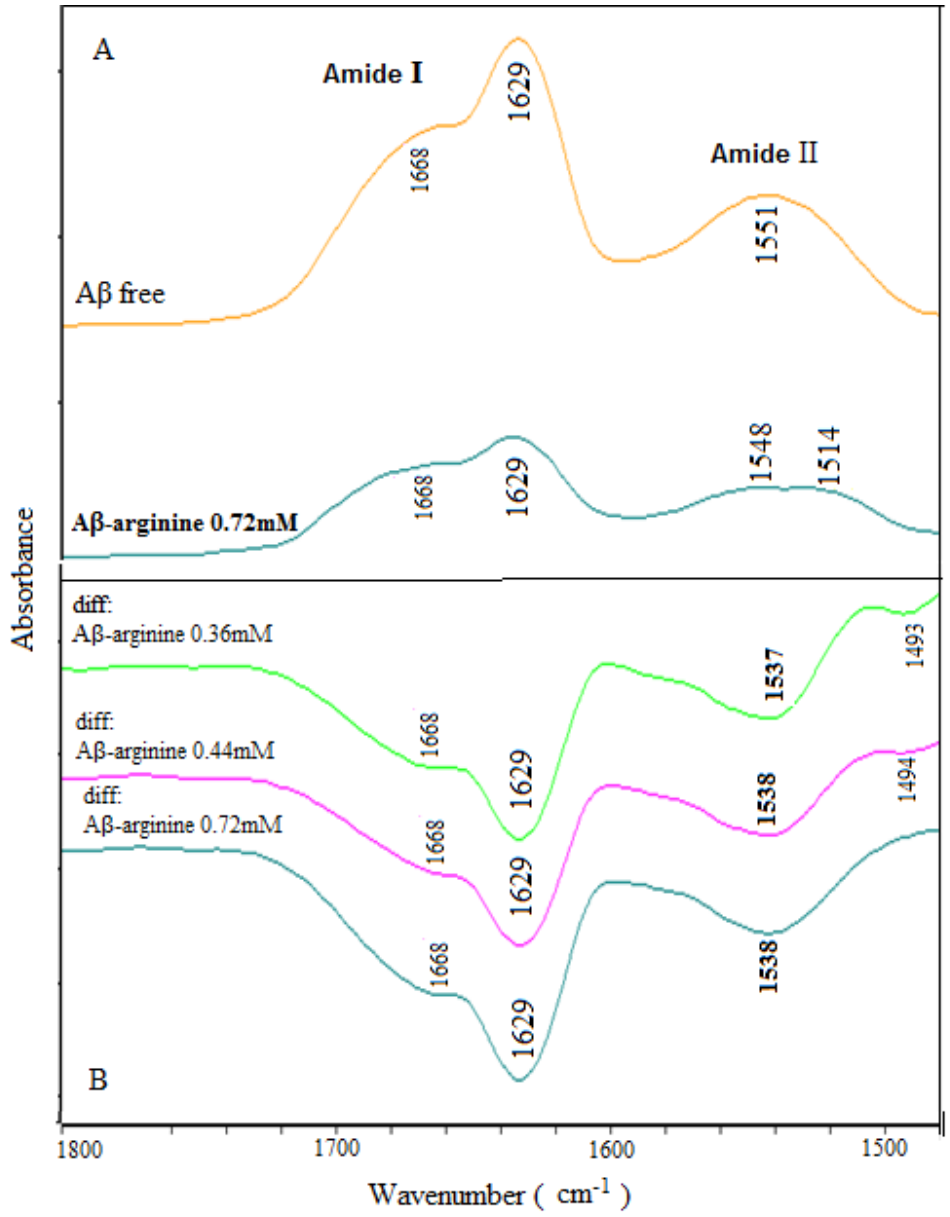

Figure 4.14: A: The FTIR spectra for Aβ free and Aβ-L-arginine complex 0.72mM, and B: the difference spectra of Aβ and its complexes with different L-arginine concentrations in the region 1480-1800cm^{-1}.

4.3.2. Secondary structural changes:

To determine the secondary structure of Aβ and its propofol or L-arginine complexes, the procedure described by Byler and Susi has been followed (Susi & Bayler 1983). A quantitative analysis of Aβ secondary structure for the free Aβ and for Aβ with different concentrations of propofol and L-arginine has been determined from the spectra of the amide I, and amide II bands. Baseline correction has been performed in the ranges (1700-1600 cm^{-1}), and (1600-1480 cm^{-1}), to bring the minimum point to zero and to align the baseline of all the spectra. FSD was applied in these two ranges to increase the resolution of spectra and estimate the position, the number, and the area of each component band. A curve fitting process has been carried out using OPUS software (version 5.5) to obtain the best Lorentzian shaped curves that fit the original spectrum.

The major peaks in each amide band are contours of multiple peaks interfere. Every peak is assigned to a secondary structural element. On the basis of previous infrared studies on other proteins (Lee 1986, Sarroukh et al 2010, Darwish et al.2012), on Aβ(1-28) (Juszczyk 2008), and on Aβ(1-40) (Lin 2003). The amide I bands range 1600-1612 cm^{-1} are assigned to anti-parallel β-sheet, 1612-1630cm^{-1} were assigned to parallel β-sheet, 1630 to 1650 cm^{-1} to random coil, 1650 to 1670 cm^{-1} to α-helix, 1670 to 1685 cm^{-1} to β-turns, and 1685 to 1700 cm^{-1} to anti-parallel β-sheet (Lin 2003, Szabo et al.1999, Cerf et al. 2009).for amide II, the absorption bands consists of six bands assigned in the following order: 1480 to 1500 cm^{-1} to parallel β-sheet, 1500 to 1520 cm^{-1} to random coil, 1520 to 1538 cm^{-1} to anti parallel β-sheet, 1538 to 1560 cm^{-1} to α-helix, 1560 to 1580 cm^{-1} to β-turns, and 1580 to 1600 cm^{-1} to anti-parallel β-sheet (Li et al. 2009).

Based on the above assignments, the percentages for each secondary structural element of Aβ and its propofol or L-arginine complexes have been calculated from the integrated areas of the component bands in amide I, and II respectively. The area of each structural element is found, then the areas are all summed, and then we divide the area of each element by the total area. The obtained number is taken as the proportion to the poly peptide chain component band responsible for that peak, and then the percentages of each secondary structural element were determined (Sarver & Krueger1991).

The secondary structure determination for the free Aβ - propofol complexes and Aβ-L-arginine complexes are given in (Table 4.3, and Table 4.4 respectively). The curve fitted for amide I and amide II regions of the free Aβ (0.231 mM) and its propofol complex with propofol concentration of 1.44 mM, are shown in (Fig. 4.15). The curve fitted for amide I and amide II regions of the free Aβ (0.231 mM) and its L-arginine complex with arginine concentration of 0.72 mM, are shown in (Fig. 4.16)

the changes in parallel and anti parallel β- sheet intensities with changing propofol and L-arginine concentration while keeping Aβ concentration constant in amide I and amide II are shown in (Fig. 4.17)

In amide I region, free Aβ composed of the components: random coil (31%), α-helix (25%), β-sheet (35% of them 16% for parallel β-sheet and the remaining 19% for anti parallel β-sheet), and β-turns (8%). From (Table 4.3, and Fig. 4.16) the result of Aβ-propofol interaction shows that random coil structure has reduced from 31% to 28%, α-helical structure has increased from 25% to 29%, β-turn has increased from 8% to 10%, parallel β-sheet has decrease from 16% to 10%, and anti-parallel β-sheet has increased from 19% to 23%.

In amide II region free Aβ contained random coil (30%), α-helix (14%), parallel β-sheet (11%), anti parallel β-sheet (27%), and β-turns (19%), after interaction with propofol random coil has decreased from 30% to 12%, α-helix from 14% to 10%, parallel β-sheet from 11% to 6%, anti-parallel β-sheet has increase from 27% to 47%, and β-turn has increased from 19% to 24%.

It can be seen from (Table 4.4, and Fig. 4.8) that is as a result of Aβ-arginine interaction that the random coil structure has increase from 31% to 42%, α-helical structure has increased from 24% to 30%, β-turn has decreased from 9% to 5%, parallel β-sheet has decrease from 16% to 10%, and anti-parallel β-sheet has decreased from 20% to 13%.

In amide II region, after interaction with L-arginine random coil has increased from 30% to 39%, α-helix has increased from 14% to 28%, parallel β-sheet has decreased from 11% to 7%, anti-parallel β-sheet has decreased from 27% to 10%, and β-turn has decreased from 19% to 15%.

The parallel β-sheet arrangement is weaker than anti-parallel one and less stable because of its geometry of the individual amino acids composing it, which will force the hydrogen bond to occur at an angle which will make them longer and weaker, on the other hand in anti parallel arrangements the amino acids are directed opposite to each other and so hydrogen bonds between carbonyl and amines will be planar and the arrangement is stronger and more stable (Perczel et al.2005, Irie et al. 2005).

In the analysis of the absorption spectra for Aβ-propofol complexes in amide I and amide II , the relative intensity of parallel β-sheet with its peak at (1623 cm^{-1}) shows a decrease with increasing propofol concentration (Fig 4.17 A). the same observation can be made for parallel β-sheet band at (1486 cm^{-1}) in the amide II as shown in (Fig. 4.17 B).on the other hands an increase in anti-parallel β-sheet component which has peaks at (1694 $cm^{-1)}$ in amide I as shown in (Fig. 4.17A) and at (1522 and 1593 cm^{-1}) in amide II as shown in (Fig 4.17 B). The decrease in the parallel β-sheet intensity percentage accompanied with increase in anti-parallel β-sheet structures are believed to be due to the unfolding of protein in the presence of propofol as a result of H-bonding formation between propofol and Aβ (zandomeneghi et al. 2004).

Circular dichroism (CD), FTIR spectroscopy, and X-ray diffraction studies confirmed that amyloid fibrils have a β-pleated sheet structure (A. Lomakin 1996, Zandomeneghi 2004). The observed increase in the intensity of anti-parallel β-sheet as a result of Aβ interaction with propofol is an indication of fibrils formation (Sarroukh 2010, Juszczyk 2008). These changes can also be noted directly from the curve fitted curves in (Fig. 4.16).

In the analysis of the absorption spectra of Aβ-L-arginine complexes in amide I and amide II, both parallel and anti-parallel β-sheet intensity shows a gradual decrease with increasing L-arginine concentration as shown in (Fig. 4.17 C, and 4.17 D), which is a good indication of the effect of L-arginine in decreasing oligomerization by converting the insoluble (β-sheet rich) fibrils or oligomers into a more soluble entities.

Table 4.3: secondary structure determination for amide I, and amide II regions for Aβ and its propofol complexes.

Bands	**Aβ free**	**Aβ+propofol 0.48 mM**	**Aβ+propofol 0.72 mM**	**Aβ+propofol 0.96 mM**	**Aβ+propofol 1.44 mM**
Amide I					
antiparallel β-Sheets 1600-1610	0.2	0.2	0.2	0.2	0.2
parallel β-Sheets 1610-1629cm-1	16.3	14.0	11.2	12.0	10.1
Random Coil (1629-1650 cm^{-1})	31.4	29.7	29.7	30.7	28.2
α-helix (1650-1669 cm^{-1})	24.8	27.3	27.7	28.2	28.7
β-turns (1669-1685cm^{-1})	8.4	9.4	10.5	9.2	10.1
Antiparallel β-Sheets (1685-1700 cm^{-1})	18.9	19.4	20.7	19.7	22.7
Amide II					
Parallel β-sheet 1480-1500	10.8	6.0	5.0	5.0	5.6
Random Coil (1500-1520 cm^{-1})	29.9	27.4	14.1	16.4	12.2
anti-Parallel β-sheet (1520-1540 cm^{-1})	15.5	18.9	25	22.5	26.6
α-helix (1540-1560 cm^{-1})	13.8	13.7	12.0	12.3	10.4
β-turns (1560-1580 cm^{-1})	18.8	20.7	25.3	24.3	24.1
Anti-parallel β-sheet 1580-1600	11.2	13.3	18.7	19.4	21.0

Table 4.4: secondary structure determination for amide I, and amide II regions for Aβ and its L-arginine complexes.

Bands	**Aβ free**	**Aβ+L-arginine 0.24mM**	**Aβ+L-arginine 0.36 mM**	**Aβ+L-arginine 0.48 mM**	**Aβ+L-arginine 0.72 mM**
Amide I					
Antiparallel β-Sheets	0.2	0.2	0.2	0.1	0.1
(1600-1610 cm^{-1})					
parallel β-Sheets	16.3	11.2	10.7	8.6	10.2
1610-1629cm-1					
Random Coil	31.4	35.4	36.7	40.4	42.1
(1629-1650 cm^{-1})					
α-helix	24.8	28.0	29.8	31.7	30.0
(1650-1669 cm^{-1})					
β-turns	8.4	7.6	7.3	6.0	4.7
(1669-1685cm^{-1})					
Antiparallel β-Sheets	18.9	17.6	15.3	13.2	12.9
(1685-1700 cm^{-1})					
Amide II					
Parallel β-sheet	10.8	10.9	7.7	7.5	7.3
1480-1495					
Random Coil	29.9	33.6	37.1	38.9	39.2
1498-1515					
Anti-parallel β-Sheets	15.5	14.7	11.4	10.9	9.9
1515-1538					
α-helix	13.8	17.1	22.1	25.4	28.3
1538-1560					
β-turns	18.8	14.6	15.3	15.0	15
1560-1577					
anti-parallel β-Sheets	11.2	9.2	6.4	2.3	0.4
1577-1600					

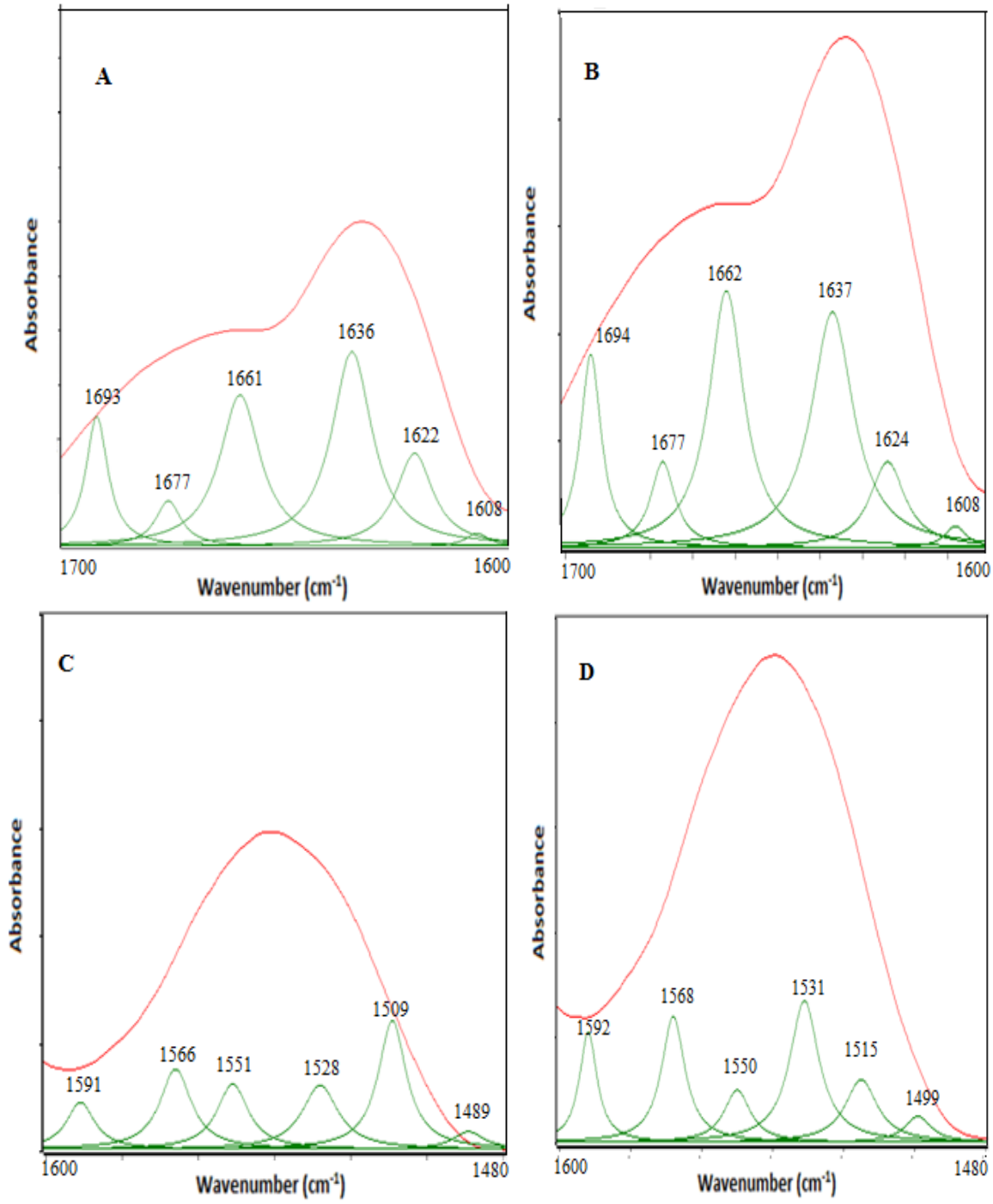

Figure 4.15: Curve fitted graphs for (A) free Aβ in amide I region, (B) Aβ-prop. Complex with 1.44mM Propofol concentration in amide I region, (C) free Aβ in amide II region, (D) Aβ-propofol complex with 1.44mM Propofol concentration in amide II region.

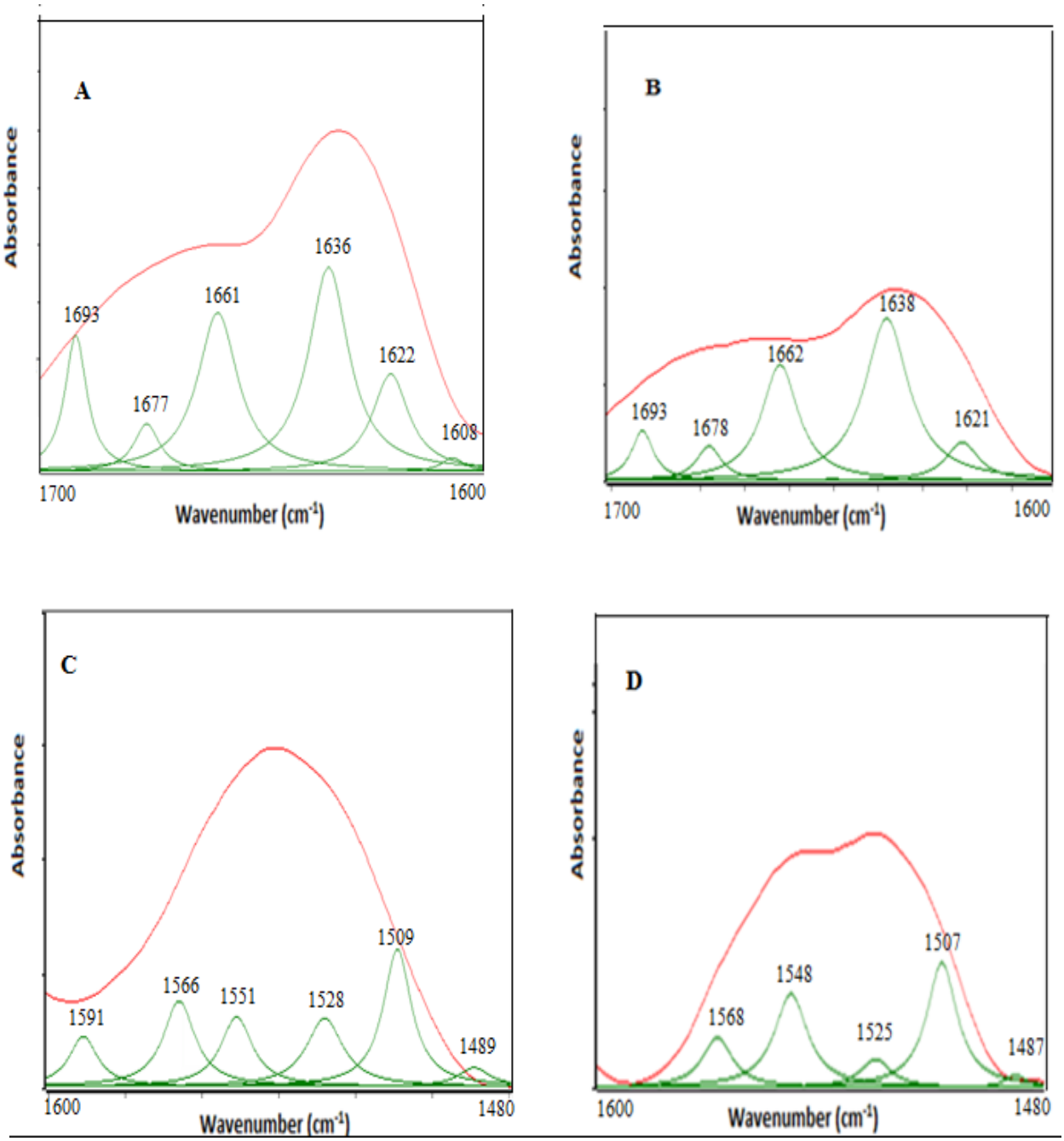

Figure 4.16: Curve fitted graphs for (A)free Aβ in amide 1 region, (B) Aβ-L-arginine. Complex with 0.72 mM L-arginine concentration in amide 1 region, (C) free Aβ in amide II region, (D) Aβ-L-arginine complex with 0.72mM L-arginine concentration in amide II region.

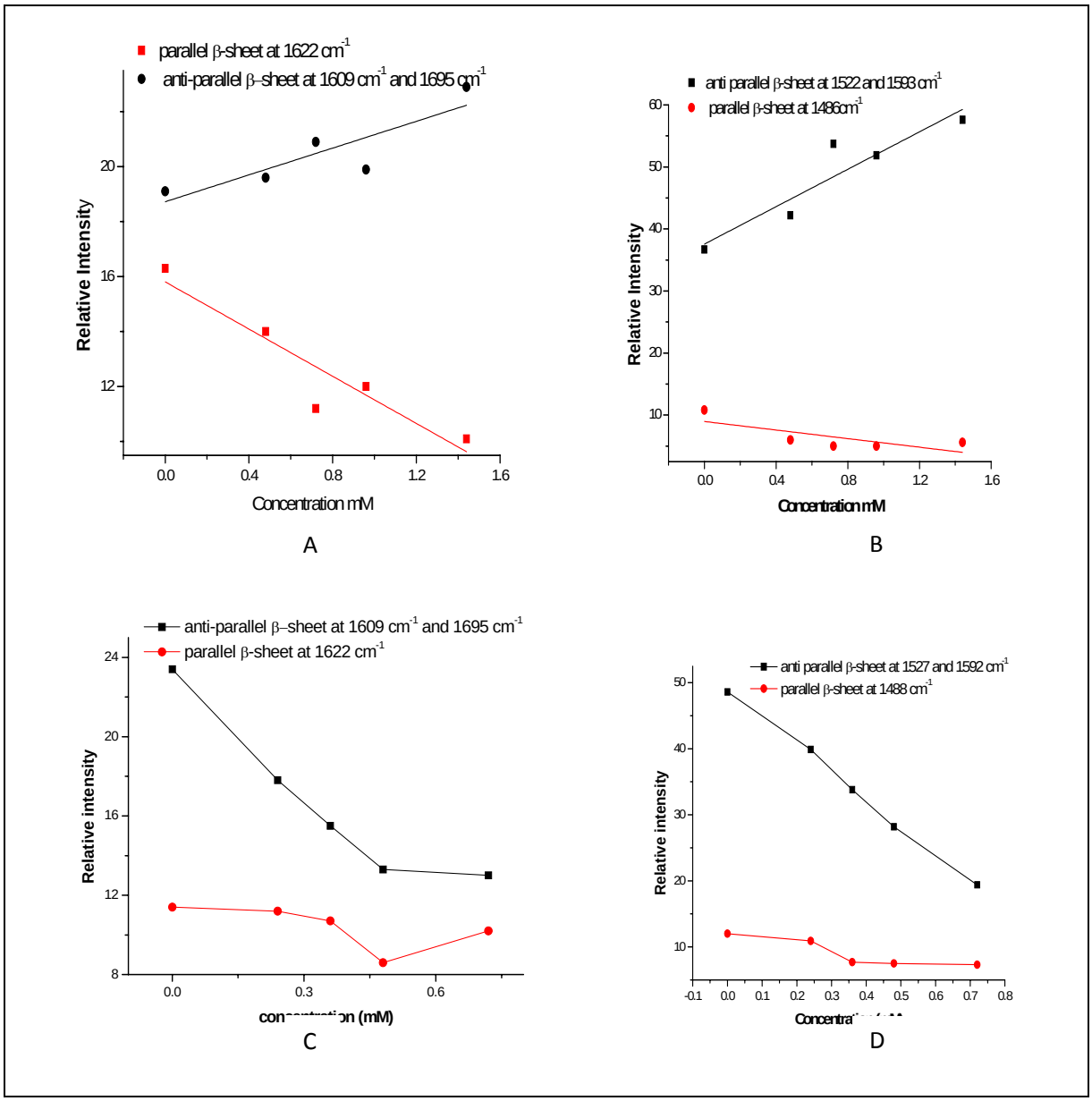

Figure 4.17: Relative intensity variation for different concentrations of A: Aβ-propofol complexes in amide I region, B: Aβ-propofol complexes in amide II region, C: Aβ-L-arginine complexes in amide I region, D: Aβ-L-arginine complexes in amide II region.

4.3.3. Effect of temperature:

The effect of increasing temperature on Aβ free, Aβ-propofol complex, and Aβ-L-arginine complex have been studied in both amide I and amide II bands. The effects of increasing temperature on parallel and anti-parallel β-sheet in amide I were shown in (Fig. 4.18 A,B, and C respectively). The effects of increasing temperature on parallel and anti-parallel β-sheet in amide II were shown in (Fig. 4.19 A,B, and C respectively).

For Aβ free no appreciable shifts in peaks are noticed. No changes in parallel or anti parallel β-sheet composition is noticed with increasing temperature in both amide I and amide II as shown in (Fig4.18 A, and 4.19 A).

For Aβ propofol complex upon the analysis of the spectra of Aβ-propofol complex with changing temperature from (20 to 80 C^0) it is noticed that: peaks have little or no appreciable shifts in their positions, the intensity for the bands of parallel β-sheet (1623 cm^{-1}) gradually decrease with increasing temperature, and anti-parallel β-sheet intensity (1694 cm^{-1}) gradually increase with increasing temperature. The relative intensity versus temperature for Aβ-propofol complex in amide I region is shown in (Fig 4.18 B), while the relative intensity versus temperature in amide II region is shown in (Fig 4.19 B).

The gradual decrease in parallel β-sheet intensity is believed to be mainly as a result of the unfolding of protein due to the formation of H-bonding between Aβ and propofol. The newly formed H-bonding will cause the C-N bond to assume a partial double bond character with C=O bond as a result of the electron flow from C=O to C-N, which will decrease the intensity of molecular vibration. The increase in anti-parallel β-sheet intensity with increasing temperature reflects more stability and low conversion of C=O bond of Aβ-propofol complex with increasing the temperature. (Lee 1986, Szabo et al.1999, Darwish et al. 2012)

For Aβ-L-arginine spectra with increasing temperature, no appreciable peak shifts is observed in amide I region, while in amide II region the peak at 1567cm^{-1} has been shifted to 1561cm^{-1} and the peak at 1551cm^{-1}, which is believed to be due to disappearance of alpha-helix.

A gradual decrease in anti-parallel β-sheet accompanied with an increase in parallel β-sheet intensity until the temperature reaches 33 C^0 is noticed. Then anti-parallel β-sheet starts to

increase, and parallel β-sheet starts to decrease gradually. The same behavior is noticed in both amide I and amide II as shown in (Fig 4.18 C, and 4.19 C).

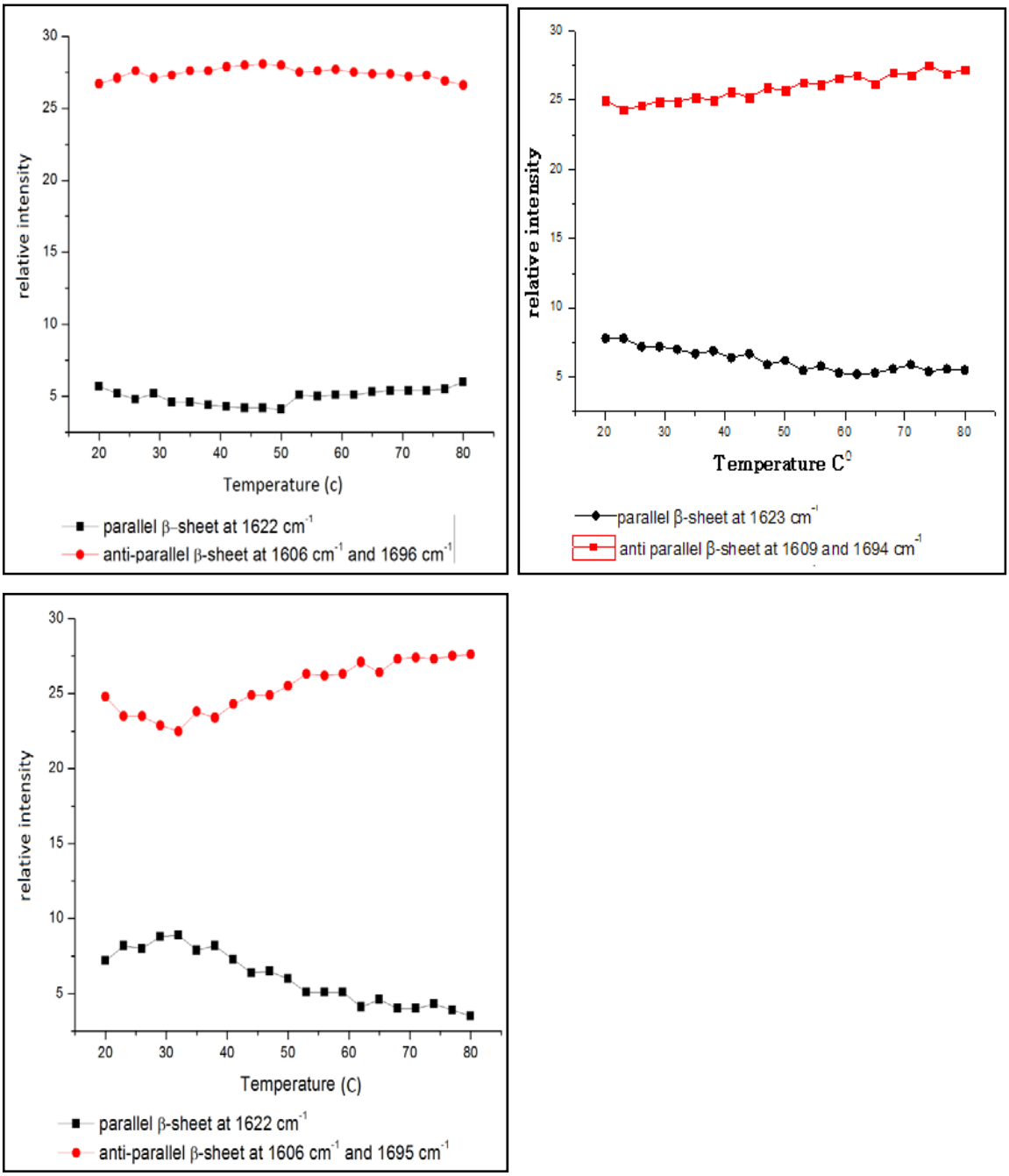

Figure 4.18: relative intensity versus temperature change in amide I band for A: Aβ-free (0.231mM), B: Aβ-propofol complex 0.48mM, and C: Aβ-L-arginine complex 0.48mM for bands at 1606, 1623, and 1694 cm^{-1}.

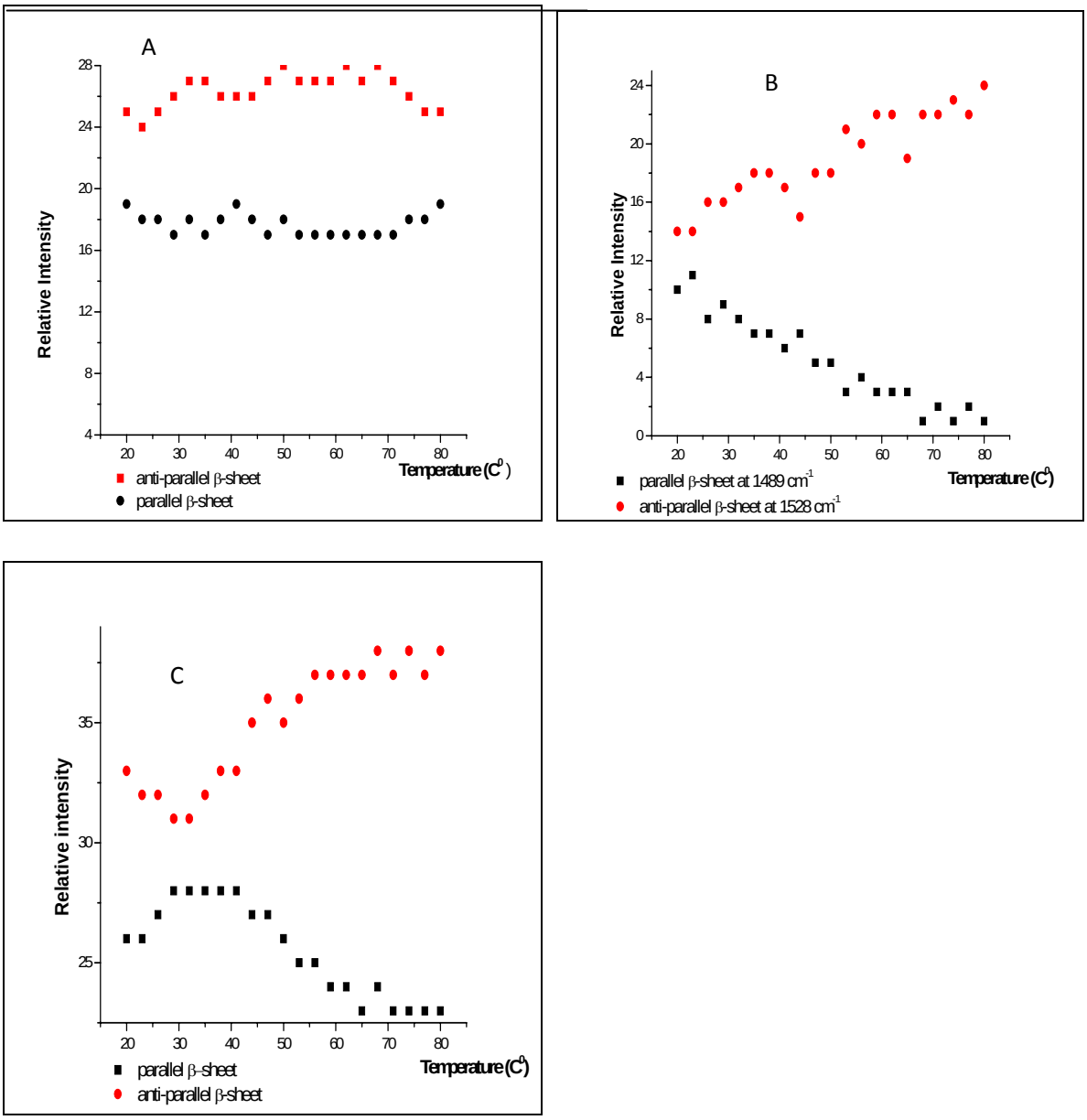

Figure 4.1**9**: relative intensity versus temperature change in amide II band for A: Aβ-free (0.231mM), B: Aβ-propofol complex 0.48mM, and C: Aβ-L-arginine complex 0.48mM for bands at 1489, 1528, and 1585 cm^{-1}.

In the process of interpreting the effect of protein oligomerization memory function, one may assume that information and images are saved in the precursor proteins as oscillations with certain frequencies of formed bonds. Plaques formation and its effect on memory can be explained by assuming that propofol interaction with proteins in the brain produces a polarized dielectric material that is sandwiched between the unfolded β-sheet to create capacitor-like structure. The presence of this dielectric material will increase the internal energy of the arrangement leading to a more stable complex. The rigid structure is expected to prevent β-sheet from folding due to the additional constraints on its surface leading to plaques formations. The new solid structure causes the loss of the original frequency related to the saved information. L-arginine can be assumed to act as a dielectric material with low dielectric constant and this explains its different effect on Aβ.

Radiation emitted and reflected from objects falls on human eye, this radiation is then turned to an oscillating signal of specific properties. This signal will pass through neurons searching for an identical signal saved in the brain. When the identical signal is found, brain tells what the object that has been seen is, and in this way memorizing occurs. When plaques formed they bind to neurons, this will cause bad transmission of signal. This will lead to memory loss accompanied with Alzheimer disease.

4.4 Atomic force microscopy (AFM)

AFM technique has been used as an additional method to investigate the effect of propofol and L-arginine on Aβ by taking images for Aβ solution, Aβ-propofol complex, and Aβ-L-arginine complex as shown in (Fig. 4.20)

AFM images for Aβ-free, Aβ-propofol, and Aβ-L-arginine complexes are shown in (Fig 4.20 A, 4.20 B, and 4.20 C respectively). The heights of species or clusters in each of these complexes when scanning the surface of the samples of Aβ-free, Aβ-propofol, and Aβ-L-arginine are shown to the right of each image in the same figure (Fig 4.20).

It has been found from AFM that Aβ species have clustered in a certain area as a result of interaction with propofol, this have not been noticed in the case of Aβ-L-arginine interaction.

From graph shown in (Fig. 4.20 A) the height of the clusters in Aβ-free sample was found to be between (30-35nm), while for Aβ-propofol sample it has been found to be (250-300nm) as shown in the graph in (Fig 4.20 B), for Aβ-L-arginine sample the height has been found to be (25-50).

These results clearly indicate the effect of propofol in increasing the sizes of the clusters which are shown as spherical shaped objects. This confirms the results already found by FTIR spectroscopy that propofol enhances plaques formation.

A little change in the heights of Aβ is noticed upon interaction with L-arginine as shown in (Fig. 4.20 A, and C). So L-arginine interacts with Aβ in a way different from that of propofol. These results confirm the results already found by FTIR spectroscopy.

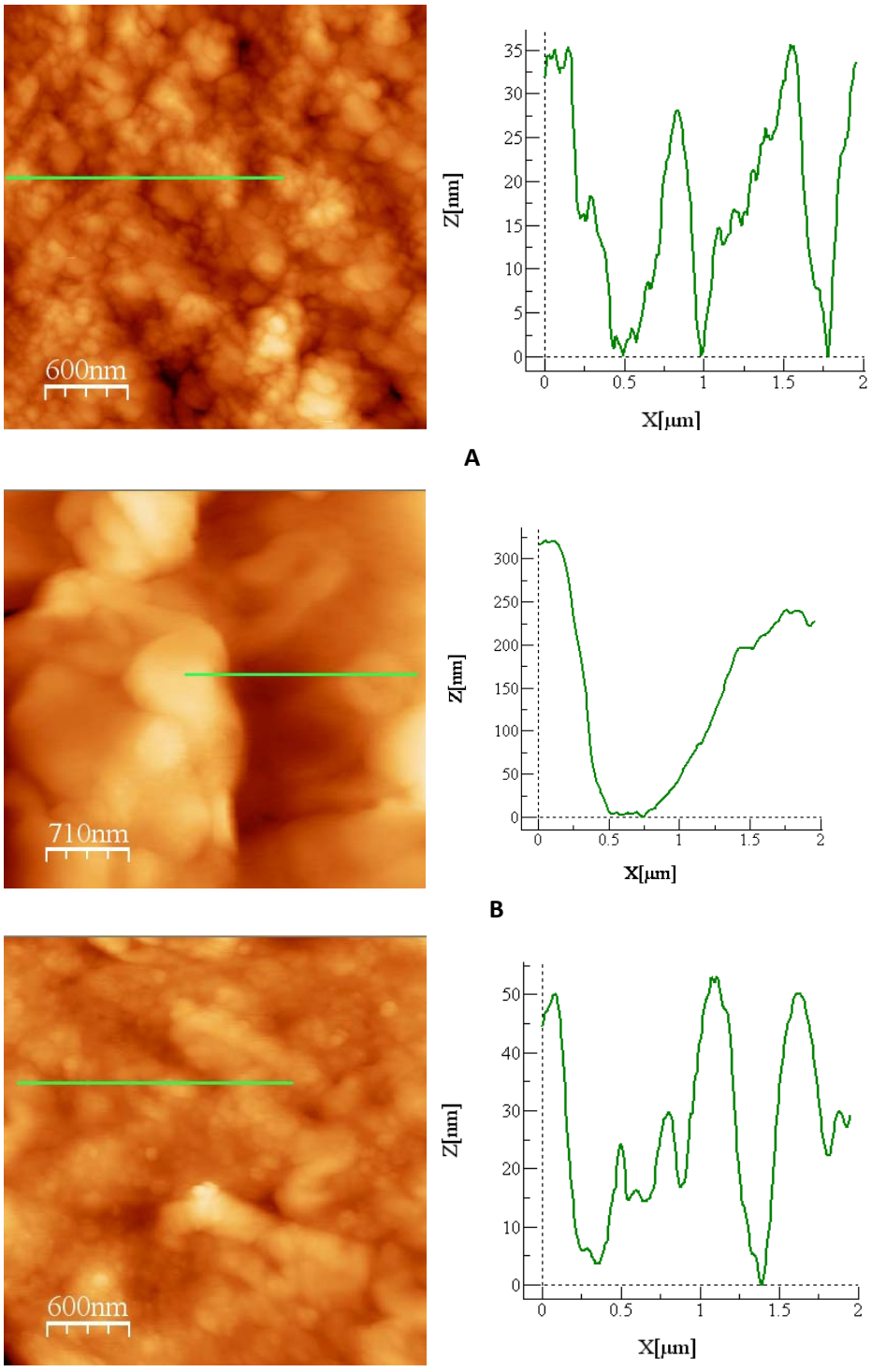

Figure 4.20: AFM image of A: Aβ solution, B: Aβ-Propofol (0.96mM) complex, and C: Aβ-L-arginine complex (0.96mM). The graph at the right to each image shows the changes in height at the surface of the sample responsible for that image.

Chapter Five

Conclusions and future work

5.1 Conclusions

In this research, the interaction of propofol and L-arginine with Aβ has been studied using UV-vis spectroscopy, fluorescence spectroscopy, FTIR spectroscopy, and AFM. The binding parameters for the binding of propofol and L-arginine with Aβ have been determined: For Aβ-propofol and Aβ-L-arginine the binding constants are calculated by UV-vis spectroscopy to be K= $2.13\times 10^{2}M^{-1}$, and $0.35\times10^{2}M^{-1}$ respectively. The obtained values of the binding constants K by using fluorescence spectroscopy are $2.81\times10^{2}M^{-1}$, and $0.37\times10^{2}M^{-1}$ respectively. Which agree with the values obtained by UV-vis spectroscopy. In addition, the values of Stern-Volmer quenching constants for both propofol and L-arginine are estimated to be (1.21×10^{3}L mol^{-1} s^{-1}, 1.49×10^{3}L mol^{-1} s^{-1}) respectively.

These experimental results confirm the fact that dynamic quenching is not the main mechanism that causes the fluorescence quenching, and the decrease in fluorescence intensity occurred as a result of static quenching, which is indicative of a complex formation between the protein and the drug molecule. Also the low binding constant between the drug (propofol or L-arginine) and Aβ is due to the effective hydrogen bonding between these drugs and Aβ.

Analysis of the FTIR spectra reveals that Aβ-propofol interaction has induced reduction in the absorption band of parallel β-sheet and random coils accompanied with an increase in anti-parallel β-sheet and α-helix with different proportionality due to the different accessibility of H-bond formation in these components. This increase in the intensity of anti-parallel β-sheet with increasing propofol concentration is an indication that propofol increases the rate of oligomers or fibrils formation. On the other hand, analysis of the FTIR spectra for Aβ-arginine interaction reveals that a reduction in the intensity of the absorption band of anti-parallel β-sheet and parallel β-sheet with increasing arginine concentration has occurred; also an increase in the intensity of random coil and α-helix is noticed.

It is noticed that the behavior of L-arginine when interacting with Aβ is different than that of propofol; means that each one of them interact with Aβ in a different manner. Many studies have proven that amyloid oligomers or fibrils which are found in the brain of patients with Alzheimer disease are rich in β-sheet especially the more stable anti-parallel β-sheet. (Murphy 2002, kirkitadze 2001, Lidgren 2010) Since increasing propofol concentration was shown to

increase the intensity of the absorption band of anti-parallel β-sheet, one can deduce that propofol increases the rate of oligomerization or fibrils formation. On the other hand arginine has the opposite effect as increasing its concentration decreases the intensity of anti-parallel β-sheet. It can be concluded that arginine not only does not induce oligomerization, but it also may decrease the rates of oligomerization.

Temperature study has shown that for Aβ-free no appreciable changes in the intensity of parallel and anti-parallel β-sheet with increasing temperature have noticed, while for Aβ-propofol complex anti-parallel β-sheet intensity has increased gradually accompanied with a decrease in parallel β-sheet intensity. For Aβ-L-arginine complex, intensity of anti-parallel β-sheet has decreased until temperature reached 33^0C then it started to increase, while parallel β-sheet has increased until 33^0C, then it started to decrease. This have been found in both amide I and amide II regions.

AFM images have been taken for Aβ free, Aβ-propofol complex, and Aβ-arginine complex. All these complexes have the same concentration of Aβ. A difference between these three images is noticed. These pictures confirm the formation of oligomers seen as clusters when propofol is added to Aβ, while the addition of L-arginine is shown to have different effect on Aβ oligomers formation.

5.2 Future work

The binding study of propofol and arginine with Aβ is of great importance in pharmacology and biochemistry. Our research can provide important information to medical and clinical researches about Alzheimer disease. It can provide theoretical basis for a new drug design. Further investigations are still needed to explain the role of anesthetics in initiating oligomers formation in proteins, and more clinical studies are needed to test these expectations.

References:

- Amaro, M. et al. (2013). Initial stages of beta-amyloid $A\beta_{1-40}$ and $A\beta_{1-42}$ oligomerization observed using fluorescence decay and molecular dynamics analysis of tyrosine, Methods Appl. Fluoresc, vol 1, 5006-5019.
- Aruldhas, G. (2007). Molecular structure and spectroscopy, 2nd ed., PHI learning private limited, New Delhi.
- Aschenbrenner, D.S., Venable, S.J. (2009). Drugs therapy in nursing, 3rd ed. Walters Kluwer Helth, Lippincott Williams & Wilkins.
- Atassi, M.Z. (2006). Protein Misfolding, Aggregationand Conformational Diseases, Springer Science&Business Media, Inc.
- Bai, Y., and Nussinov, R. (2007). Protein Folding Protocols, Humana Press Inc.
- Ball, D.W. (2001). The basics of spectroscopy, SPIE- the international society for optical engineering.
- Bowen, W.R., Hilal, N. (2009). Atomic force microscopy process engineering: an introduction to AFM for improved processes and products, Elsevier Ltd.
- Braga, P.C., and Ricci, D. (2004), Atomic force microscopy: biomedical methods and applications, Vol. 242, Humana press Inc., Totowa, New Jersy.
- Buxbaum, E. (2007), Fundamentals of protein structure and function, Springer Science & Business media, LLC.
- Buxbaum, E. (2011). Biophysical chemistry of proteins: an introduction to laboratory method, springer science+ Business media. LLC.
- Carnini, A. et al. (2007), Current Alzheimer Research, 4,No.3, 233-241.
- Cerf, E. et al. (2009). Biochem.J. 421, pp415-423.
- Chiti, F., and Dobson, C.M. (2006), Annu. Rev. Biochem., 75,333–366.
- Chiti, F., and Dobson, C.M. (2009), Nature chemical biology, 5 num. 1, 15-22.
- Collins, J.S., Dawes, M.A. (2007). Effect of Propofol on beta Amyloid induced cell death pc-12 cell, ProQuest LLC.
- Cote, J. et al. (2009), A practice of anesthesia for infants and children, 4th ed., Saunders, Elsevier Inc.

- Curey, J.A., Garavaglia, M.J. (2008). The Direct Effects of Propofol on Amylase Release of AR42J Cells, ProQuest LLC.
- Darwish, S.M. et al. (2012), spectroscopic investigation of pentoparbital interaction with Transthyretin, vol 2013, p10, journal of spectroscopy.
- Duce, J.et al. (2010). Cell 142, 857–867.
- Eckenhoff et al., (2004), Anesthesiology, 101:703–709
- El-Agnaf, O. et al. Oligomerization and toxicity of β-amyloid-42 implicated in Alzheimer disease, Biochemical and biophysical research communication, 273, 1003-1007.
- Fasman, G.D. (1990). Prediction of Protein Structure and the Principles of Protein Conformation, Plenum press, NewYork.
- Fodale, V. et al., (2006), British Journal of Anaesthesia 97 (4): 445–52.
- Fodale, V. et al., (2010), Journal of Alzheimer's Disease 22, S1–S3.
- Griffith, P.R., Haseth, J.A. (2007). Fourier Transform Infrared Spectroscopy, 2nd ed., John Wiley & sons. Inc.
- Haass,Cet al. (2012). Trafficking and Proteolytic Processing of APP Cold Spring Harbor Laboratory Press.
- Hollas, M.J. (2004). Modern spectroscopy. 4th ed., John Wiley & sons, Chichester, England.
- Hsu,C.P. Infrared spectroscopy, Research and Product Development Mallinckrodt, Inc.Mallinckrodt Baker Division.
- Ignarro, L.J. (2000). Nitric Oxide: Biology and Pathobiology, academic press.
- Irie, K. et al. (2005), Review: Structure of β-amyloid fibrils and relevance to their neurotoxicity: implication for the pathogenensis of Alzheimer disease, Journal of bioscience and bioengineering, Vol 99, no 5, 437-447.
- Jimenez, J.P. (2005). Systematic study of amyloid beta peptide conformations: implication for Alzheimer disease, thesis and dissertation, university of south Florida.
- Juszczyk, P. (2009). J. Pept. Sci. , 15, 23–29.
- Kalsi, P.S. (2004). Spectroscopy Of Organic Compounds, 6th ed., New Age international publishers Ltd.

- Kirkitadze, G. et al.(2001). J. Mol. Biol, 312, 1103-1119.
- Kong, J., and Yu,S. (2007). Acta Biochimica et Biophysica Sinica, 39(8), 549–559.
- Krebs, M. et al., (2005). Journal of Structural Biology, 149, 30–37.
- Kumar, P. et al. (2011). Int. J. Mol. Sci., 12, 694-724.
- Lakowicz, J.R. (2002). Topics in fluorescence spectroscopy, Vol 5, Kluwer academic publishers.
- Lakowicz, J.R. (2006). principles of fluorescence soectroscopy, 3rd ed., springer science+ Business media. LLC.
- lampman, G.M., Pavia, D.L. (2012) spectroscopy, 4th edition. Brooks Cole.
- Lee, D.C., and Chapman, D. (1986). infrared spectroscopic studies of biomembranes and model membrane, Bioscience reports, Vol 6, no. 3.
- Lee, J.S., and Park, C.B. (2010). Biomaterials, 31, 6789-6795.
- Li, H. et al. (2009). Amyloid and protein aggregation – analytical method, John Wiley and sons, pp 1-32.
- Lin,S.Y. (2003). International Journal of Biological Macromolecules. 32, pp173-177.
- Lindgren, M., Hammarstrom, P. (2010). The FEBS Journal. 277, 1380-1388.
- Lomakin, A.et al. (1996). Proc. Natl. Acad. Sci. USA. Vol 93, pp 1125-1129.
- Miller, R.D., Pardo, M.C. (2011). Basics of anesthesia, 6th ed., Elsevier Saunders.
- Miloro, M. et al. (2004). Peterson's Principles of Oral and Maxillofacial Surgery,vol 1, 2nd ed. , BC Decker Inc..
- Murphy, R. (2002). peptide aggregation in neurodegenerative disease, Annu. Rev. Biomed. Eng., 4, 155-174.
- National research council of the national academy of science, (2006), Nutrient Requirements of Dogs and Cats, printed in United States of America.
- Pavis, D. et al. (2008). Introduction to spectroscopy. 4th ed., cengage learning.
- Perszel, A. et al. (2005). Journal of Computational Chemistry. vol. 26, no. 11, pp. 1155–1168.
- Petsko, G.A., Ringe, D. (2004). Protein structure and function, New Science Press Ltd.
- Planque, M.R. (2007). J. Mol. Biol., 368, 982–997.
- Pravat, P.K. et al. (2006). Neurochem Res, 31, 883–890.

- Raaman, N. (2006). Phytochemical Techniques, New India publishing agency.
- Ramiraz, M. et al. (2010). Protein Misfolding Diseases, A John Wiley & sons, INC., PUBLICATION.
- Rice, P.A., Correl, C.C. (2008). Protein-Nucleic Acid Interactions: Structural Biology, Royal society of chemistry.
- Rubin N. et al.(2010), J. Am. Chem. Soc,, 132, 4242–4248.
- Samori, P. (2008), STM and AFM studies in (bio)molecular systems: unraveling the nano world, Springer- Verlag Berlin Heidelberg.
- Sarroukh, R. et al. 2011, Transformation of amyloid β(1-40) oligomers into fibrils is characterized by a major change in secondary structure, Cell. Mol. Life Science, Vol 68, no 8, pp 1429-1438.
- Sarver, R.W., Krueger, W.C. (1991). Protein secondary structure from fourier transform infrared spectroscopy: a data base analysis, Vol. 194, 89-100.
- Sathyanarayana, D.M. (1983). vibrational spectroscopy: theory and application. 1st ed., New age international (P) Ltd., New Delhi.
- Schulman, S.G. (1977). Flurescence and phosphorescence spectroscopy: physiochemical principles and practice, Vol 59, A. Wheaton & Co. Ltd, Exeter.
- Sharma, B.K. (2007). Spectroscopy. 20th ed., Goel Publishing house, Meerut, Delhi.
- Sheehan, D. (2009). Physical Biochemistry: principles and applications. 2nd ed., John Wiley & sons Ltd.
- Silverstein, J.et al. (2008). Geriatric Anesthesiology, 2nd ed., Springer science-business media, LLC.
- Smith, B.C. (2011), Fundamentals of Fourier Transform Infrared Spectroscopy, 2nded., CRC press, tailor and Francis Group LLC..
- Stargrove, M.B., Stargrove, L.B. (2008). Herb Nutrient and Drug Interactions: Clinical Implications and Therapeutic Strategies, library of congress.
- Stayton, M. et al. (2008). Regulation of Arginine Metabolism Following Acute Myocardial Infarction in Mice, ProQuest LLC.
- Stein, T.D. et al., (2004), The Journal of Neuroscience, 24(35):7707–7717.
- Stuart, B. (2004). Infrared spectroscopy fundamentals and applications,ANTS.

- Susi, H., Bayler, D.M. (1983). Protein structure by fourier transform infrared spectroscopy: second derivative spectra, Vol. 115, No. 1, 391-397
- Szabo, Z. et al. (1999). Biochemical and Biophysical Research Communications 265, 297–300.
- Takahashi R.H., Nam E.E., Edgar M., Gouras G.K., (2002), Histol Histopathol, 17: 239-246.
- Thirumalai, D.et al. (2003) Current Opinion in Structural Biology, 13, 146–159.
- Tjernberg, L. et al. (1999). Chemistry and biology, 6, 53-62.
- Turro, N.J. (1991). Modern Molecular Photochemistry, University science books, America.
- Vetri, V. (2010), Biochimica et Biophysica Acta 1804 , 173–183.
- Walsh, D. et al.(1999), The Journal of biological chemistry. 274, No. 36, pp 25945–25952.
- Wang, H. et al. (2008). PNAS, 105, 7159-7164.
- Wang, T., et al. (2008), Spectroscopic investigation on the binding of bioactive pyridazinone derivative to human serum albumin and molecular modeling, Collides and surfaces B, Vol 65, no 1, pp 113-119.
- Whitford, D. (2005). Proteins: Structure and Function, John Wiley & Sons Ltd.
- Williams, D. (1976), methods of experimental physics: spectroscopy, vol 13, part A, Academic press Inc.
- Wilson, R.A., and Bullen, H.A. Introduction to Scanning Probe Microscopy (SPM): Basic Theory Atomic Force Microscopy (AFM). Department of Chemistry, Northern Kentucky University, Highland Heights, KY 41099.
- Xie, Z. et al. (2006). Anesthesiology; 104,988–994.
- Xie,Z., and Tanzi, R.E. (2006). Alzheimer's disease and post-operative cognitive dysfunction , Experimental Gerontology 41 346–359.
- Yadav, L.D. (2005). Organic spectroscopy, Klower academic publisher, New Delhi, India.
- Zandomeneghi, G. et al. (2004).Protein science , 13, 3314-3321

دراسة تأثير البروبوفول و الأرجنين على البيتا أميلويد بواسطة تقنيات مطيافية الجزيئات

اسم الطالبة: شروق يوسف محمد عيايدة

اسم المشرف: د. صقر درويش

ملخص

تم دراسة التفاعل بين كل من الدواء المخدر (البروبوفول) والأرجنين مع البروتين المعروف باسم (بيتا أميلويد) باستخدام مطياف الأشعة فوق البنفسجية (UV-vis. spectroscopy) وجهاز انبعاث الاشعاع (Fluorescence spectroscopy) وجهاز مطياف تحويل فورييز للأشعة تحت الحمراء (Fourier transform infrared spectroscopy) حيث تم حساب ثابت الترابط (binding constant) للبروبوفول والارجنين عن طريق جهاز مطياف الأشعة فوق البنفسجية وجهاز مطياف انبعاث الإشعاع عند درجة حرارة (293K) والقيم هي: ($2.13x10^2M^{-1}$ و $2.81x10^2M^{-1}$) للبروبوفول و($0.35x10^2M^{-1}$ و $0.37x10^2M^{-1}$) للأرجنين. بالاضافة الى ذلك تم حساب ثابت (Stern-Volmer constant) وهي للبروبوفول ($1.21x10^3L\ mol^{-1}$) و ($1.49x10^3L\ mol^{-1}$) للأرجنين.

ومن النتائج التي تم التوصل اليها أن شدة امتصاص الأشعة فوق البنفسجية للبيتا أميلويد تزداد بزيادة تركيز البروبوفول وتقل بزيادة تركيز الارجنين مع بقاء تركيز البيتا أميلويد ثابت.

ومن خلال استخدام جهاز انبعاث الاشعاع وجد أن شدة الاشعاع المنبعث نتيجة تفاعل كل من البروبوفول والارجنين مع البيتا أميلويد تقل بزيادة تركيز كل من الدوائين وبقاء تركيز البروتين ثابت حيث أن هذا الانخفاض في شدة الإشعاع المنبغث يشير إلى أن كلا من البروبوفول والارجنين لديه قدرة قوية على خفض او التقليل من الإشعاع المنبعث ذاتيا من البيتا أميلويد من خلال الية (static quenching).

باستخدام جهاز مطياف تحويل فوريير للأشعة تحت الحمراء (FTIR) مع تطبيق عدد من التقنيات الموجودة في هذا الجهاز مثل تقنية (Fourier self deconvolution) و (second derivative resolution) بالإضافة الى تقنية (curve fitting) تم تحليل منطقة الأميد الاول والأميد الثاني لبروتين البيتا أميلويد من أجل تحديد بنية البروتين الثانوية (secondary structure) والية ارتباط كل من البروبوفول والأرجنين معه حيث تم تحديد جميع مواقع القمم (peaks) في مناطق الأميد الاول والثاني وتفسير التغيرات في مواقع القمم نتيجة تغيير تركيز الأدوية المضافة (البروبوفول والأرجنين).

يشير الطيف المقاس بواسطة جهاز (FTIR) الى تغير في شدة حزم الامتصاص (Absorption bands) نتيجة تغير تركيز الأدوية المضافة (البروبوفول والأرجنين). إضافة الى ذلك ظهر من خلال النتائج أن هناك زيادة في حزم الامتصاص التابعة لل(anti parallel β-sheet) بزيادة تركيز البروبوفول وبالمقابل لوحظ نقصان في حزم الامتصاص التابعة لل(anti parallel β-sheet) بزيادة تركيز الأرجنين.

تمتاز التراكمات (Amyloid oligomers or fibrils) الناتجة في دماغ المصابين بمرض الزهايمر- والتي ترتبط بالنهايات العصبية فتعيق انتقال السيالات العصبية مما ينتج عنه الأعراض المرافقة لمرض الزهايمر من فقدان الذاكرة وغيرها- بزيادة في (anti parallel β-sheet) في بنيته الثانوية وهذا مؤشر على تأثير البروبوفول في تحفيز تكوين (oligomers) وتأثير الارجنين المختلف عن تأثير البروبوفول.

ومن خلال تقنية AFM (Atomic Force Microscopy) وجد أن البروبوفول يزيد من حجم التراكمات الناتجة في البيتا أميلويد عند اضافته اليه كما ولوحظ أن تأثير الارجنين كان مختلفا تماما حيث كانت الزيادة في حجم التراكمات صغيرة جدا وبشكل مختلف عن التراكمات الناتجة عن البروبوفول وهذا يدعم ما تم التوصل اليه بطرق التحليل الأخرى.